FORMATION AND CHARACTERIZATION OF SILK FIBROIN / HYALURONIC ACID COMPLEXES AND THEIR USE IN IONTOPHORETIC DRUG DELIVERY

A Thesis Submitted to
the Graduate School of Engineering and Sciences of
İzmir Institute of Technology
In Partial Fulfillment of the Requirements for the Degree of

MASTER OF SCIENCE

in Chemical Engineering

by
Özge MALAY

July 2005
İZMİR

We approve the thesis of **Özge MALAY**

Date of Signature

..... **26 July 2005**
Assist. Prof. Dr. Ayşegül BATIGÜN
Supervisor
Department of Chemical Engineering
İzmir Institute of Technology

..... **26 July 2005**
Assist. Prof. Dr. Oğuz BAYRAKTAR
Co-supervisor
Department of Chemical Engineering
İzmir Institute of Technology

..... **26 July 2005**
Assoc. Prof. Dr. Sacide ALSOY ALTINKAYA
Department of Chemical Engineering
İzmir Institute of Technology

..... **26 July 2005**
Assoc. Prof. Dr. Ahmet YEMENİCİOĞLU
Department of Food Engineering
İzmir Institute of Technology

..... **26 July 2005**
Assist. Prof. Dr. Figen TOKATLI
Department of Food Engineering
İzmir Institute of Technology

..... **26 July 2005**
Prof. Dr. Devrim BALKÖSE
Head of the Department
İzmir Institute of Technology

.....
Assoc. Prof. Dr. Semahat ÖZDEMİR
Head of the Graduate School

ACKNOWLEDGEMENT

This study was carried out at the Department of Chemical Engineering, İzmir Institute of Technology during the years 2003-2005.

I express my warmest gratitude to my supervisors Dr. Ayşegül Batıgün and Dr. Oğuz Bayraktar for introducing me to the interesting world of polyelectrolyte complex systems and transdermal drug delivery, for guidance and endless optimism during the years.

My special thanks go to Dr. Sacide Alsoy Altınkaya, Dr. Ahmet Yemenicioğlu and Dr. Figen Tokatlı for their valuable comments.

I wish to express my gratitude to professor Devrim Balköse, the Head of the Department of Chemical Engineering, for providing me excellent facilities for the instrumental analyses.

I am grateful to the whole stuff of Department of Chemical Engineering for their help and technical assistance.

I express my thanks to all my friends and colleagues (Serdar Özer, Can Aksakal, Öniz Birsoy, Sevde Seza Bozacıoğlu and others) for their friendship, support and for taking my mind out of the work from time to time.

I thank my parents, Esin and Ziya Kaşlı, and my brother Tahir Emre, for their unfailing encouragement and loving support during my whole life.

I express my thanks to Lale and Hasan Malay for being in my life with all their love, support and belief in me.

Finally, my warmest thanks belong to my dear life-mate Umut Malay for his neverending love, understanding support and for being sunshine of my life.

The financial support from Research Fund of İzmir Institute of Technology for this thesis and the general technical support of State Planning Organization on researches in İzmir Institute of Technology are gratefully acknowledged.

ABSTRACT

This study aimed the investigation of the pH-induced complexation of silk fibroin (SF) and hyaluronic acid (HA), and the potential use of the films casted from the aqueous mixtures of the SF-HA complexes in iontophoretic drug delivery applications.

In the present study, SF-HA complex coacervation was investigated by turbidimetric, conductometric, gravimetric and viscosimetric analysis with respect to changes in total biopolymer concentration and biopolymer weight ratio. SF-HA complexes were formed within the pH-window of 2.5-3.5 regardless of the total biopolymer concentration, biopolymer ratio or mixing order.

SF-HA aqueous complex mixtures, prepared under previously determined conditions, were casted and dried under controlled conditions. The resultant insoluble and transparent films were subjected to instrumental analysis such as DSC, XRD, FT-IR, SEM and AFM. Swelling kinetics of the films was studied for pH window of 2.5-7.4 and cyclic swelling test was performed to determine the pH-responsiveness of the films. It was shown that films swelled more in alkaline conditions and responded to the changes in pH of the medium. The permeability of the films were tested with modified-diffusion-vessels method at pH 2.5 and 7.4 and it was demonstrated that the complex films had higher permeability in alkaline condition. Eventually, iontophoretically assisted drug permeation and release studies were performed with a custom-made diffusion cell under both passive condition and electric field applied in pulsatile fashion. In conclusion, SF-HA complex films were found promising for the iontophoretic delivery of high molecular weight and charged drugs for a membrane-permeation controlled formulation. In this study, timolol maleate (TM) was used as the model drug.

ÖZET

Bu çalışmada, ipek fibroin (SF) and hyaluronic asitin (HA) pH'a bağlı olarak kompleks oluşturması ve sıvı karışımda oluşan kompleks çözeltilerin dökümü ve uygun şartlar altında kurutulması sonucunda elde edilen filmlerin iyontoforetik ilaç salım sistemlerinde kullanılma potensiyeli araştırılmıştır.

SF-HA kompleks koazervasyonu, turbidimetrik, kondaktometrik, gravimetrik ve vizkozitemetrik yöntemlerle incelenmiş ve toplam biyopolymer konsantrasyonu ve karışımda bulunan biyopolymerlerin ağırlık oranları açısından incelenmiştir. Bu analizler sonuncunda, SF-HA kompleks oluşumu, toplam biyopolymer konsantrasyonu, polymerin karışım oranı ve karışım sırasından bağımsız olarak pH 2.5-3.5 aralığında gerçekleşmiştir. En fazla koazervasyon maksimum turbidite ve minimum vizkozite değerlerinde elde edilmiştir.

Belirlenen şartlar altında hazırlanan kompleks karışımından filmler dökülmüş ve kontrollü olarak kurutulmuştur, ve sonuç olarak suda çözünmeyen, şeffaf, ipek filmlere göre mekanik olarak daha dayanıklı filmler elde edilmiştir. Elde edilen filmler DSC, XRD, FT-IR, SEM ve AFM cihazları aracılığıyla karakterize edilmiştir. Filmlerin şişme kinetiği pH 2.5 - 7.4 aralığında çalışılmış ve filmlerin pH duyarlılığını ölçmek için siklik şişme testi uygulanmıştır. Kompleks filmlerin alkalin ortamda daha fazla şişme gösterdiği ve pH değişimlerine duyarlı olduğu tespit edilmiştir. Buna bağlı olarak da farklı pH değerlerinde (2.5 ve 7.4) gerçekleştirilen geçirgenlik deneylerinde alkalin ortamda daha fazla ilaç geçirgenliği gösterdiği belirlenmiştir. Son olarak, hem pasif durumda hem de kesikli elektrik alan uygulaması altında iyontoforetik ilaç geçirgenliği ve ilaç yüklenmiş filmden ilaç salımı özel yapım difüzyon hücresi kullanılarak incelenmiştir. SF-HA kompleks filmlerin kontrollü ilaç iletimi için kullanılabileceği gösterilmiştir. İlacın kesikli tarzda kontrollü salımı başarılmıştır. Çalışmada model ilaç olarak timolol maleate kullanılmıştır.

TABLE OF CONTENTS

LIST OF FIGURES viii

LIST OF TABLES xi

LIST OF ABBREVIATIONS xii

CHAPTER 1. INTRODUCTION 1

CHAPTER 2. REVIEW OF LITERATURE 3

2.1. Controlled Drug Delivery 3

2.2. Transdermal Drug Delivery 5

2.2.1. Enhancement of Transdermal Permeation 7

2.2.1.1. General Aspects 7

2.2.1.2. Iontophoresis 9

2.2.2. Polymeric Systems in Transdermal Drug Delivery 11

2.3. Polyelectrolyte Complexes (PEC) 17

2.3.1. General Aspects 17

2.3.2 Protein-Polysaccharide Complexation 20

2.3.3. Models on Formation of Coacervate Systems 24

2.3.3.1. Silk Fibroin 29

2.3.3.2. Hyaluronic Acid 35

CHAPTER 3. AIMS OF THE STUDY 39

CHAPTER 4. EXPERIMENTAL 40

4.1. Materials 40

4.2. Methods 40

4.2.1. Part I. Preparation and Properties of SF and HA Stock Solutions 41

4.2.1.1. Preparation of Stock Solutions 41

4.2.1.2. Molecular Weight Determination of SF 42

4.2.1.3. Electrophoretic Mobility Measurements 43

4.2.2. Part II. Preparation and Characterization of SF-HA Complexation 43

4.2.2.1. Turbidimetric Analysis 43

4.2.2.2. Conductometric Analysis 44

4.2.2.3. Gravimetric Analysis 44
4.2.2.4. Viscosimetric Analysis 45
4.2.3. Part III. Preparation and Characterization of SF-HA Films 45
4.2.3.1. Preparation of SF-HA Films 45
4.2.3.2. Swelling Measurements 46
4.2.3.3. Material Characterization 47
4.2.4. Part IV. Permeability and Release Studies 48
4.2.4.1. Choice of the Model Drug 48
4.2.4.2. Drug Permeation Tests 48
4.2.4.3. Drug Permeation and Release Tests:
Passive vs. Iontophoretic Delivery Applications 50

CHAPTER 5. RESULTS AND DISCUSSION 52
5.1. Part I. Properties of the SF and HA Dispersions 52
5.2. Part II. SF-HA Complexation 53
5.2.1. Turbidimetric Titration under Acidification 54
5.2.2. Titration of HA by SF: Conductometric Monitoring 58
5.2.3. Gravimetric Analysis 60
5.2.4. Viscosimetric Analysis 63
5.3. Formation and Characterization of SF-HA Complex Films 67
5.3.1. Morphological Examination of the SF-HA Complex Films 69
5.3.2. Thermal Analysis 74
5.3.3. X-Ray Diffraction Analysis 78
5.3.4. FT-IR Analysis 80
5.3.5. Swelling Tests 82
5.4. Drug Permeability and Release Studies 88
5.4.1. Permeability of TM Through SF-HA Complexes 88
5.4.2. Passive vs. Iontophoretic Delivery of TM 89

CHAPTER 6. CONCLUSION 92

REFERENCES 94

APPENDICES
APPENDIX A. Preparation of Dialysis Tubing. 106
APPENDIX B. Calibration Curves 107

LIST OF FIGURES

Figure **Page**

Figure 2.1. Rate control mechanisms in new generation drug delivery systems 4

Figure 2.2. Controlled drug delivery versus immediate release 5

Figure 2.3. Diagram of iontophoretic technique: as current is applied, drug cations are repelled into the skin and absorbed in the systemic circulation 9

Figure 2.4. Schematic illustration of a iontophoretic transdermal delivery patch composed of a membrane/reservoir system..... 13

Figure 2.5. Schematic representation of the aggregation of the PECs 18

Figure 2.6. Main trends in the behaivour of protein/polysaccharide mixtures. 21

Figure 2.7. Schematic representation of phase separation by complex coacervation... 22

Figure 2.8. The coacervate droplets that have partially spread over the surface of the microslide and coaleasced with each other. This picture was reproduced from the study of de Jong and Kruyt (1929)..... 23

Figure 2.9. Intrapolymer (A) and interpolymer (B) complexes..... 25

Figure 2.10. Schematically proposed model for coacervate formation for a protein/polysaccharide mixture..... 26

Figure 2.11. Secondary structure of SF 30

Figure 2.12. The relation between conformation, quenching or casting temperature and concentration of silk fibroin..... 31

Figure 2.13. Chemical structure of hyaluronic acid..... 35

Figure 2.14. Schematic depiction of crosslinked HA hydrogel. 37

Figure 4.1. Step-wise preparation of aqueous silk fibroin solution from silk fibers. ... 42

Figure 4.2. Structure of timolol maleate salt. 48

Figure 4.3. Vial-in-vial permeation testing system..... 49

Figure 4.4. Iontophoretic drug release set-up. 50

Figure 4.5. Custom-made diffusion cell for iontophoresis applications. 51

Figure 5.1. Electrophoretic mobility of 0.1 wt% biopolymer dispersions at 20°C. 53

Figure 5.2. Turbidity of pure SF (▲) and HA (●) solutions; and SF-HA system as a function of pH for C_p=0.5% (○) and C_p=2.5% (□) with SF:HA ratio of 32:1. 55

Figure 5.3. Turbidity of SF-HA system as a function of pH for SF:HA ratio of 32:1 (○) and 16:1 (∆) for C_p=0.5% 56
Figure 5.4. Formation of soluble and insoluble complexes with respect to pH. 58
Figure 5.5. Conductometric titration at pH 3.0. 59
Figure 5.6. Coacervation yield (%) vs. SF (g) in the complex mixture 61
Figure 5.7. Coacervate (g) recovered from the complex mixture vs. ratio of the charges of the biopolymers at constant pH. 62
Figure 5.8. Viscosity vs. pH for C_p=1.5% and SF:HA=32 (■) ; C_p=0.5% and SF:HA=32 (▲); C_p=0.5% and SF:HA=16 (●). 65
Figure 5.9. Viscosity vs. shear stress plots of SF-HA complex mixtures at pH=3.0. The curves represents C_p=1.5% and SF:HA=32 (■) ; C_p=0.5% and SF:HA=32 (▲); C_p=0.5% and SF:HA=16 (●) 66
Figure 5.10. Appearence of dry (a) and wet (b) insoluble SF-HA complex films 68
Figure 5.11. SEM photographs of the SF-HA complex film magnified at 2000x (a) and 15000x (b) 69
Figure 5.12. Cross section images of SF/HA complex film with a magnification of 100x (a), porous (b) and dense (c) regions of insoluble SF/HA film (15000x).. 70
Figure 5.13. AFM images of SF-HA PEC film with height view (a), view of roughness analysis (b), deflection view (c) and 3D height view (d) 71
Figure 5.14. SEM photograph of SF-HA complex films dried under controlled conditions (a) and at room temperature (b). 72
Figure 5.15. AFM images showing the formation of cracks on the complex film dried at room temperature given as height image for 50x50 μm^2 (a) and for 10x10 μm^2 (c); deflection image for 50x50 μm^2 (c) and for 10x10 μm^2 (d). 73
Figure 5.16. AFM images of SF-HA complex film (a) and SF control sample with silk II conformation (b) dried under controlled controlled conditions. 74
Figure 5.17. DSC curves of the films. SF film-II (F1), SF film-I (F2), SF-HA blend (SF:HA=20) (F3), SF-HA complex film (SF:HA=20) (F4), SF-HA complex film SF:HA=30) (F5), phase-separated coacervate network (F6), coacervate film (F7), ... 75
Figure 5.18. X-ray diffraction patterns of SF film-II (F1), SF film-I (F2), SF-HA complex film (SF:HA=20) (F4), SF-HA complex film (SF:HA=30) (F5), HA film (F8). 79

Figure 5.19. ATR-IR spectra of the casted films; HA (a), SF (b); SF-HA complex film (c) and drug loaded SF-HA complex film (d)..... 81
Figure 5.20. pH-dependent swelling kinetics of the SF-HA complex film at 37°C. pH 2.5 (◊); 3.2 (□); 6.5 (○); 5.5(Δ); 7.4 (●)..... 83
Figure 5.21. pH-dependent swelling kinetics of the SF-HA complex film at 50°C. pH 2.5 (◊); 3.2 (□); 6.5 (○); 5.5(Δ); 7.4 (●).....84
Figure 5.22. Equilibrium swelling percentages of the SF-HA complex films with respect to pH at 50°C (●) and 37°C (○). 85
Figure 5.23. pH responsive changes of water content in SF-HA complex films. 87
Figure 5.24. Timolol maleate concentration in permeate through SF-HA complex film at pH 7.4 and 2.5. 88
Figure 5.25. TM delivery profiles through SF-HA complex film. TM permeation through the film in passive mode (a), iontophoretically assisted TM permeation form the film (b), release (c) from the drug loaded film, (d) applied electric field profile. 90
Figure B.1. Calibration curve of TM dissolved in PBS at pH = 7.4 evaluated at λ = 294 nm in UV-visible spectrophotometer 107
Figure B.2. Calibration curve of TM dissolved in PBS at pH = 2.5 evaluated at λ = 294 nm in UV-visible spectrophotometer 107
Figure B.3 Calibration curve of aqueous SF solution evaluated at λ = 272 nm in UV-visible spectrophotometer 108
Figure B.4. Calibration curve of aqueous HA solution evaluated at λ = 217 nm in UV-visible spectrophotometer 108

LIST OF TABLES

Table **Page**

Table 2.1. Methods to enhance transdermal permeability of macromolecular drugs..... 8

Table 2.2. Factors studied for some protein/polysaccharide systems in literature. 28

Table 4.1. Detailed description of the preparation conditions of the complexes..... 46

Table 5.1. Calculated vs. Measured Viscosity..... 64

Table 5.2. Degree of dissociation for HA with respect to pH. 84

Table 5.3. Equilibrium swelling of various SF films with respect to pH and ionic strength. 86

LIST OF ABBREVIATIONS

AFM	Atomic force microscopy
Ala	Alanin
Asp	Aspartic acid
β-lg	Lactoglobulin
BSA	Bovine serum albumin
Cp	Total biopolymer concentration
DDS	Drug delivery system
DNA	Deoxyribo-nucleic acid
DSC	Differential scanning calorimetry
FT-IR	Fourier transform infrared
GA	Glutaraldehyde
Glu	Glutamine
Gly	Glycine
HA	Hyaluronic acid
HPLC	High pressure liquid chromatography
IEP	Isoelectric point
LHRH	Luteinizing hormone releasing hormone
MW	Molecular weight
NTU	Nephelometric unit
PBS	Phosphate buffer saline
PEC	Polyelectrolyte complex
PEG	Polyethylene glycol
PEO	Polyethylene oxide
p*K*a	negative logarithm of dissociation constant
Pr:Ps	Protein to polysaccharide weight ratio
PVA	Polyvinyl alcohol
PVP	Poly(vinyl) propylene
R	SF-HA weight ratio
RH	Relative humidity
RSF	Regenerated silk fibroin
SEC	Size exclusion chromatography
SEM	Scanning electron microscopy
Ser	Sericine
SF	Silk fibroin
TM	Timolol maleate
Tyr	Tyrosine
Val	Valine
XRD	X-ray diffraction

CHAPTER 1

INTRODUCTION

Controlled delivery of drugs to achieve predictable and reproducible drug concentration in the blood stream is the aim of the search on the alternative routes for drug administration. Production of new peptide-based drugs due to extensive research in genetics has accelerated the studies in this area, as these drugs require specific conditions for effective delivery regimes.

Transdermal drug delivery is an alternative route for drug delivery. It offers many important advantages over oral drug delivery, e.g., avoids gastrointestinal tract and hepatic first pass biotransformation and metabolism, controls absorption rate, increases patient compliance, and provides ease of termination if needed. There is a number of successful transdermal drug delivery systems commercially available at present. However, the need remains to extend their operating parameters so that more sustainable and variable delivery regimes can be achieved. Iontophoresis is a process, by which the transport of ions into and through the skin is increased by the application of an external field. This process has been used to enhance controlled transdermal delivery of the drugs which have low permeability through the skin such as hydrophilic, very lipophilic, of high molecular weight or charged ones, e.g. peptide-based drugs.

The heart of the transdermal therapeutic systems is the transdermal patch. Transdermal patches are polymeric materials that can be in the form of a membrane controlled permeation system including a reservoir or matrix-diffusion controlled system in which the drugs were dissolved or evenly distributed. Several synthetic natural polymeric systems have been attempted to meet the needs of an effectively functioning transdermal patch. Polyelectrolyte membranes comprising natural and/or synthetic polymers have been found promising for the iontophoretic transdermal drug delivery systems since they have high responsiveness to the environmental changes such as to alterations in ionic strength, pH or electric field of the system.

The phenomena of interpolymer interactions have been the focus of intensive fundamental and applied research on polyelectrolyte complexes (PECs). The PECs

prepared from natural polymers such as proteins and polysachharides have the additional advantage of being non-toxic and bioabsorbable.

Protein-polyelectrolyte interactions have been concerned widely with biotechnological and biomedical applications such as protein purification, enzyme immobilization, immunosensing and bioactive sensors. Several globular proteins and polyelectrolytes (natural or synthetic) have been matched for various techniques and objectives of investigation. Protein-polyelectrolyte interactions often leading to coacervation and resulting in biopolymer complexes arises mainly from electrostatic interactions. This complexation is dependent on the ionization degree of these macromolecules and thus the pH. The aqueous complexation mixtures obtained under specific conditions can be processed into several forms such as films, gels, sponges, etc. The recent trend is to replace the natural biopolymers used with the new ones to allow precise control over resultant material properties along with the opportunity.

Several researches have been concentrated on the PECs that occur in protein-polyelectrolyte mixtures. However, silk fibroin and hyaluronic acid complexation has not been studied in terms of complex coacervation. Fibroin, a fibrous silk protein, is produced by silkworm *Bombyx mori*, is an excellent film former. This protein has been found to be a good starting material for preparation of fibroin-based materials such as gel, powder or film, and it has potential uses in contact lenses, artificial corneas, burn wound dressings, artificial lungs and drug delivery devices. On the other hand, HA is a natural anionic polysaccharide that has been used in the formation of PECs. It is considered as an attractive building block for the production of novel biomaterials with potential applications in drug delivery and tissue engineering.

The specific objectives of this work were to investigate the complex formation between SF and HA, to characterize the films produced by this complexation and to determine the capability of the complex films, whether they can be utilized in iontophoretically assisted transdermal drug delivery systems.

CHAPTER 2

REVIEW OF LITERATURE

2.1. Controlled Drug Delivery

The development of newer and more powerful drugs and the need for prolonged and better control of drug administration are the leading factors for the search of the alternative ways of drug administration. In the light of advancing technologies such as genome mapping, there has been a dramatic increase in peptide and protein drugs that are mostly injectable. These facts reveal that there is a great commercial potential for the controlled delivery systems that uses the alternative routes (Fletcher 1998).

Studies on drug delivery systems were initiated to achieve the controlled delivery of drugs for predictable and reproducible rate of drug input to the blood stream to enhance the treatment of the diseases. The initial aim in the field of controlled drug delivery has been attaining sustained zero-order release of a therapeutic agent over a prolonged period of time (Sershen and West 2002). Zero-order kinetics have been attempted by using several techniques including, osmotically driven pumps, matrices with controllable swelling, diffusion or erosion rates, non-uniform drug loading profiles, and multilayered matrices.

Recently, the biologically active peptides have been artificially synthesized by genetic engineering techniques. These peptides are easily degraded under physiological conditions and they may also encounter absorption problems due to their high molecular weight. Hence, they cannot be utilized in conventional dosage forms. Moreover, in order to maximize efficiency and minimize side effects, the new generation of drug delivery systems has been attempted. The challenge appeared to be the controlled delivery of a therapeutic molecule, gene or protein in a pulsatile or staggered fashion when the drug is required or by targeting the drug to a specific site in addition to utilizing the conventional rate-controlling systems. By these means, the recent improvements on controlled drug delivery can be examined by a division into two classes: temporal control and distribution control (site-specific delivery) as shown in Figure 2.1 below (Kumar M. and Kumar N. 2001, Okano and Yoshida 1993).

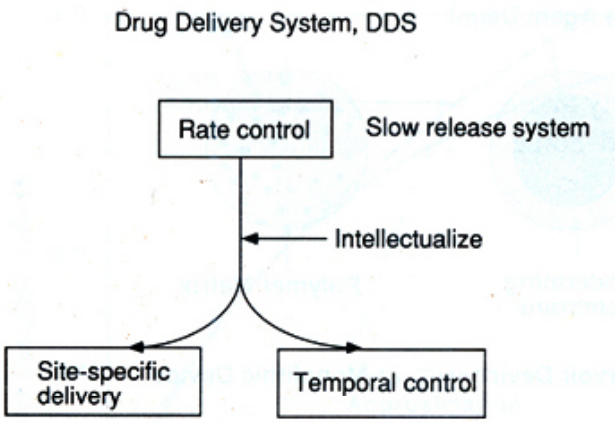

Figure 2.1. Rate control mechanisms in new generation drug delivery systems (Source: Okano and Yoshida 1993).

In case of temporal control, the drug release is achieved over an extended period or at a specific time during treatment. This can be achieved by constructing a pre-programmable system that can deliver the agent at a pre-set rate or in pulses of a predetermined sequence. Alternatively, a responsive system can be formulated that can respond to alterations in the local environment such as pH, electric field, temperature, absence or presence of a specific molecule (Kost and Langer 2001). In case of traditional administration routes, fluctuations occur in the blood plasma levels. By the temporal control, the rate of drug release matches the rate of drug elimination, and hence the concentration of drug stays within the therapeutic window (effective drug plasma range between the excessive toxic level and subtherapeutic level) during a specified interval (Figure 2.2). This avoids waste of drug and toxic effects due to overdosing while maximizing the benefits of the drug.

On the other hand, the distribution control aims the “target release” of the drug to the precise site of activity. This improvement is especially beneficial for the cases when the traditional routes are not capable of distributing the drug molecules to the site action or when the natural distribution caused side effects as the drug molecules encounter tissues as in the case of chemotherapy (Kumar M. and Kumar N. 2001).

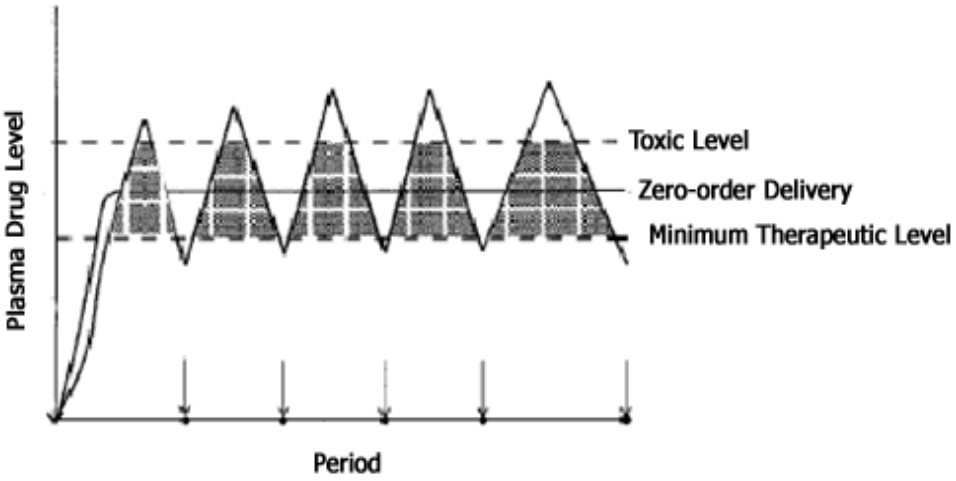

Figure 2.2. Controlled drug delivery versus immediate release
(Source: Kumar M. and Kumar N. 2001).

2.2. Transdermal Drug Delivery

The improvements in controlled drug delivery regimes provides a competitive situation between the administration routes, which can be listed as peroral (osmotic minipumps), transdermal (membrane/matrix), oral (targeted formulations), parenteral (nanoparticles and nanocapsules), subcutenaous (implants), intracavitary, nasal, buccal, etc. (Vasil'ev et al. 2001). Among these controlled drug delivery systems, transdermal therapeutic systems has gained considerable success while generating lots of interest with the ongoing enhancements on this technique and has found wide applications.

Transdermal drug delivery systems offer the controlled plasma levels of potent drugs with short biological half-lives. These systems allow the administration of drugs with narrow therapeutic window. By this parenteral route of administration, the potential irritant side effects of the drugs on the gastrointestinal tract can be decreased. In addition to this, transdermal administration brings out the bypass of the hepatic first-pass metabolism, which may result in lost of activity or generation of toxic metabolites. By this way, the drug wasted by the metabolism is also avoided, and hence the dose to be administered decreases. On the other hand, when compared to other mucosal routes, proteolytic activity is relatively low in skin, and this reduces the degradation at the site of administration (Banga et al. 1999). This noninvasive technique minimizes trauma, risk of infection, damage to the wound. Additionally, the continuous mode of

administration increases patient compliance to the therapy and it brings out the ease of discontinue the delivery in case of toxic effects.

The skin, as the largest organ of the human body with a surface area of about 2 m^2, was thought to function just as an impermeable barrier that precludes the entry of foreign agents into the body (Stamatialis et al. 2002). By the development of transdermal drug administration systems, skin gained another function as a route of administration for the topical or continuous systemic delivery of drugs. Transdermal administration comprises stage-wise delivery of the drug. The first stage is the delivery of the drug molecule from the transdermal device (acting as a reservoir) to the skin surface. The second stage is the permeation of the molecule through the skin and the final stage includes the distribution of the molecule to the site of action via systemic circulation. Thus, permeation rate limiting factor is characterized by the drug permeation properties of either the skin or the membrane, or both. Obviously, the release of the drug from the device can be controlled more exactly than the permeability of drug in the skin. In passive delivery the transport of the molecule across the *stratum corneum*, the outermost layer of the skin, is the rate-limiting step since this layer constitutes the most impermeable membrane in humans with its rigidly arranged, lipophilic structure. The controlled transdermal delivery systems are designed so that the delivery from the device, by the diffusion of the molecule in a polymeric membrane of the product, is the rate-limiting step. The main drawback of these systems is seen for the drugs that require high blood levels and for the drugs that are charged, of high molecular weight, hydrophilic or very lipophilic (Wang et al. 2005).

Biological factors of transdermal drug delivery, which are generally less easily controlled, can be summarized as the intra- and intersubject variability, the regional blood flow and the skin pH. This underlines the need of the individual dosage even for the same patient for the variable states that determine the sweat counterflow, skin temperature, etc (Vasil'ev et al. 2001). Better control of biological variability in transdermal drug absorption has been attempted with enhanced systems. Selection of external conditions (e.g. ionic strength, pH) and/or drug properties (e.g. charge, lipophilicity, molecular weight, etc.) and the enhancements on the characteristic properties of the transdermal device can be applied to control the release kinetics of a drug from transdermal systems. By such manipulations, controlled drug delivery can be promisingly achieved by the transdermal therapeutic systems to obtain presumably reproducible drug delivery.

2.2.1. Enhancement of Transdermal Permeation

2.2.1.1. General Aspects

The first transdermal drug delivery system (TDDS) was developed for scopolamine for motion sickness in 1981 (Panchagnula 1997). Since then many TDDS have appeared in market with great success, but the need remains to extend their operational parameters to obtain more sustainable and variable delivery regimes. Inherent limitations of TDDS stems from the variability of physico-chemical properties of the penetrant, low drug levels in plasma and skin irritation caused by some drugs or formulations. Passive permeability of drugs across the highly lipophilic stratum corneum is especially difficult to compounds which are hydrophilic, very lipophilic, of high molecular weight (MW > 400 g/mol) or charged (Wang et al. 2005, Vasil'ev et al. 2001). Several approaches to overcome these problems and to enhance the transdermal drug delivery are summarized in Table 2.1.

Approaches to increase the drug permeation across the skin to achieve and maintain therapeutic concentration of drug in blood can be expressed as: chemical, biological and physical approaches. Chemical enhancers such as sorption promoters or biological enhancement studies such as synthesis of bio-convertible pro-drugs have been found to increase transdermal drug transport via several mechanisms, including increased drug partitioning into the *stratum corneum*, fluidization of the lipid bilayers, and disruption of the intracellular proteins. Even though chemical enhancers have the potential to alter the properties of skin, many of them are irritants, and safe and effective methods to be used in this field properly are still under development (Sebastiani et al. 2005). In case of prodrugs, enhancement can be accomplished due to enzymatic activity in the epidermis; however, high prodrug concentration in the skin can lead to enzyme saturation, which hinders the conversion of the prodrug into an active drug molecule.

Physical approach mainly includes sonophoresis (phonophoresis), iontophoresis and electroporation techniques. Sonophoresis is the application of ultrasound (Mitragotri et al. 1995) whereas iontophoresis and electroporation refer to "low-voltage" and "high voltage" treatments, respectively (Pachagnula 1997). Iontophoresis acts primarily on the drug by variable applications while electroporation acts on the

lipid bilayer of the skin and creates transient aqueous pathways by short high-voltage pulses (Banga et al. 1999).

Table 2.1. Methods to enhance transdermal permeability of macromolecular drugs.

Method	**Mode of Action**
Chemical enhancers	Compromisation of the tightly structured *stratum corneum* lipid bilayers
Lipid vesicles	Cumulation of drugs in the *stratum corneum*
Iontophoresis	Low current/voltage electrostatic repulsion, electroosmosis
Low-frequency ultrasound	Local thermal effect, weakened bilayers of the *stratum corneum* by cavitation
Electroporation	High voltage short term electrical pulses
(Micro)needles	Transient holes in the skin
Pressurised He-gas	Invasive "gene-guns"

There are also several attempts such as creating a synergistic effect on transdermal drug delivery by a combined approach. The use of iontophoresis with a chemical enhancer is proposed to achieve higher drug penetration, whereas it may also reduce the side-effects such as irritation caused by high concentration of enhancers or stronger electric forces. Combination of iontophoresis and electroporation is suggested for further enhancement of drug transport since it may allow rapid delivery of a bolus dose with a precise control of drug delivery modulation and programmability. Synergy between low-frequency ultrasound and iontophoresis has been found to increase the transdermal drug transport to a greater degree. On the other hand, as reported, the combination of microneedles and iontophoresis may offer the possibility of macromolecule transdermal delivery with precise electronic control (Wang et al. 2005, Pachagnula et al. 2000, Sebastiani et al. 2005). Iontophoresis applications in conjunction with ion-exchange materials has also provided promising improvements on transdermal drug transport (Jaskari et al. 2000).

The novel approaches in transdermal drug delivery are obviously built around iontophoresis showing that iontophoresis could be the answer for the effective transdermal drug delivery, especially for the novel biotechnologically developed drugs such as peptides and proteins that are hydrophillic, charged macromolecules and susceptible to proteolysis, chemical change and denaturation (Banga et al. 1999, Tabata and Ikada 1998).

2.2.1.2. Iontophoresis

Iontophoresis is a transport phenomenon, and it stems from the movements of ions in solution due to an applied electric field across two electrodes. Iontophoretic drug delivery implies the use of small amounts of physiologically acceptable electric current across a membrane to drive charged molecules into the body. By using an electrode of the same polarity as the charge of the drug, the drug is driven into the skin by electrostatic repulsion (Stamatialis et al. 2002) as illustrated in Figure 2.3 below. The electric field applied results in an electric current, which is transformed into an ionic current at the electrode/liquid or electrode/skin interface. This ionic current carries the drug ions into the skin while the counter-ions that are more mobile complete the circuit (Coston and Li 2001).

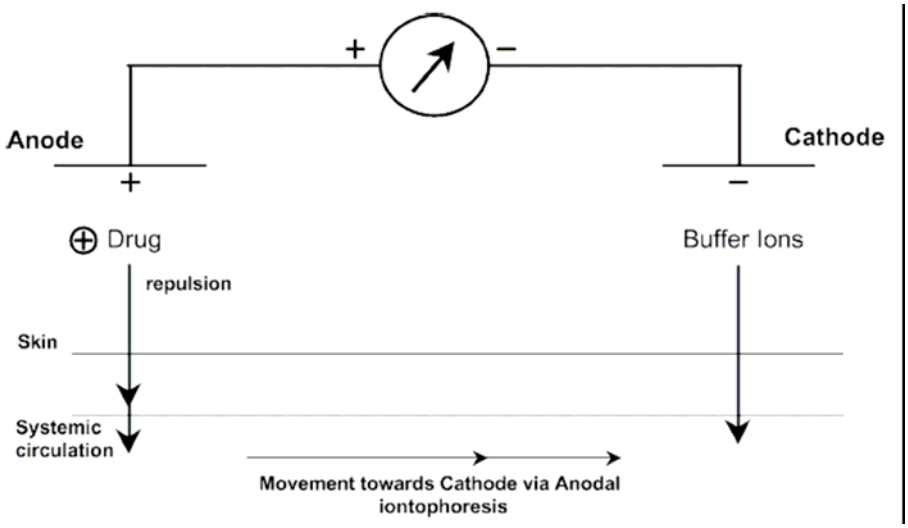

Figure 2.3. Diagram of iontophoretic technique: as current is applied, drug cations are repelled into the skin and absorbed in the systemic circulation
(Source: Wang et al. 2005).

In addition, bulk fluid flow or volume flow occurs in the same direction as the flow of counter-ions. This phenomenon, which accompanies the electrostatic repulsion, is called electro-osmosis. By the contribution of electroosmosis and increased passive permeation (increased permeability of the skin) by the applied potential difference across the skin, the transport rate of uncharged and zwitterionic molecules is also increased (Sebastiani et al. 2005).

Numerous attempts have been made to define the rate of iontophoretic flow. The rate equation would include flux due to electrochemical potential gradient across the skin, change in the skin permeability due to applied electric field and the electro-osmotic flow. The general rate equation including these flux terms is given as:

$$J^{ionto} = J^{electric} + J^{passive} + J^{convective} \tag{2.1}$$

$J^{electric}$ is the flux due to electric current application; $J^{passive}$ is the flux due to passive delivery through skin and $J^{convective}$ is the flux due to convective transport due to electroosmosis (Singh et al. 1994).

There are several factors affecting the results of iontophoresis. These include the physico-chemical properties of the drug (molecular size, charge, hydrophobicity, concentration), drug formulation (type of the system, buffer, pH, viscosity, presence of other ions), equipment used (available current range, constant vs. pulsed current, type of electrode), biological variations (skin site, regional blood flow, age, sex), skin temperature and duration of iontophoresis (WEB_1 2003).

The skin surface's isoelectric point (IEP) ranges from 3 to 4, which is about the isoelectric point of keratin in the stratum corneum layer. Therefore, for a drug donor solution with a pH value higher than the IEP of the skin surface, skin is a negatively charged membrane, and hence the electroosmotic flow may enhance the delivery of positively charged drug permeation across the skin. In this point of view, the anodic delivery is facilitated, whereas the cathodic delivery is retarded by the electroosmotic flow, in addition to being a major mode of transport for neutral molecules (Panchangnula et al. 2000). However, it was reported that electro-repulsion constitutes the dominant mechanism for the transdermal iontophoresis of the ionic smaller solutes, whereas electroosmosis becomes more important in the transport of larger ions such as proteins as shown by the study of Guy et al. (2000). These findings suggest that the charge of the skin rather than the charge of the permeant may be the predominant

transport mechanism depending on the physicochemical properties of the drug. This dictates that the iontophoretic delivery regimes can be manipulated by changing the pH of the formulation (Panchangnula et al. 2000).

Over the years a wide range of protein and peptides such as tyrotropin-releasing hormone (Huang et al. 1996), vasopressin (Banga et al. 1995), calcitonin (Chang et al. 2003), LHRH (Luteinizing Hormone Releasing Hormone) (Raiman et al. 2004) and human parathyroid hormone (Medi et al. 2003). These studies approved that iontophoresis not only achieves enhanced transdermal drug transport but the lag time required for the delivery is also reduced.

Consequently, iontophoresis provides a means of local, non-invasive, painless drug administration when compared with the traditional administration. Importantly, iontophoresis can be used to deliver peptides and protein drugs not suitable for oral administration (Green et al. 1992). The technique has been observed to enhance the transdermal permeation of varying types of drugs several fold and this shows that iontophoresis is promising to make a lasting impact in drug delivery. Most importantly, this method also offers the possibility of an individualized dose titration by modulation of the current density. The adjustable and pre-programmable drug delivery is the unique opportunity of the iontophoresis and parallel developments in the fields of bioengineering and microelectronics support the improvements on the iontophoretic technique. This is specifically important for some therapies such as Parkinson's disease since an individual dose arrangement is required to obtain an optimum therapy with the minimum side effects (Nugroho et al. 2005).

2.2.2. Polymeric Systems in Transdermal Drug Delivery

The earliest drug delivery systems, first introduced in 1970s, were based on polymers. Today, polymeric materials still provide the most important material of choice for research, primarily because of the ease of processing and control over their chemical and physical properties. The polymeric controlled delivery systems are being applied for a wide range of drugs in various environments. These systems can be formulated as hydrogels, films, membranes, matrices or tablets. Such polymeric systems usually contain a base polymer, a plasticizer to provide a suitable degree of flexibility and an excipient. The excipients are water-soluble materials that, as they leave the

matrix, create channels in the polymeric material and hence facilitate the diffusion of the drug. The choice of the prepared polymeric materials suitable for delivery systems characterized by several factors as biocompatibility, environmental stability during the time of complete drug delivery, appropriate mechanical and thermal properties, appreciable swelling characteristics, ease of fabrication and cost (Kumar M. and Kumar N. 2001).

Controlled release of active agents from a polymeric delivery system can be tailored by three primary mechanisms: diffusion, degradation and swelling followed by diffusion. These mechanisms can stand alone or all may exist in a given release system. Polymer structure is the key parameter for the diffusion through polymers, whereas the macromolecular structure is effective on diffusion as it influences the rate of partitioning into the medium. On macroscopic scale the diffusion can occur through the pores in the polymer membrane/matrix, and on molecular level, by passage of the drug molecules between polymer chains. In case of transdermal drug delivery, there exists additional series of diffusional and active transport steps after the penetration of the drug through the skin (Brannon-Peppas 1997).

In transdermal drug delivery systems, skin is utilized for the delivery of a drug via polymeric patches and the drug release from these patches can be controlled by two mechanisms: membrane permeation controlled and matrix diffusion controlled systems (Jain et al. 2003). Vasil'ev et al. (2001) claimed that these two systems do not differ in principal on the drug delivery, both capable of achieving the effective plasma concentration for a prolonged period of time.

Matrix and membrane systems may be developed as various combinations of hydrophilic and lipophilic polymers, whether natural or synthetic.

The membrane system mainly consists of a reservoir where the drug is loaded, a membrane that does not contain any drug but serves to control the rate of release of the drug from the reservoir. Other components of the system are a drug-impermeable cover film (mechanically fastening the whole system and preventing the drug from diffusing in undesired directions and from loss on storage) and a pressure sensitive biocompatible adhesive for mounting the patch on the skin (Figure 2.4).

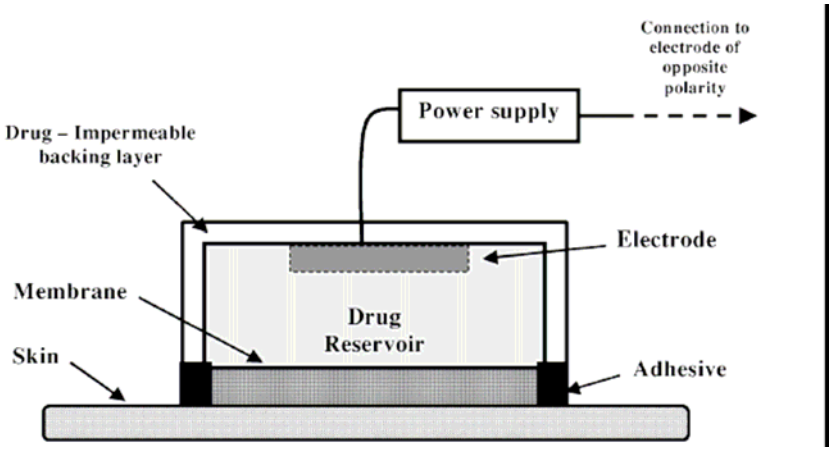

Figure 2.4. Schematic illustration of a iontophoretic transdermal delivery patch composed of a membrane/reservoir system (Source: Stamatialis et al. 2002).

In the membrane type systems, reservoir is employed to supply the drugs, dissolved or dispersed in liquid phase (solvent) or entrapped in a gel and the drugs diffuses from this phase through the control membrane. Most drugs exist in stable protonated form, nitreous bases, which exhibit poor permeation profiles through nonpolar epidermis. Therefore, drugs are prepared in nonprotonated liquid form or unstable solid state. Silicon oils and minerals, that are capable of dissolving drugs, have been used to fill the reservoir or gels containing the drugs have been used as reservoirs (Vasil'ev et al. 2001). In addition to this, to maintain a constant driving force for the mass transfer, drug is loaded to the reservoir over its saturation concentration.

Hydrogels that are highly swollen, hydrophilic polymer networks have found various applications in biomedical applications. Several systems such as resin gels have been used as reservoirs and recently, cross-linked poly(ethylene glycol) (PEG) networks are evolved as reservoirs for delivery of proteins via transdermal route. Thacharodi and Rao (1995) reported permeation controlled transdermal drug delivery systems using chitosan. Studies on propanolol chloride delivery systems using various chitosan membranes with different cross-link densities as drug release-controlling membranes and chitosan gel as the drug reservoir was performed. In vitro released profiles showed that devices constructed with chitosan membranes released propanolol chloride in a reliable and reproducible manner, and the minimum release was observed at the maximum crosslinking density (Thacharodi and Rao 1995). In another study of Thacharodi and Rao, indicated the use of collagen-chitosan composite membranes as

membrane-permeation-controlled transdermal devices for the release of propranolol and nifedipine. Jain et al. (2003) has also used the system of glutaraldehyde crosslinked chitosan membranes for the release-rate control and chitosan gels for drug reservoir for transdermal delivery of diltiazem hydrochloride, which resulted in zero-order kinetics for the drug release. On the other hand, several commercial membranes with various properties have been attempted.

Membrane is the crucial component of the drug delivery patch as it in direct contact with the skin and acts as the interface between the drug reservoir and the skin to give optimal control for the transdermal drug delivery (Stamatialis et al. 2002). In addition to the factors in the choice of polymers for the drug delivery systems and specific to transdermal applications, the membrane should be biocompatible to prevent skin irritation, it should have the control over the drug release (with lower drug permeability than skin) and it should have low drug adsorption. In case of iontophoresis applications membranes with low electrical resistance is also required for better utilization of the power source.

For a transdermal patch, the total permeability of a drug through the membrane + skin is expressed as (Flynn et al. 1974):

$$\frac{1}{P_{total}} = \frac{1}{P_{memb}} + \frac{1}{P_{skin}} \tag{2.2}$$

where P_{memb} and P_{skin} represents the permeability of the drug through the membrane and skin, respectively. The drug delivery is considered as membrane-rate controlled when P_{memb} / P_{skin} ratio is less than 0.2, and as skin-rate controlled when this ratio is larger than 5. Between these values, the delivery rate is controlled by both skin and membrane (Baker and Kochinke 1989).

Drug flow through the membrane following zero-order kinetics is given by (Barker 1987);

$$J = \frac{\varepsilon D}{\gamma} \cdot \frac{C_s}{L} \tag{2.3}$$

where J [mg/(cm^2.s)] is the drug flow through the membrane, ε is the membrane constant (i.e., the ratio of the pore volume to the membrane volume), D [cm^2/s] is the coefficient of drug diffusion through the pores, γ is the pore form factor (i.e., the ratio

of the molecular path length in the pores to the membrane thickness, C_s [mg/cm^3] is the saturated drug solution concentration in the reservoir and L [cm] is the membrane thickness. Drug release from the membrane is assumed to be constant since C_s is constant until the overload is exhausted (zero-order kinetics) while it is provided the membrane properties remain unchanged during the transdermal system functioning.

For a continuous membrane, the drug release from the transdermal system is described by Fick's Law

$$J = \frac{KD\Delta C}{L} = PC_s \tag{2.4}$$

where J is the transdermal drug supply rate, K is the coefficient of drug distribution between the system and the membrane, D is the coefficient of drug diffusion in the matrix, ΔC is the gradient of the drug concentration between the system and blood, L is the epidermis thickness, C_s is the saturated drug solution concentration in the reservoir and P is the permeability of the membrane.

The matrix systems offer a simplified case for the design of transdermal therapeutic systems. In matrix systems, the drugs are dissolved and dispersed in material of the system so that an appropriate matrix diffusion profile determining the delivery rate of the drug molecules from the system is handled (Conaghey et al. 1998). The maximum drug diffusion (release) time depends on the matrix/membrane thickness, drug concentration, and the skin permeability for the given drug. These facts reveal that transdermal systems can be controlled by changing the matrix/membrane thickness and composition (drug concentration and limiting solubility), whereas manipulation can be handled by implying structural changes during the preparation of these materials.

For the matrix type systems with assumed overload, the flow rate J [μg/(cm^2.s)] at a current time instant T is given by the Higushi equation:

$$J = \sqrt{\frac{M_0 DC_s}{2T}} \tag{2.5}$$

where M_0 is the initial drug content in the transdermal system. As can be evaluated from the system, these systems do not obey stationary kinetics.

Transdermal patches comprising matrices of PEG/Vaseline oil and PEG/Poly(vinyl alcohol) (PVA), commercialized with the name 'Percutens', carrying

various drugs has been exploited (Vasil'ev et al. 2001). Nicotin loaded cross-linked ion-exchange resins for both passive and iontophoretically assisted transdermal delivery systems (Conaghey et al. 1998), polyacrylamide and *p*-HEMA hydrogels for the transdermal release of protein/peptide drugs (Banga and Chien 1993) were attempted. There are several studies representing the ongoing research on this area such as matrices of Eudragit L(or E)-100/PVP and Eudragit L(or E)-100/PEG for diltiazem hydrochloride (Jain et al. 2003). In this study, diltiazem release was higher at the higher contribution of the hydrophilic polymers. Fractional dissolution of hydrophilic polymers in the matrix led to formation of gelaneous pores, which decreased the mean diffusional path length of the drug molecules to release into the diffusion medium. It has been reported that the simplest type of matrix patches contains a drug dissolved in an adhesive that is applied to an impermeable backing membrane. The reported studies include salicylic acid and chlorpheniramine maleate dissolved in a polymethacrylate amino ester copolymer matrix, lidocane and ketoprofen in acrylic/rubber (polyisobutylene) copolymers (Vasil'ev et al. 2001).

Studies performed up to date show that hydrophilic matrices and membranes are more effective than hydrophobic ones in transdermal drug delivery systems. Hydrophilic matrices are also preferred for iontophoresis applications since hydration of the system is crucial for this application to allow the passage of the ions. The use of water-soluble polyelectrolytes as constituents of the hydrogel matrix in the formation of iontophoretic patches have been signified in the light of these findings (Kupperblatt et al. 1999). Electro-responsive or electrically stimulated pH sensitive polyelectrolyte membranes and hydrogels such as chondroitin 4-sulphate hydrogels (Jensen 2002), PMMA polyelectrolyte membrane (Grimshaw 1990) have been suggested to be promising for the iontophoretic delivery of large charged macromolecules such as proteins and peptides (Kost and Langer 2001). Such polyelectrolyte membranes may enhance the iontophoretic drug delivery by several mechanism such as enhanced membrane permeability due to electrically and chemically induced swelling, electrostatic partioning of the charged solutes into the membrane, electroosmotic augmentation of solute flux within the membrane or electrophoretic augmentation of solute flux within the membrane (Grimshaw et al. 1989).

2.3. Polyelectrolyte Complexes (PEC)

2.3.1. General Aspects

Macromolecular complexation of different polymers are formed by various intermolecular interactions, such as hydrogen bonding, Coulomb forces, Van der Waals forces, transfer forces, and hydrophobic forces. According to the nature of the dominating interactions, the complexes are named as polyelectrolyte complexes (sometimes called coacervate complexes), hydrogen-bonding complexes or charge-transfer complexes (Peniche et al. 2003, Dumitriu and Chornet 1998). In case of polyelectrolyte complexes, electrostatic interactions play the major role in determining the mixed polymer behaviour. Secondary binding forces such as hydrogen bonding or covalent bonding may also participate in the formation.

Polyelectrolytes are macromolecules carrying a relatively large number of functional groups that either are charged, or under suitable conditions can become charged. The molecules can exist as polyanions or cations, since the net charge of the macromolecules depends on the functional groups, which may be either positively or negatively charged, or both (Şimşek-Ege et al. 2002). One of the most interesting features of polyelectrolytes is their ability to form stable complexes as a result of ionic interactions. Therefore, Coulumbic interactions between polyelectrolytes may be either repulsive or attractive depending on whether the electrical charges are of the same or opposite sign. On the other hand, the interactions may be either short-ranged (weak) or long-ranged (strong) depending on the degree of ionization and the polyelectrolyte concentration. Therefore, the overall electrostatic interactions, which depends on the physicochemical character (e.g. charge density and molar mass), concentration and ratio of the polymers, is very sensitive to variations in pH and ionic strength of the complexation medium. Furthermore, temperature, shear and pressure can affect the formation and stability of the complexes (Dickinson 1998, Weinbreck et al. 2003a).

Complexation between two oppositely charged polyelectrolyte can lead to:

- Precipitation (insoluble solid phase)
    - Driven by charge neutralization on hydrophobic polymers
    - Driven by macro-aggregate formation
- Coacervate formation (dense liquid phase)
- Soluble Complexes

The formation of complexes occurs by a step-wise process. Initially, a primary complex is formed with respect to Coulumbic interactions. Second step implies the formation of new bonds and/or correction or the distortion of the polymer chains resulting in a new conformation of the complex. Finally, secondary complexes aggregate mainly due to hydrophobic interactions at the third stage (Figure 2.5).

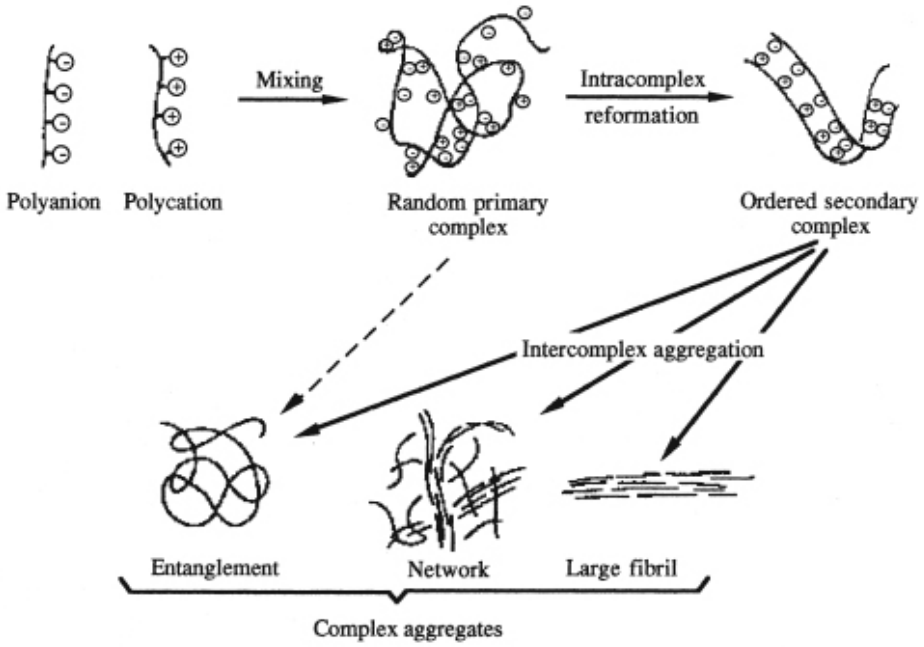

Figure 2.5. Schematic presentation of the aggregation of the PECs
(Source: Kokufuta et al. 1979).

Most pronounced secondary complex conformations are ladder or scrambled egg models. The resulting structures of polyelectrolyte complexes are explained by two models, ladder and scrambled egg, in the literature. “Ladder-like structure” refers to complex formation on a molecular level via conformational adaptation, whereas the “scrambled egg model” denotes the incorporation of high number of chains into a particle. PEC formation between polyions with weak ionic groups may lead to soluble complexes with a ladder-like structure. However, in most applications of PEC formation results in highly aggregated systems obeying the scrambled egg model (Dautzenberg 2000). On the other hand, in highly diluted solutions quasi-soluble particles on the colloid level are formed.

Polyelectrolyte complex formation is widely used for the preparation of membranes, gels, films, etc., with special properties, microencapsulation of biological components, isolation and fractionation of proteins, enzyme immobilization, and controlled delivery, but also as carriers for proteins and nucleic acids, supports for catalysts, implants for medical use and food ingredients (Dautzenberg 2000, Schmitt et al. 1999). The use of natural and/or synthetic polyelectrolytes as building blocks, preparation techniques and the resulting properties of the complexes characterize the potential end uses of these systems.

Complex formation between synthetic polyelectrolytes such as poly(sodium styrene sulfonate) and polyvinylbenzyl trimethylammonium chloride have been studied extensively. The membranes produced by the specified PEC system have been found promising for desalination of seawater, dialysis, ultra-filtration and purification of aqueous solutions containing colloids, micro- and macroparticles. There are numerous synthetic polyions and polycations employed to polyelectrolyte complexation.

Recently, the use of natural polymers in polyelectrolyte complexes for encapsulation of drugs, proteins and viable cells, and stimuli responsive systems has received much attention because of their biocompatibility. There are any kinds of natural polyelectrolytes such as proteins and polysaccharides to be used for complexation. Polysaccharides are natural polyelectrolytes whether anionic or cationic and proteins are polyampholytes (polymers containing both positively and negatively charged segments).

Chitosan, a biocompatible and biodegradable polysaccharide, has been utilized in several studies as polycationic partner in PEC formation. Chitosan based PEC with natural polymers such as sodium alginate, κ-carrageenan, heparin, pectin, xanthan or synthetic polymers such as poly(acrylic acid), polystyrene sulfonate have been reported. Chitosan-sodium alginate membranes were proposed for wound-dressing material with respect to its noncytotoxicity, capability of supporting cell proliferation and pH-dependent water uptake, whereas chitosan-xanthan complexes as reported to be an appropriate drug delivery vehicle with enhanced swelling characteristics.

Protein-protein interactions were also investigated in terms of polyelectrolyte complexation. Macromolecular interactions between oppositely charged proteins led to enhanced functional properties of including foaming, aggregation phenomena and gelation. The parameters effective through enhancement were reported to be concentration of each protein in the mixture, pH and ionic strength of the solution. The

complexation systems of proteins with synthetic polyelectrolytes such as heparin/PVA were also studied.

Protein-polysaccharide complexation, which is also called complex coacervation, has suggested as a special case of polyelectrolyte complex formation and it is evidenced by coacervate formation. Besides their biotechnological and biomedical utilization, the detailed information and the structure of the complex coacervates can also be helpful to understand the mechanisms of complex biological processes as the formation of polymeric complexes of proteins and polysaccharides simulate the intermolecular interactions during the formation of biological systems. For this reason, proteins and polysachharides complexes can be used in products that are directly contact with the living organism with the less allergic risks compared with synthetic polymers since they are of biological origin (Schmitt et al. 1998). Additionally, certain properties of protein/polysaccharide coacervates were found to be better than those of the pure protein and pure polysaccharide (Schmitt et al. 2000), and their complexation has been found very promising as constituents of biomaterials with respect to enhanced physicochemical properties, film-forming capability and environmental stability. However, further work on these complexes is required to make up the global characterization of the formation, stability, structure and techno-functional properties of these complexes.

2.3.2 Protein-Polysaccharide Complexation

Protein-polysaccharide interactions have been investigated widely with respect to its promising applications in biotechnological and biomedical areas as well as its biological aspects. In living organisms, proteins and polysaccharides can be naturally associated to maintain cell integrity in the formation of membranes, and participate in cell division through histone/DNA complexes or enzyme catalysis, whereas they can be incompatible as they involve in cell partition.

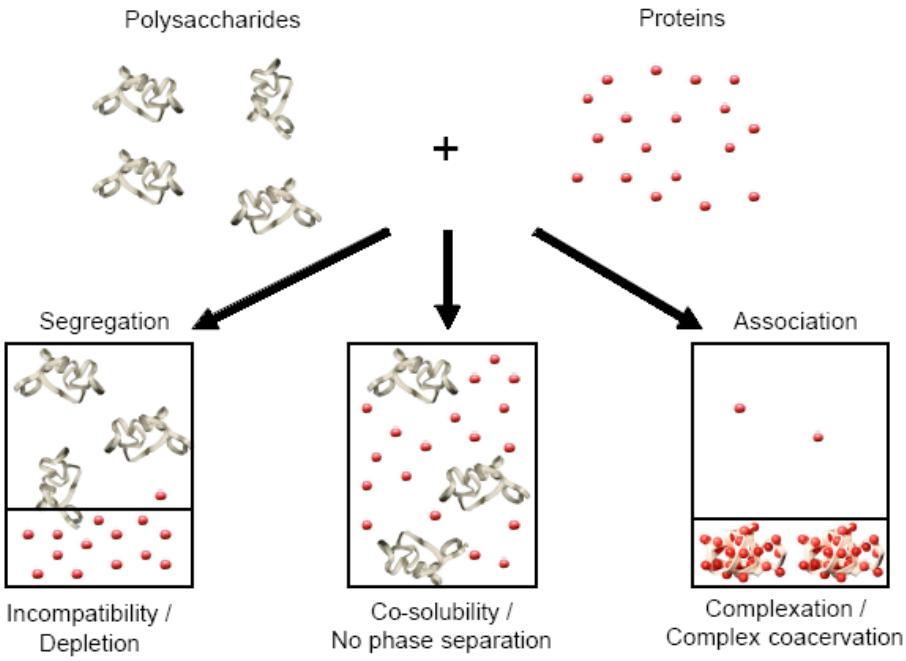

Figure 2.6. Main trends in the behavior of protein/polysaccharide mixtures (Source: WEB_2 2005).

The mixtures of protein and polysaccharides generally lead to phase separation due to phase separation through thermodynamic incompatibility or complex coacervation (Turgeon et al. 2003) as illustrated in Figure 2.6. As the protein and polysaccharide are incompatible, they repel each other and a thermodynamic phase separation, which is also called segregation or depletion interaction, occurs. Phase separation results in a mixture with two phases, one is rich in protein and one is rich in polysaccharide. A diluted and non-reactive biopolymer mixture of proteins and polysaccharides may also exhibit co-solubility. On the other hand, if they attract each other through electrostatic interactions, the biopolymers associate excluding the solvent from their vicinity. This gives rise to the formation of protein/polysaccharide complexes. Associative phase separation of the mixture results in two phases: the lower phase containing the protein/polysaccharide complex and the upper phase containing mainly the solvent.

Coacervation describes the phase separation of a liquid polymer rich-phase from a macromolecular solution, representing the separation of two liquid phases in a colloidal system. The phase more concentrated in colloid component is the coacervate and the other phase is the equilibrium solution (de Kruif et al. 2004). In the mixture, electrostatically attracted and bound complexes can also be either soluble or insoluble.

The coacervate layer occurs as the insoluble complexes concentrate in liquid coacervate droplets followed by the further coalescence and phase separation (Figure 2.7).

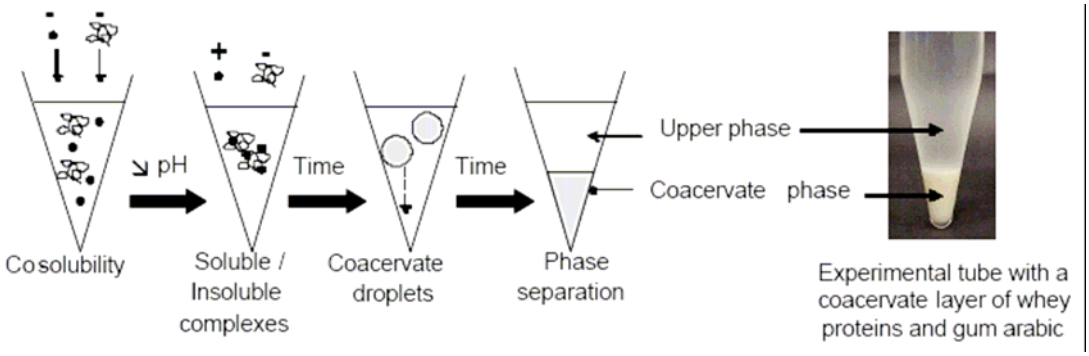

Figure 2.7. Schematic representation of phase separation by complex coacervation (Source: WEB_2 2005).

The complex coacervation was discovered by Tiebackx in 1911, and the term 'coacervate' was first introduced by Bungenberg de Jong (1949). Coacervate was derived from the Latin word "acervus" which means aggregation, and "co" means together. Thus, "coacervation" denotes the union of the colloidal particles. By colloidal particles, de Jong signified the liquid droplets, primarily induced by demixing (Figure 2.8). The word 'coacervate' was specifically preferred instead of precipitate to explain this phenomenon since the complex remains liquid, rather than forming a precipitation (de Kruif and Tuinier 2001). The detailed study of Bungenberg de Jong (1949) revealed under which conditions complex coacervation occurred, such as pH, ionic strength, polymer concentration, polymer ratio, and temperature. Simple coacervation was described in this study as the coacervation process involving only one biopolymer. It occurs by the excluding the solvent from a hydrophilic colloid by introducing a competing hydrophilic substance, such as salt or alcohol, to the solution medium. This is also called as 'salting out' and results in simple coacervation (Peniche et al. 2003).

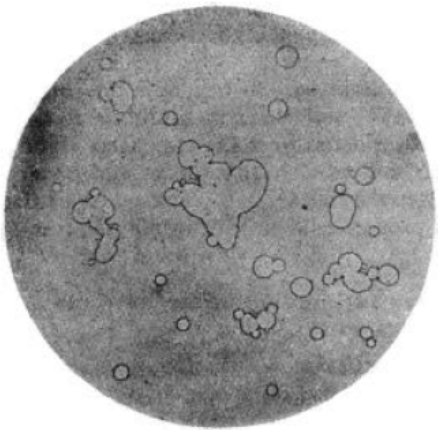

Figure 2.8. The coacervate droplets that have partially spread over the surface of the microslide and coaleasced with each other. This picture was reproduced from the study of de Jong and Kruyt (1929) (Source: WEB_2 2005).

The ternary system (two biopolymers and a solvent) of coacervation is characterized by a one- or two-phase equilibrium state. Complexation depends on biopolymer-biopolymer and biopolymer-solvent interaction forces (enthalpic effects), and dominantly on the size and structures of biopolymers (entropic effects) (Schmitt et al. 1999). Therefore, the formation of these biopolymer complexes governed by electrostatic interactions represents the key parameters of charge density, geometry (shape and flexibility of charge distribution), swelling, counterion hydrophilicity, and screening (Weinbreck et al. 2004) that explains the strong dependency on pH ad ionic strength of the medium.

The knowledge of protein/polysaccharide complexation inspires the researches to build biological systems on this phenomenon. For instance, DNA-gelatin nanoparticles formed by salt-induced complex coacervation of gelatin and plasmid DNA have been used for the development of a novel system for gene delivery. Besides the fundamental interest on biological phenomena, complex coacervation has been used in the fields of pharmaceuticals, medicine, foods, cosmetics, etc. Complexation has been studied in the purification and recovery of the macromolecules (e.g. protein) on the lab scale and offered several advantages such as high removal levels and more thermal stability through complexation. Microencapsulation based on the ability of the coacervates to form a coating around sensitive materials (e.g. drug particle or an oil droplet containing flavors) has been investigated extensively and commercialized.

Promising results on the gelatin/gum arabic microcapsules had led to extensive investigations on this system and have been proposed applications in the fields of pharmacy, cosmetics, carbonless copy paper production, biotechnology, and food ingredients. Addition to this system, milk protein/xanthan gum system was also suggested as a food ingredient, e.g. fat substitute and meat replacer (Chen et al. 1989).

The biodegradability of the complexes offers the use of the complexes as biopackaging or edible food packages based on the film formation properties of the complexes. It has been reported that the coacervate films of sodium caseinate/wheat or starch corn displayed good mechanical and gas barrier properties. On the other hand, polyelectrolyte films produced by the chitosan/alginate coacervates have represented good biocompatibility and found promising in biomedical applications. There have been several studies indicating the potential of protein/polysaccharide complexes as constituents in the production of biomaterials such as wound dressings, sutures, blood substitutes or artificial prostheses, grafts or vessels.

2.3.3. Models on Formation of Coacervate Systems

When the protein and polysachharide dispersions are mixed together at a pH and weight ratio where interactions are strong, they can form complexes. However, it has been reported that, it is a challenging work to follow the very fast initial events and to study the different structural transitions. To overcome this drawback, such mixtures are firstly prepared at a pH where no interactions take place, and then acidification is performed to focus the specific pH range to determine the potentiometric conditions where interactions occur. Upon lowering the pH, the interpolymeric complexes occur at a critical pH_c value. The critical pH value can be observed above isoelectric point (IEP) of protein due to heterogeneous charge distribution and/or randomly charged patches on the protein surface. The very first small variations in turbidimetric signals are attributed to this formation of soluble intrapolymeric complexes. Further decrease of the pH leads to coacervation at pH_ϕ. By analogy to the colloidal systems (Leisner and Imae 2003), at the critical pH_ϕ, the coacervates interact together to form a fully percolated system that phase separates from the solvent. The pH_ϕ is generally detected by a more or less ‘strong’ increase in system turbidity.

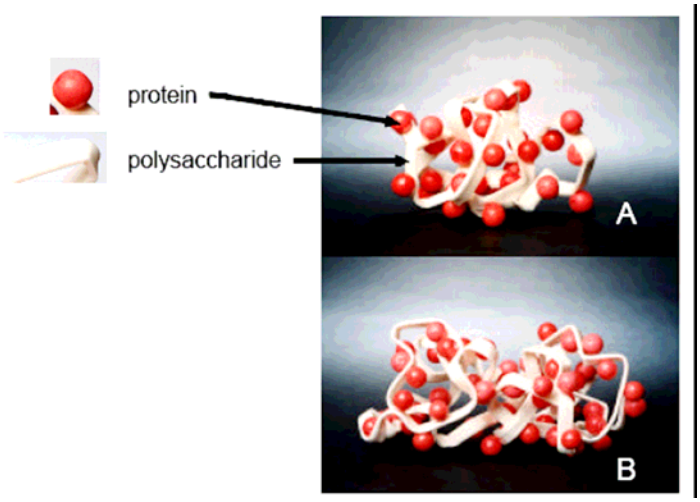

Figure 2.9. Intrapolymer (A) and interpolymer (B) complexes
(Source: de Kruif et al. 2004).

Consequently, for all systems studied, two major structural transitions in the mechanism of complexation have been observed. Thus, the process of complex formation was explained by 3-step formation of coacervates

1. intrapolymeric complexes at pH_c
2. Interpolymeric soluble and insoluble complexes
3. insoluble complexes and macroscopic phase separation at pH_ϕ (coacervation or precipitation)

There are only a few studies on the structure of the soluble complexes, coacervate droplets and coacervate phases that occur during the transitional formation of complexes. The recent light-scattering technique based study of Leisner and Imae has represented the structure of the complexes through the transitions of interpolymeric complexes to coacervates, for the first time. Proposed model, describing the subsequent associative micro- and macrophase separation, is schematically shown in Figure 2.10.

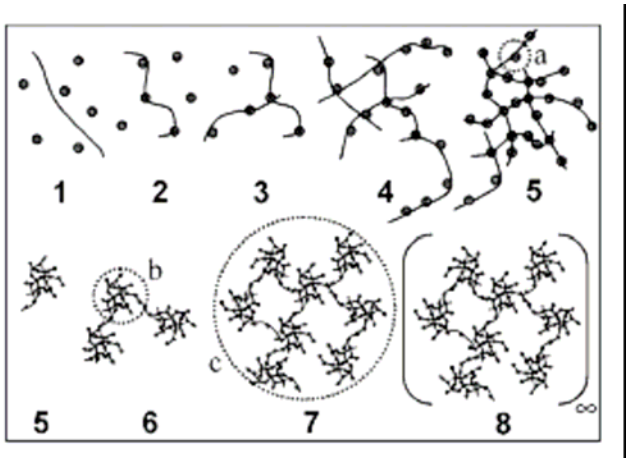

Figure 2.10. Schematically proposed model for coacervate formation for a protein/polysaccharide mixture (Source: Leisner and Imae 2003).

The model describes the coacervation mechanism with respect to protonation of the protein that occurs below its isoelectric point. Independent protein and polysaccharide (**1**) interact attractively to form transient 'monomolecular' interpolymeric complexes (**2**), which remains highly negatively charged but with positively charged patches localized at the side of the protein away from the chain. By this mean, the protein cation can form transient crosslinks between two polysaccharide chains and this formation constitutes the first step to multimolecular interpolymer complexes (**3**). This is followed by aggragation to microgels (**4**) that is limited by the net charge of the biopolymers. By further protonation of the protein almost neutral high molecular weight interpolymer complexes (**5**) with partially collapsing center is formed. As the critical size/charge ratio for attraction between microgels is reached, microgels stick together to form a microgel cluster (**6**). However, a complete collapsing is hindered due to overcharging or steric hinderence. After a time consuming swelling/deswelling process of the microgels for cooperative coupling, eventually, a hierarchically branched intramolecular structure (**7)** with the charge stabilization occurs. The equilibrium would be reached at a macroscopic phase separation to the coacervate (**8**) through coagulation of the stabilized microgel clusters (**7**), leaving an upper phase with only sporadically clustered microgels (**5**). As a consequence, coacervates are reported as randomly branched gels with a sponge-like morphology and compact and smooth microgel homogeneities larger than 20 nm.

Various physico-chemical parameters influence the electrostatic interactions between two biopolymers and thus the complex formation. For instance, pH plays a key role in the strength of electrostatic interaction as it determined the charge density of both polymers. Moreover, the ionic strength of the system has a significant effect on coacervation since it has been reported that addition of salt created screening of the interactions between two components. Table 2.2 chronologically represents the research on the formation of protein/polysaccharide systems based on these parameters by several experimental methods such as turbidimetric titration, dynamic and static light scattering, viscosimetry, etc.

Complex coacervation systems have been studied extensively through the investigations on complexation of the proteins with both polysachharides and synthetic polyelectrolytes. The work reported in this thesis focuses on the complex formation of protein/polysaccharide mixtures.

The trend nowadays, to replace the protein and polysaccharide components by other biopolymers to form complexes offering complexation mixtures that may result in novel properties and application areas. Among several biopolymers, silk fibroin, as a fibrous protein, and hyaluronic acid, as a widely used polysaccharide, has not been worked on with respect to coacervate complexation and the potential application of the material processed through complexation. The work reported in this thesis focuses on the complexation of silk fibroin ad hyaluronic acid and its potential applications in the fields of biotechnology and biomedicine. The following subsections represent the extensive information on these natural biopolymers.

Table 2.2. Factors studied for some protein/polysaccharide systems studied in literature.

REFERENCES	SYSTEMS	EXPERIMENTAL TECHNIQUES	PARAMETERS
Bungenberg de Jong 1949	Gelatin / GA	Light microscopy, Viscosity, Turbidity, Phase diagrams	pH, Pr:Ps*, Cp, ionic strength, types of ions
Burgess and Carless 1984	Gelatin / GA	Microelectrophoretic mobility	pH, Pr:Ps, pl of gelatin, ionic strength
Burgess and Carless 1985	Gelatin / Gelatin	Microelectrophoretic mobility, Preparation of gelatin microcapsules	pH, ionic strength, temperature, gelatine concentration, Pr:ps, time, drug content
Burgess and Carless 1986	Gelatin / Gelatin	Microelectrophoretic mobility Coacervate yield determination Photon correlation spectroscopy	pH, ionic strength, temperature, time, treatment of gelatin solutions
Burgess 1990	Gelatin / GA BSA / GA	Microelectrophoretic mobility Dry coacervate yield determination	pH, ionic strength, Cp, time
Burgess 1991	BSA / GA	Microelectrophoretic mobility Dry coacervate yield determination	pH, ionic strength, Cp
Burgess 1994	Gelatin / GA BSA / GA	Microcapsule production Particle size stability Scanning electron microscopy	pH, Pr:Ps, stirring speed, time
Girard et al. 2002	β-lg / Pectin (low- and high-methylated)	Potentiometric titrations Determination of the quantity of â-lg complexed to pectin (ultrafiltration)	Pr:Ps, pH, NaCl, urea, temperature
Girard et al., 2003	β-lg / Pectin (low- and high-methylated)	Isothermal titration calorimetry (binding constant, stoichiometry, enthalpy, entropy) Overlapping binding site model	Pr:Ps, time
Plashchina et al. 2001	Faba bean legumin / chitosan	Ultraviolet spectroscopy, Viscometry, Calorimetry, Turbidimetric titration, Surface tension, Emulsion stability	Pr:Ps, ionic strength, pH
Sanchez et al. 2002	β-lg / GA	Confocal laser microscopy, small angle static light scattering (SASLS), Time resolved SASLS, Turbidity	Time, Pr:Ps = 1:1 and 2:1
Schmitt et al. 2000	β-lg / GA	Confocal scanning laser microscopy, Diffusing wave spectroscopy	Pr:Ps, â-lg with or without aggregates, time, Cp = 1% or 5%, pH 4.2 or 4.5
Tuinier et al. 2002	Casein micelles / pectin	Dynamic light scattering Adsorption measurements Renneting experiments	Time, concentration in GDL, pectin concentration, percentage of renneting
Weinbreck et al. 2004	Whey Protein/ Gum Arabic	Small Angle X-Ray Scattering Turbidimetric titration	Pr:Ps, ionic strength, pH

*Pr:Ps denotes the protein/polysaccharide weight ratio in the biopolymer mixture.

2.3.3.1. Silk Fibroin

Silks are protein polymers that are biosynthesized by the epithelial cells within the glands of silkworms and spiders. Silk proteins are secreted into the lumens of these glands and then spun into fibers (Altman et al. 2003). The most abundant and extensively characterized silk is produced by the domestic silkworm *Bombyx mori*. Silk synthesized by *B. mori* consists of two kinds of protein, sericin and fibroin. Fibroin is the structural fibrous protein and constitutes 70% of the intact silk, and sericin is the water-soluble glue-like protein that surrounds and binds the fibroin fibers (Magoshi et al. 1996). Sericin can be easily removed from the silk fiber by a traditional degumming process (treatment of fibers with an alkali salt solution at ~100 °C), and hence silk fibroin is also called degummed silk (sericin-free silk fiber).

Silk has been commercially used as surgical sutures for decades and as a source of textile-grade fibers for centuries. The attractive properties stem from the physical chemistry of silk since this protein is made up of almost all fiber (Zhou et al. 2001). Recently, interest has been concentrating and dramatically increasing on the use of several processed forms of the solubilized silk fibroin in biotechnological materials and biomedical applications. On the other hand, fibroin is widely used in cosmetics and also suggested as a pharmacological agent or as a food additive. Silk fibroin contains about 6% essential amino acid and in addition to this, it lowers the blood glucose level with respect to its alanine content and enhances the alcohol metabolism of the liver with respect to its glycine content (Lue et al. 1993).

A fibroin molecule is composed of a heavy chain and a light chain connected by a disulfide linkage. The larger heavy chain having a molecular mass of ~350 kDa is composed of 12 repetitive domains that constitutes crystalline ordered clusters of oligopeptides Gly-Ala-Gly-Ala-Gly-Ser, $[Gly\text{-}Ala]_n$-Gly-Tyr and $[Gly\text{-}Val]_n$-Gly-Ala (n = 1-8). These domains are separated by 11 amorphous regions in which peptides are mainly in the sequence of Gly-Ala-Gly-Ser and Gly-Ala-Gly-Ala-Gly-Ser (Hossain et al. 2003, Yamada et al. 2001). It is mostly reported that the primary structure of silk fibroin is characterized by the crystallizable repeating sequence of six amino acidic residues $(Gly\text{-}Ala\text{-}Gly\text{-}Ala\text{-}Gly\text{-}Ser)_n$ since this simple and regular unit forms ~70% of the amino acid sequence. The heavy chain of the silk fibroin comprises mostly hydrophobic amino acid residues, whereas the hydroxyl residues of Ser and Tyr along

the chain provide affinity to water. The charged amino acid residues, glutamic acid (Glu) and aspartic acid (Asp), that reside in two chain ends and in the amorphous region illustrate the polyelectrolyte nature of the heavy chain. Light chain of the fibroin with a molecular mass of ~25 kDa has a non-repetitive sequence including higher contents of charged amino acids, and it is hydrophilic in nature. However, the light chain has a minor contribution in the fiber characteristics (Hossain et al. 2003, Zhou et al. 2001).

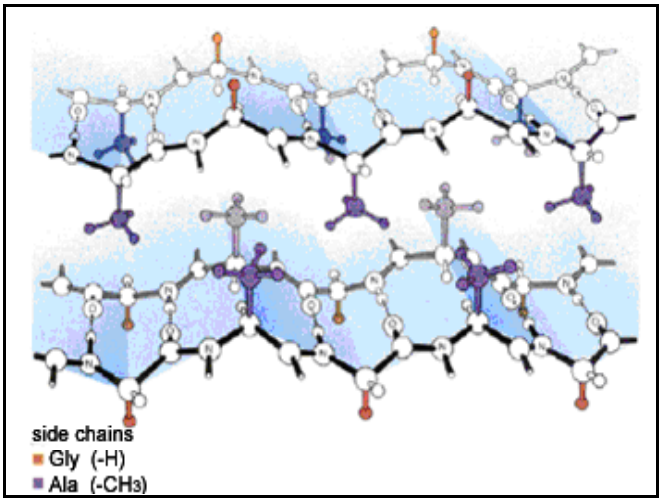

Figure 2.11. Secondary structure of SF
(Source: WEB_3 2005).

The major secondary structures of silk fibroin are described as two different conformations: silk I (α-helix, random coil) and silk II (β-sheet). Silk I is the water-soluble structure of fibroin that mimics its liquid structure in the silkworm glands. Silk II is the well-oriented anti-parallel β-sheet conformation of the water-insoluble spun fibers as shown in Figure 2.11. In this conformation, the polypeptide chains are aligned and adjacent chains are connected with hydrogen bonds (>C=O···HN<) (Yamada et al. 2003). The lately reported silk III structure of fibroin represents its surfactant behaviour and builds at the water-air interface in thin films (Valuzzi et al. 1999).

Numerous researchers have reported that the conformational change, from silk I to silk II, during the fiber spinning of the silkworm is induced as a result of the applied shear and elongation stresses. The silk fibroin fibers with β-sheet confirmation establish sufficiently strong intermolecular hydrogen-bonding, which prevents the separation of molecules, and hence their dissolution to pure water. However, the fibers are easily redissolve in water with very concentrated neutral salt solutions (LiBr, LiSCN, $CaCl_2$)

without inducing hydrolytic degradation (Tsukada et al. 1994). By the contribution of high concentration of ions, intermolecular interactions are screened and a pathway for dissolution is created. Following dialysis after the dissolution provides the preparation of the salt-free fibroin solution.

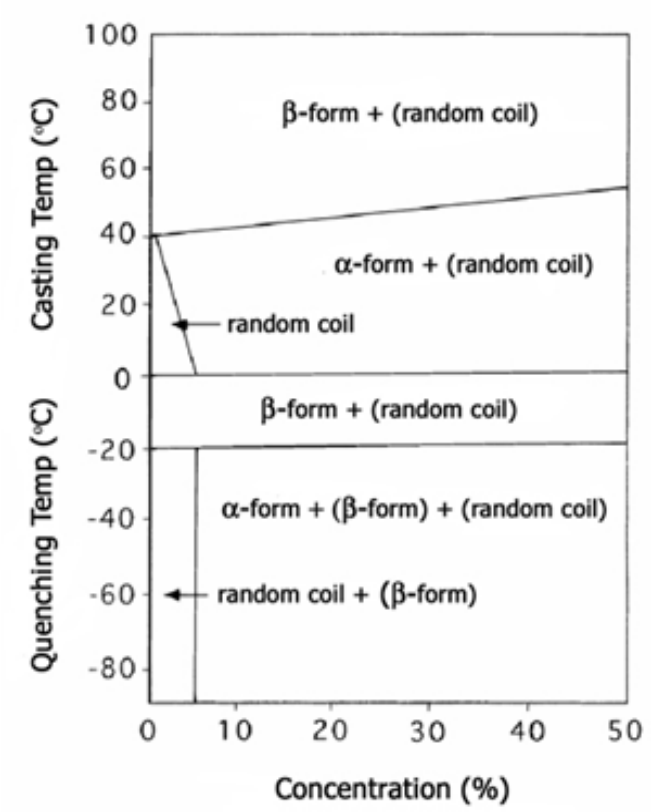

Figure 2.12. The relation between conformation, quenching or casting temperature and concentration of silk fibroin

(Source: Magoshi et al. 2000).

Aqueous fibroin solution, which is also called regenerated silk fibroin (RSF), is environment-friendly and used in various applications. RSF is of interest as it represents a good starting material for the preparation of different forms of materials by the application of various processing techniques. Furthermore, the easily controlled characteristics of the end product by changing the processing conditions or by applying post-processing treatments represent the reason of this interest. The silk I structure is metastable and easily changes to the silk II, and therefore the solubility and the mechanical charateristics of fibroin-based materials can be controlled by utilizing the conformational change of fibroin. Adjustable processing conditions can be summarized

as solution concentration, solution temperature, quenching temperature, drying temperature, drying time, presence of an electric field, pH and presence of certain enzyme (Putthanarat et al. 2002). Figure 2.12 shows the change of the conformation of the casted aqueous silk fibroin samples by quenching or casting temperature and the concentration of silk fibroin (Magoshi et al. 2000). Furthermore, the influences of initial protein concentration, temperature and pH have been previously designated with respect to high hydrogelation tendency of aqueous SF solutions. This brings a material option for preparation of biomaterials in the form of hydrogels. In aqueous solution at neutral pH, dissolved fibroin takes the random coil structure (Nemoto et al. 1999). It has been reported that the random coil to silk I transformation occurs at pH > 6 as the negative charges provide a strong repulsive component to protein-protein interactions. As the pH is lowered, this repulsion decreases and allows a closer approach of neighboring molecules. This increases the potential for the formation of a β-sheet structure through hydrophobic interactions with a simultaneous increase in viscosity of the solution (Hossain et al. 2003). At the pH values closer to the isoelectric point (IEP) (IEP = 3.8-3.9) of fibroin, especially pH < 4.5, transition from random coil to silk II occurs, and concurrently, gelation of the silk fibroin molecules accelerates. Such an observation can be interpreted as a typical behaviour of proteins that aggregate near their isoelectric points (Kim et al. 2004). The gelation time of fibroin decreases with increasing the initial concentration of fibroin and temperature, and gelation is reversible, if its exposure to acidic conditions is brief. Otherwise, gelation is irreversible since the hydrogen bonds are too strong to be broken at mild conditions (Terry et al. 2004, Kang et al. 2000).

If the end product is a fibroin-based film, casting surfaces are also stated to be effective. It was reported that casting onto different surfaces such as polyethylene, glass, polystyrene, platinum wire may influence the conformation. As the fibroin-based material is processed, numerous reports notice the possibility of further treatments on the material to improve its collective properties. The widely applied post-processing treatments are stretching, heating and immersion in hydrophilic polar solvents (e.g. methanol). Rate and ratio of stretching, heating temperature, concentration of the solvent and their application time are used to control the molecular conformation, and hence the properties of the resulting fibroin-based material such as solubility and morphology (Putthanarat et al. 2002, Nam et al. 2000).

Among the possible processed forms of the silk fibroin, there has been a growing interest in fibroin films and membranes within the last few decades. Silk fibroin has good film-forming capability, and amorphous, water-soluble silk fibroin films casted from aqueous regenerated fibroin solution can be made insoluble by means of simple physicochemical treatments as they undergo transitions from random coil to β-structure. The insoluble silk fibroin films are soft and flexible in wet state and it was suggested that water in the films serves as a plasticizer (Minoura 1996). However, these films suffer from poor tensile strength in dry state, in non-aqueous environments or on exposure to ambient air, and hence, they are very brittle and unsuitable materials for practical use. Therefore, the physical properties of silk films require improvement by physical or chemical modification. Several studies highlighted that the collective properties of these films can be improved by polymer blending as an effective and economical technique. Silk blends have been extensively studied as binary systems with respect to film formation by many researchers. Blends with synthetic polymers such as poly(ethylene oxide) (Jin et al. 2004), polyacrylamide (Freddi et al. 1999), poly(vinyl alcohol) (Tsukada et al. 1994, Yamaura et al. 1990) , poly(ethylene glycol) (Gotoh et al. 1997), polyallylamine (Arai et al. 2002) or with natural polymers such as chitosan (Rujiravanit et al. 2003, Park et al. 1999, Chen et al. 1997), cellulose (Freddi et al. 1995), sodium alginate (Liang and Hirabayashi 1992) have been studied to improve the mechanical or thermal or membrane properties of silk films. Silk fibroin/PEO blend films showed improved mechanical properties and predictable surface morphology based on the based on the PEO content. Thermal and mechanical properties of fibroin/polyacrylamide blend films represented significant improvements, whereas silk/PVA blend films showed increased permeability to neutral salts. By blending with cellulose, films with excellent elastic behaviour was prepared and porous cellulose membranes were produced by dissolving the silk in 10% NaOH. In case of chitosan addition, conformational transition to silk II is induced and resulted in increased crystallinity and mechanical strength in the fibroin/chitosan blend films. Blends may have included crosslinking agents such as glutaraldehyde (Rujiravanit et al. 2003), (1-ethyl-(3-3-dimethylaminopropyl)carbodiimide hydrochloride (EDC) (Bayraktar et al. 2005) or cosolvents such as water, formic acid (Park et al. 1999) and acetic acid (Chen et al. 1997).

Consequently, silk fibroin, as a representative fibrous protein, takes the attention of various scientists and technologists as a promising resource with respect to its unique

mechanical properties, the versatility in processing, as well as its biocompatibility, biostability and slow rates of biodegradation (Sofia et al. 2001, Perez-Rigueiro et al. 1998). Fibroin aqueous solution reformed into gel, sponge, powder, film and membrane with given properties and environmental stability pointed out its applicability in the production of biotechnological and biomedical materials. In addition to these, the minimal inflammatory reaction of these silk-based biomaterials supported its suitability as scaffolds for tissue engineering, cell culturing applications or implant materials (Fini et al. 2005, Meinel et al. 2005, Gotoh et al. 2004). Fibroin hydrogel have been found potentially useful as bone replacement material as it improves bone healing and maturation (Fini et al. 2005). Fibroin membranes and fibroin/PVA composites have been proposed for immobilized matrix of enzymes for the second generation of biosensors (Zhang 1998, Qian et al. 1996). It has been also reported that silk fibroin membranes have high-dissolved oxygen permeability and water-vapor permeability in the wet state, similar to that of human skin, which suggest the potential of fibroin in the development of wound dressing artificial skin, soft contact lenses with high oxygen permeability, artificial corneas. These promising applications represent fibroin as a soft-tissue compatible biopolymer (Minoura et al. 1990).

As a result of benefits of being nontoxic, biocompatible and biodegradable, fibroin has been suggested to be used in drug preparation and in drug delivery systems. Fibroin gels have been proposed for oral dosage form (Hanawa et al. 1995), membranes as controllable medicine-releasing carriers (Li et al. 2001) and fibroin/chitosan matrices for a transdermal drug delivery system (Rujiravanit et al. 2003). Chen at al. (1994) studied the transport of pharmaceuticals through silk fibroin membranes and reported that fibroin membrane as an amphoteric ion-exchange membrane composed of both weak acidic and basic groups represents pH-dependent drug permeability. It has shown that transport rate of penetrant through a fibroin membrane can be controlled by changing the charge-state of the membrane. Membrane permeability can be significantly influenced since the effective charge density of membranes composed of fibroin molecules can change with pH, if pharmaceuticals can also be ionized with pH (Chen et al. 2000). Therefore, it has been stated that fibroin membranes are considered to have great potential for controlling the transport of pharmaceuticals such as in drug delivery systems.

2.3.3.2. Hyaluronic Acid

Hyaluronic acid (HA) is a naturally-occurring linear polysaccharide that is a copolymer of N-acetyl-D-glucosamine and D-glucuronic acid disaccharide units connected by regularly alternating β-(1→3) and β-(1→4) glucosidic bonds (Figure 2.13). This endogenic biopolymer was discovered first by Meyer and Palmer (1934) and is present in the extracellular matrix of all higher animals as the only non-sulfated glucosaminoglycan (Šoltés and Mendischi 2003, Luo et al. 2000). Chosen by Meyer in 1934, the name *hyaluronic acid* comes from *hyaloid* (meaning "vitreous") and *uronic acid*. The term *hyaluronate* refers to the conjugate base of hyaluronic acid. Because the molecule typically exists *in vivo* in its polyanionic form, it is most commonly referred to as *hyaluronan* (WEB_4 2005).

HA is found in high concentrations during fetal skin development and it contributes to cell migration and differentiation, and it has been reported that HA is the first macromolecule to appear in the extracellular matrix during wound healing (Alexander et al. 1980). It is also called hyaluronan, as assigned by Balázs et al. (1986), and in some cases, hyaluronan is a major constituent of the mature tissues; as, for example in the vitreous of human eye, or in synovial joint fluid or it exists as an important component such in connective tissues (e.g. cartilage). Industrially, HA is obtained from animal tissue such as eyeball, umbilical cord, and it can be produced on a large scale by biotechnology as it is also present in the capsule of some strains of *Streptococci*.

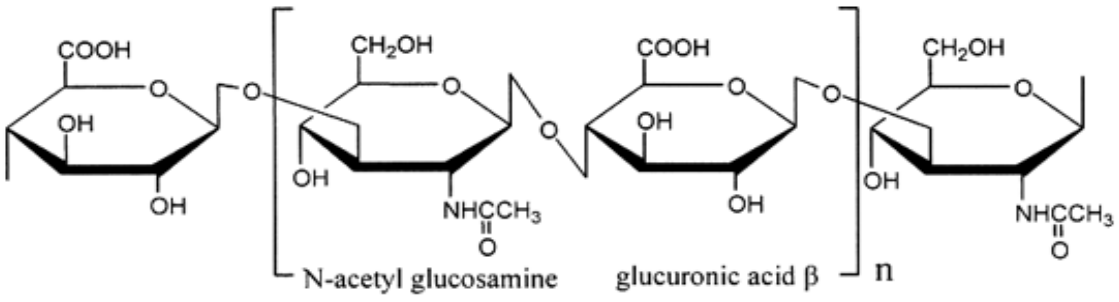

Figure 2.13. Chemical structure of hyaluronic acid
(Source: Kim et al. 2003).

Under physiological conditions, HA is a polyanion ad its pK_a value is estimated to be 2.9 (Šoltés and Mendischi 2003). The molecular weight of HA changes in the ranges from hundreds of thousands to several millions of Daltons and its extremely high molecular weight yield a highly viscous solution even at low concentrations such as 0.1 wt%. In solution, HA chains assume an expanded 'somewhat-stiff' random coil conformation. The size of the HA 'globule' varies with pH and salt concentration as expected for a flexible polyelectrolyte (Cleland 1968). It has been reported by Gibbs et al. (1968) that at pH 2.5 the HA solutions were more elastic and exhibited a 'paste-like' nature on gentle shaking or stirring, which was attributed to a pronounced stiffening of HA chains. This was interpreted to occur as a result of a critical balance between the repulsive forces (provided by the ionized carboxyl groups) and the attractive interactions (electrostatic or hydrogen bonds originated) functioning between the molecular chain elements. In addition, Ghosh et al. (1993) indicated that at alkaline pH, HA gains a more compact, flexible random coil conformation as the hydrogen bonds taking part in the structural organization of HA chains are destroyed resulting in a large loss of the intrinsic stiffness.

Unmodified hyaluronic acid has been found many applications owing to its unique viscoelastic nature. This lubricous biopolymer has been used for medical purposes for surgical treatments in ophthalmology as a viscoelastic biomaterial protecting ocular cells during surgery or in orthopedics for the treatment of joint disease through injection of the aqueous solution. Additionally, it is used in cosmetic applications to moisturize the skin with respect to its high water retention ability.

Hyaluronic acid is also an attractive building block for novel biocompatible and biodegradable biomaterials with potential applications in drug delivery (Surini et al. 2003, Luo et al. 2000, Simon et al. 1997) and tissue engineering (Park et al. 2002) and with proposed applications in the production of artificial blood vessel and artificial skin (Choi et al. 1999, Nishida et al. 1993). Such applications require modification/derivatization of HA since it is very soluble in water or in aqueous salt solutions and it has quick hydrolytic degradation in biological environment. By these means, the recent studies focus on the methods to tailor the physicochemical properties and in vivo residence time of HA to specific applications while keeping its excellent water absorptivity, intrinsic biocompatibility, biodegradability, and lack of immunogenicity thereof. Modified HA based biomaterials can be produced in the form of films, gels, sponges, composites, etc.

Crosslinking is one of the mechanisms used to make HA-based materials water-insoluble. Many attempts has been proposed to prepare cross-linked gels of HA having reduced water solubility including 1,2,3,4-diepoxybutane in alkaline medium, divinyl sulfone in alkaline medium, formaldehyde, glutaraldehyde, dimetylolurea, dimethylolethylene urea, ethylene oxide, polyaziridine, polyisocyanate and water-soluble carbodiimides. Among these reagents, relatively more biocompatible EDC, which has good solubility properties, has been widely used. It has been reported that the HA crosslinks are obtained by the intermolecular formation of ester bonds between the hydroxyl and the carboxyl groups in different molecules (Tomihata and Ikada 1997). Balazs et al. (1986) stated that crosslinked gels of HA can slow down the release of a low molecular weight substance dispersed therein but not covalently attached to the gel macromolecular matrix. It was also reported that delayed and pulsatile release of protein-based drugs are found to be potentially useful through partially esterified HA membranes (Simon et al. 1997). In another study, crosslinked hyaluronic acid hydrogels, Figure 2.14, are reported to exhibit reverse swelling and drug release behaviour under applied electric field. When the electric field is applied, rapid contracted and deswelled due to partial protonation of the ionized polyelectrolyte network and the drug release was reduced and stopped. On the other had, when the current is switched off, the gel swells again and the drugs can diffuse out by the 'pore' mechanism (Tomer et al. 1995).

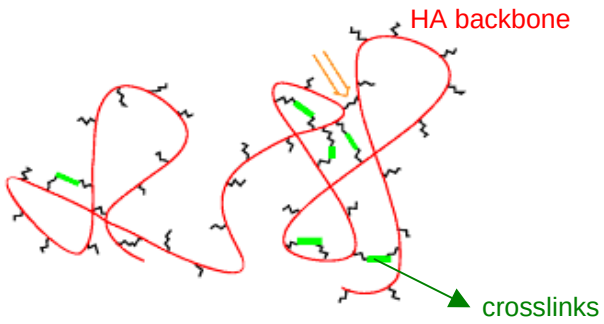

Figure 2.14. Schematic depiction of crosslinked HA hydrogel (Source: WEB_5 2005).

Another group of study represents crosslinked HA blends through both amide and ester bond formation including the binary systems of HA/PVA (Kim et al. 2003), HA/gelatin (Choi et al. 1999) and HA/collagen (Park et al. 2002). Crosslinking was applied to the systems through immersion in crosslinking agent solutions, or adding the

powder form or solutions of these agents into blend solutions. Crosslinked HA/PVA hydrogels showed an electrical and pH sensitive behaviour that can be utilized in drug delivery systems, whereas crosslinked HA/collagen porous matrices were suggested to be used as scaffolds in tissue engineering with improved resistance to enzymatic digestion and mechanical properties.

The formation of water insoluble biocompatible hyaluronic acid polyion complexes, without the contribution of a crosslinking agent, was illustrated by the patented study of Nishida et al. (1993). In this study, polyion complexes were formed through ionic bonds between the carboxyl groups of hyaluronic acid and the amino groups of a high molecular weight natural compound and the mixture ration was 1:1. The resulting complex was insolubilized to water while retaining excellent water absorptivity. It was proposed that the polyion complex can be used a film, tube, etc. for an artificial organ such as an artificial heart, an artificial blood vessel and skin etc. owing to the excellent biocompatibility of both polyelectrolytes. Later, in 2003, Surini et al. attempted to develop a polymeric implant device for the sustained-release of a protein drug by utilizing the interaction between chitosan and hyaluronic acid. In this study pH and polymer mixing ratio dependence of polyion complexes composed of hyaluronic acid and chitosan were investigated. Chitosan, which is also a natural polysaccharide, was used as the high molecular weight cationic polyelectrolyte pronounced in the study of Nishida et al. This study represented the formation map of polyion complexes with respect to pH and weight ratio of the biopolymers. The results highlighted the formation of complexes within the pH range where two polyions were oppositely charged with a binding ratio of 1:1. The complexes formed were used to prepare pellets, which were employed to in vitro insulin release studies. The results suggested that polymer-mixing ratio is effective on the release. The release was controlled by the three-dimensional network structure of the complexes. In addition to this, Kim et al. (2003) reported the electrical sensitive bending behaviour of polyelectrolyte complexes composed of chitosan/hyaluronic acid. The bending angle measurements were performed in the non-contact DC electric field. Polyelectrolyte complexes have shown quick and significant bending that is reversible under the applied electric field. The swelling and bending characteristics of the films based on pH and medium ionic concentration was also investigated. The results of the study signified that such a PEC system can be useful for artificial organ components, sensors, switches and electric current mediated drug delivery systems.

CHAPTER 3

AIMS OF THE STUDY

The main goal of this thesis was to investigate the complexes formed between silk fibroin (SF) and hyaluronic acid (HA). The main motivation is to be able to control the delivery of a charged model drug through films, prepared by silk fibroin-hyaluronic acid complexes, iontophoretically.

The specific aims of the study can be summarized as follows:

- To get insight into complex coacervation between silk fibroin and hyaluronic acid and characterize SF/HA complexes
- To characterize the formation of the SF/HA complex films
- To study the effect of temperature and pH on the swelling characteristics of SF/HA complex films.
- To study the effect of iontophoresis on the permeation and release of a model drug through SF/HA complex films.

CHAPTER 4

EXPERIMENTAL

4.1. Materials

Silk Fibroin (SF) was obtained in reeled form from Bursa Institute for Silkworm Research (Bursa/Turkey). Hyaluronic acid (HA) sodium salt (MW: 1,600,000 Da, form *Streptococcus equi*) was provided by Fluka-BioChemica (Buchs, Switzerland) in powder form. Di-sodium hydrogen phosphate, phosphate dihydrogen phosphate (acid and base components for phosphate buffer), ethanol (absolute GR for analysis) and sulfuric acid (98+%) were from Merck (Darmstadt, Germany). Calcium chloride-2-hydrate and sodium chloride were supplied from Riedel-de Haën (Seelze, Germany), sodium carbonate (99.5+%) was from Aldrich-Chemie (Steinheim, Germany) and timolol maleate salt (MW=432.5) was from Sigma (St. Louis, MO, USA). Dialysis tubing (MW Cut-off: 12,000-14,000) was obtained from Sigma (St. Louis, MO, USA) and Medicell (London, UK). Sodium sulfide hydrate was provided by Fluka Chemie (Buchs, Switzerland). Deionized water was used during all experiments.

4.2. Methods

The methods included were divided into four parts. The first part included the preparation and characterization of the SF and HA stock solutions. Second part explained the analysis employed for the characterization of the complex coacervation between SF and HA, and third part included the preparation and characterization of the SF-HA complex films by instrumental analysis. In the last part, the methods applied for permeability and diffusion studies were described.

4.2.1. Part I. Preparation and Properties of SF and HA Stock Solutions

4.2.1.1. Preparation of Stock Solutions

Silk fibroin solutions were prepared by subsequent processes of degumming and dissolution as described in Figure 4.1. During the degumming process, raw silk was kept in 50 times (v/w) of boiling aqueous 0.05% Na_2CO_3 for 30 minutes and this treatment was repeated three times. This was followed by washing several times with deionized water and the degummed silk was left drying at room temperature.

To obtain aqueous SF solution, 1.2 g degummed silk was added to 20 times (v/w) of Ajisawa's reagent ($CaCl_2$/ethanol/water, 111/92/144 in weight) in a Schott bottle with a volume of 250 ml (Yamada et al. 2001). Higher amounts per batch of dissolution were avoided due to observed gelation during dialysis. The mixture was stirred at 78 °C to form a clear solution for 2 hours. The resulting SF solution was then dialyzed against deionized water for at least 3 days at sub-ambient temperature to remove the neutral salts using a cellulose tubing. Preparation of the cellulose dialysis tubings prior to usage is given in Appendix A. Dialysis was accomplished in 2 liter Erlenmeyer flasks. The water change was done for half-an-hour intervals for the first 2 hours and then for 12-hour intervals for the rest of the 3 days. Eventually, the dialysis was ended as the dialysate tested negative for chloride ion by performing silver chloride precipitation test using $AgNO_3$.

It has been observed that undissolved fibers and particles may have a seeding effect during the concentrating step. Therefore, the dialyzed fibroin solution is filtered with a Filtrak 389 filter paper (Barenstein, Germany). The pure aqueous fibroin solution with a concentration of 1-2% (w/v) was obtained after filtration. The concentration of the SF solution was controlled using a rotary vacuum evaporator, Heidolph Laborota 4001, run at 30°C and 30 rpm to avoid crystallization induced by temperature and shear stress. It was preferred that aqueous silk fibroin solution is prepared by Ajisawa's method just prior to use since the waited samples has shown tendency to form a gel.

HA was provided in powder form and it was soluble in water or any buffer solutions considered. However, HA particles were prone to coagulation during dissolution; therefore HA solution was stirred overnight to ensure complete solubilization.

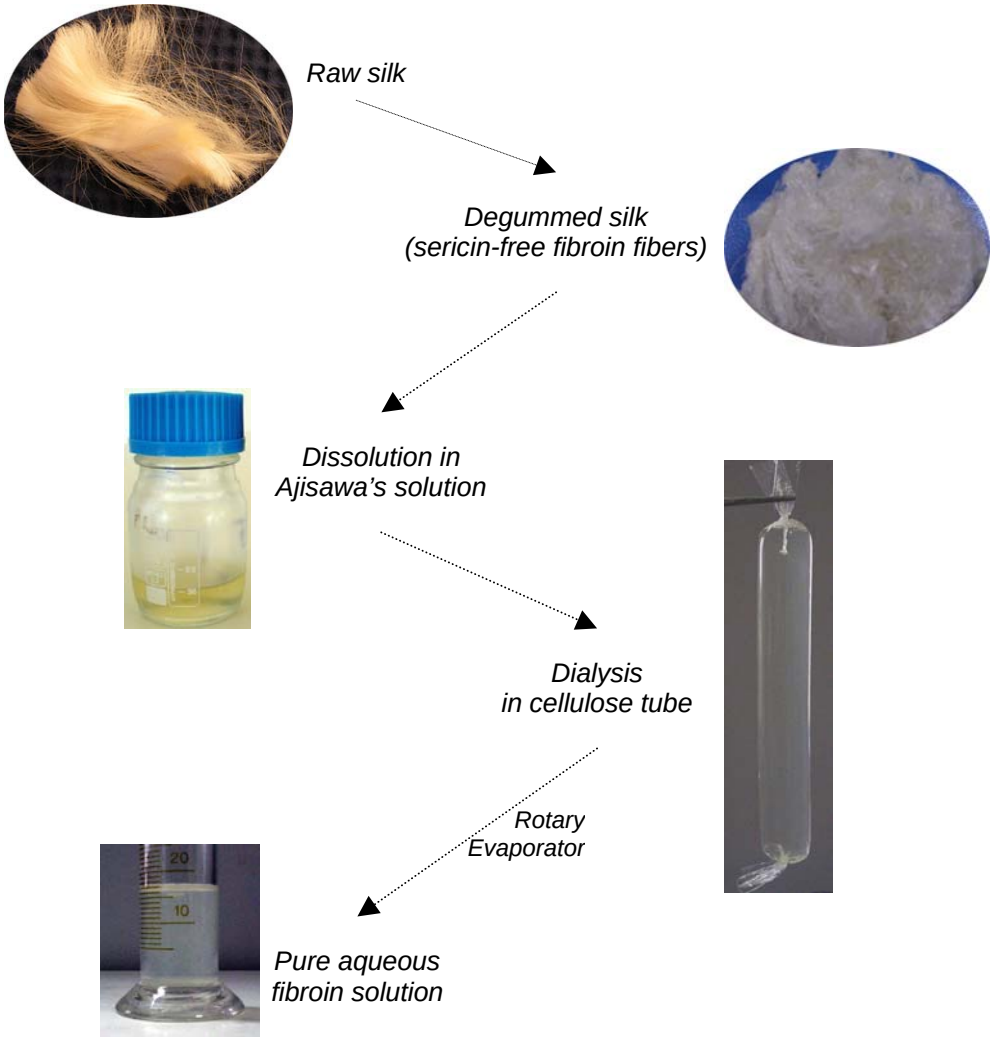

Figure 4.1. Step-wise preparation of aqueous silk fibroin solution from silk fibers.

4.2.1.2. Molecular Weight Determination of SF

The SF average molecular weight (MW) was determined by size exclusion chromatography (SEC). The system consisted of ZORBAX GF-250 column, HPLC (Agilent Tech. 1100) and a UV detector. The column was calibrated with two albumin standards: Egg Albumin (MW = 45,000) and Bovine Albumin (MW = 66,000) obtained from Sigma. 20 μl of sample dispersion (0.5 wt%) was injected into the column after filtration through 0.45 μm filters. Mobile phase was 200 mM sodium phosphate (pH 7.0). Flowrate through the column was kept at 2 ml/s.

4.2.1.3. Electrophoretic Mobility Measurements

Measurements were performed with Zeta-Sizer (Malvern Ins.) apparatus. The biopolymer dispersions were injected using a plastic shringe into a quartz-measuring cell containing two electrodes. Three experiments (and three runs per experiment) were performed. 0.1 (w/v) % HA and SF dispersions were prepared with 10^{-3}M KCl solution.

4.2.2. Part II. Preparation & Characterization of SF-HA Complexation

All experiments based on silk fibroin – hyaluronic acid complex coacervation was studied in salt free systems since it has been reported that salt has a screening effect on the ionic interaction between the two polymers constituting a binary polyelectrolyte system (de Kriuf et al. 2004, Weinbreck et al. 2003a). The analyses were performed at room temperature since variations in temperature does not influence the coacervation which also signifies that complexation does not include a strong contribution of hydrophobic interactions (Kaibara et al. 2000).

4.2.2.1. Turbidimetric Analysis

As a simple method to evaluate biopolymer complexation between SF and HA, turbidity of the mixed solution was measured at varying total biopolymer concentrations (0.1-2.5 wt%) and biopolymer ratios with respect to pH. The pH of the mixture was measured with WTW pH-meter (Inolab) equipped with a Sentix 41 pH electrode, which was calibrated with pH 7 and pH 4 buffers. Initially, the pH of the mixture was adjusted to pH 5.4 by 0.1 M NaOH. The turbidity of the solution was measured as a function of pH by titrating with 0.1 M NaCl with gentle magnetic stirring. Prior to each measurement, acid tirated mixture (30 ml) was stirred until the preset pH level was reached to a constant value. Then, the mixture was dispensed to the special glass bottles of the turbidimeter. The turbidity of the SF-HA mixtures was then monitored by using HACH 2100AN turbidimeter.

4.2.2.2. Conductometric Analysis

Conductometric analysis were carried out to get additional information about complex formation between SF and HA through changes in conductivity of the system. All measurements were performed with WTW Cond 340i conductometer set with a probe of TetraCon 325 at room temperature (~25 °C). In order to avoid changes in pH during titration both protein and polysaccharide solutions were adjusted to the same pH level (3.0). The pH level was selected with respect to the results of turbidimetric titration measurements. A volume 40 ml HA solution (0.5 wt%) was titrated by adding a solution of 1.0 ml SF solution (2.0 wt%) as the titrant. The system was continuously stirred, and after each addition the conductivity was measured and recorded as a constant value was reached. On the other hand, pH of the system was also checked frequently.

4.2.2.3. Gravimetric Analysis

The gravimetric yield studies were based on the study of Barbani et al. (1999). Six sample mixtures were prepared by adding 3 ml (0.3 wt%) HA to each and varying the SF volume added between 0.5 – 7 ml. The final volume in each tube was brought to 10 ml by addition of deionized water at the selected pH. pH of the solutions were adjusted by 0.1 M HCl while being stirred in a 25 ml beaker. Then the mixtures were dispensed into test tubes and centrifuged at 3000 rpm for 1 hr. Same procedure was applied for pure fibroin and HA solution. The supernatants were analysed by Shimadzu UV-1600 spectrophotometer with the absorbance measuring at 272 nm (specific wavelength for fibroin) and 229 nm (specific wavelength for hyaluronic acid) to search for the excess amount of each component. On the other hand, the phase-separated coacervates were washed twice with deionized water at the same pH of the experiment, dried and weighed. The amount of coacervate formation and separation was evaluated using the formula given below:

$$\text{Coacervation yield (wt\%)} = \frac{\text{weight of complex recovered}}{\text{weight of SF} + \text{weight of HA}} \qquad (4.1)$$

and it was represented as a function of SF concentration.

4.2.2.4. Viscosimetric Analysis

Intrinsic properties of biopolymer solutions were measured using a Brookfield DV-III rotational Rheometer interfaced to a personal computer and driven by a software package supplied by the manufacturers. The range of the rotational speed was 4 - 163 rpm. Shear rate was started from 5 s^{-1} and increased up to 200 s^{-1} with an increment of 5 s^{-1}. The data was collected at 5 seconds intervals as an average of the three simultaneous measurements. The viscosity measurements were carried out at room temperature (~25°C) on 20 ml samples. Pure silk fibroin samples were 0.016 g/ml and hyaluronic acid samples with a concentration of $5x10^{-4}$ g/ml with respect to its viscous nature. The viscosity of the complexes were measured for a total biopolymer concentration of 0.5 (w/v) % at a SF:HA weight ratio of 32:1 and 16:1. The measurements were executed at three different pH values (7, 3.14 and 2.3) and repeated twice.

4.2.3. Part III. Preparation and Characterization of SF-HA Films

4.2.3.1. Preparation of SF-HA Films

Regenerated silk fibroin (RSF) solution adjusted to desired concentration and sodium hyaluronate dissolved in water are mixed at a preset ratio. RSF is slowly poured on the HA solution. The order of biopolymer mixing was reported to be effective on complex formation and structure of the complexes formed. It was suggested that as the whey protein was added to the exopolysaccharide B40, a turbid dispersion was obtained, as if to each polysaccharide chain some protein were adsorbed (Weinbreck et al. 2003b). For this reason, addition of HA on SF solution was preferred to simulate the referred system and the opposite technique was also tested.

The pH of the solution was concurrently monitored and the pH was adjusted to pH value between the pK_a of HA and IEP of SF. The mixture was stirred for 4 hours and casted on polyethylene Petri-dishes (Diameter = 5 cm) at room temperature. In case of drug loading, the films were mixed for 2 more hours after drug addition. The casted films were dried at 20 °C and at 80% RH for the first 2 hours, 65% RH for the following

2 days in an environmental chamber (Angelantoni Industrie, Italy). The preparation conditions and type of the complexes were given in Table 4.1 below.

Table 4.1. Detailed description of the preparation conditions of the complexes.

Film Label	pH	R*	Drying Condition	Description
F1	3.2	-	45°C, 65% RH	Pure SF film
F2	5.5	-	20°C, 65% RH	Pure SF film
F3	5.5	20	20°C, 65% RH	SF-HA film
F4	3.2	20	20°C, 65% RH	SF-HA film
F5	3.2	30	20°C, 65% RH	SF-HA film
F6	3.2	30	20°C, 65% RH	SF-HA coacervate particles
F7	3.2	20	room conditions	SF-HA film
F8	3.2	-	20°C, 65% RH	Pure HA film
F9	3.2	20	20°C, 65% RH	Drug loaded SF-HA film

R*: (SF:HA wt ratio)

The dried films were stored in a desiccator at 10 °C until used to avoid contamination. The solubility of the films was controlled by immersing in deionized water and buffer solutions, whereas the thickness of the dried and swollen films was measured by an electronic digital micrometer.

4.2.3.2. Swelling Measurements

Swelling measurements were performed at 5 different pH values from 2.5 to 7.4 at both 37°C and 50°C. After immersion in citric acid buffer at a desired temperature and pH, the film was taken from buffer solution, filter paper-dried by blotting to remove the absorbed water on the surface and then weighed immediately on an electronic balance. The film was repeatedly weighed and reimmersed in solution at predetermined pH and temperature until the hydrated weight reached a constant value.

The swelling defined as, the weight of water uptake per unit weight of dried films (given by Eqn. 4.2) (Kim et al. 2005), was calculated by measuring the weight of swollen films until the weight changes within 1% of the previous measurement.

$$\text{Swelling (\%)} = \frac{W_s - W_d}{W_d} \times 100 \qquad (4.2)$$

Where W_d is the weight of the dry film and W_s is the weight of the swollen film. Each swelling experiment was repeated three times and the average value was taken as the percentage of swelling value.

Cyclic pH-responsive swelling tests were performed at preset two pH levels, 2.5 and 7.4, where considerable alterations in swelling can be observed. The films were exposed to solutions at pH 2.5 and 7.4 for 30 min and the cycles were repeated for 5 times.

4.2.3.3. Material Characterization

Complexes precipitated in aqueous solutions (F6) and the homogeneous films casted from the complex mixtures (F4, F5), as well as the coacervate formation, were characterized by instrumental analysis techniques.

Thermal analysis of SF-HA coacervates and complex films were determined by a differential scanning calorimeter (DSC) (Schimadzu DSC-50) in the 25 – 450°C temperature range at a scan rate of 10°C/min using stainless-steel pans under nitrogen.

Scanning Electron Microscopy (SEM) (Philips XL 30S FEG) analyses were performed to show the morphological changes in the membranes. The films were coated with gold-palladium by Polaron SC 7610 Sputter Coater prior to imaging. The porosity and the roughness of the films were determined by Atomic Force Microscopy (Digital Instruments MMAFM-2/1700EXL). The contact mode was used and 10 and 50 μm scales were used for the area scanned.

The changes in the crystalline state were monitored by X-ray diffractometer (XRD) (Philips X'pert Pro) with CuKα radiation for 2θ from 7 to 70°.

Fourier Transform Infrared Spectroscopy (FTIR) analysis was carried out in the spectral region of 700-4000 cm^{-1} using an FTIR spectrophotometer (Digilab FTS 3000 Mx) equipped with ATR diamond cell accessory.

4.2.4. Part IV. Permeability and Release Studies

4.2.4.1. Choice of the Model Drug

Timolol Maleate (TM) is a nonselective beta-adrenergic blocking agent that is used in the management of hypertension, angina pectoris, myocardial infarction and glaucoma. It undergoes extensive first-pass metabolism and its elimination half-life is 2-2.6 h. TM (pK_a=*9.21*) exists as predominantly charged ions (98.45%) at pH 7.4. Molecular structure of TM was given in Figure 4.2. It was demonstrated that transdermal delivery of TM would avoid first-pass metabolism after oral administration and would improve the bioavailability of the drug (Kanikkannan et al. 2001).

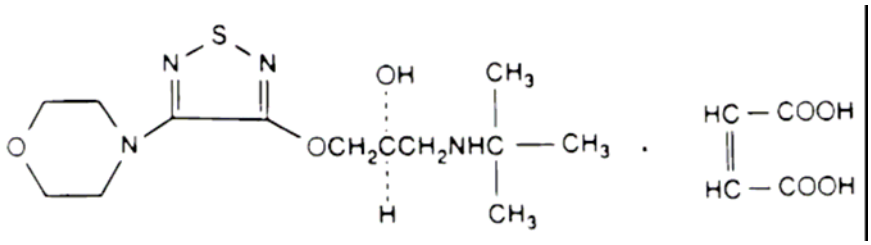

Figure 4.2. Structure of timolol maleate salt
(Source: WEB_6 2005).

Timolol was chosen as a model drug because it is transdermally well tolerated in humans, it permeates through human skin (Kubota et al. 1991), and it has suitable chemical properties (weak base, $pK_a \approx 9.2$, adequate lipophilicity) for transdermal administration (Sutinen et al. 1999).

4.2.4.2. Drug Permeation Tests

The permeability of the model drug, timolol maleate, through SF-HA complex films was measured at pH 2.5 and 7.4 at 37°C by a modified diffusion-vessels method (Yoshizawa et al. 2004). The system used in this study was schematically represented in Figure 4.3. Initially, the bottle cap of a smaller vial (20 ml) was punched and the film was placed between the cap and the packing material. Then this smaller vial, which

constituted the donor, was filled with drug solution. The vial was firmly capped with the punched cap, tested for any leakage for 2 hours, and then placed into a larger vial (180 ml) (receptor). The larger vial contains the buffer solution and shaken at 100 rpm to eliminate a boundary layer effect. Except the packing, no support material was used since the films were mechanically strong in wet state.

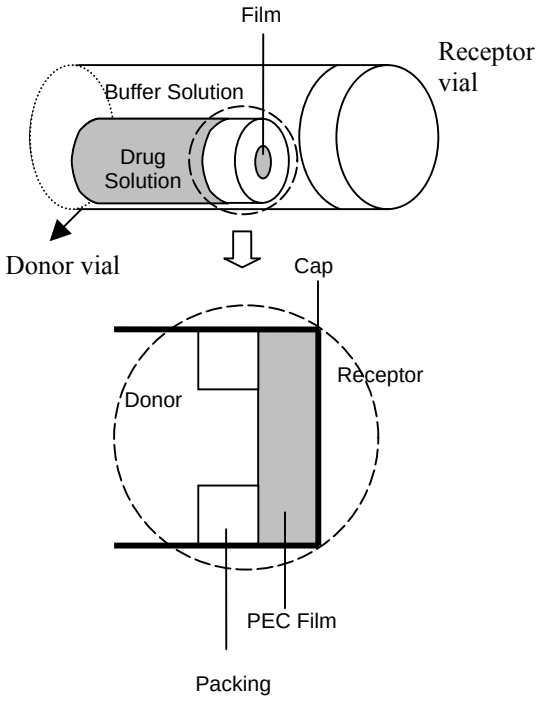

Figure 4.3. Vial-in-vial permeation testing system.

The initial donor concentration was 2.0 g/dm^3 and the effective surface area for flux was 1.5 cm^2. The pH of the donor and the receptor solutions were adjusted to the same pH level with high precision. The aliquots (0.2 ml) were taken with 1-hour interval and UV-spectroscopy (Shimadzu, UV-1601) was used to measure the concentration of the drug in the receptor solution at 294 nm wavelength.

4.2.4.3. Drug Permeation and Release Tests: Passive vs. Iontophoretic Delivery Applications

A schematic drawing of the experimental set-up for the iontophoresis applications is given in Figure 4.4. The set-up primarily consisted of a diffusion cell, the Iomed iontophoretic drug delivery device used as the power supply and the UV visible spectrophotometer with the *in situ* flow cell installed. Phosphate buffer saline ([NaCl] = 0.1 M) at the physiological pH 7.4 was used as the acceptor fluid. The flow of the buffer solution (approximately 2 ml/min) through the diffusion cell was provided by a peristaltic pump.

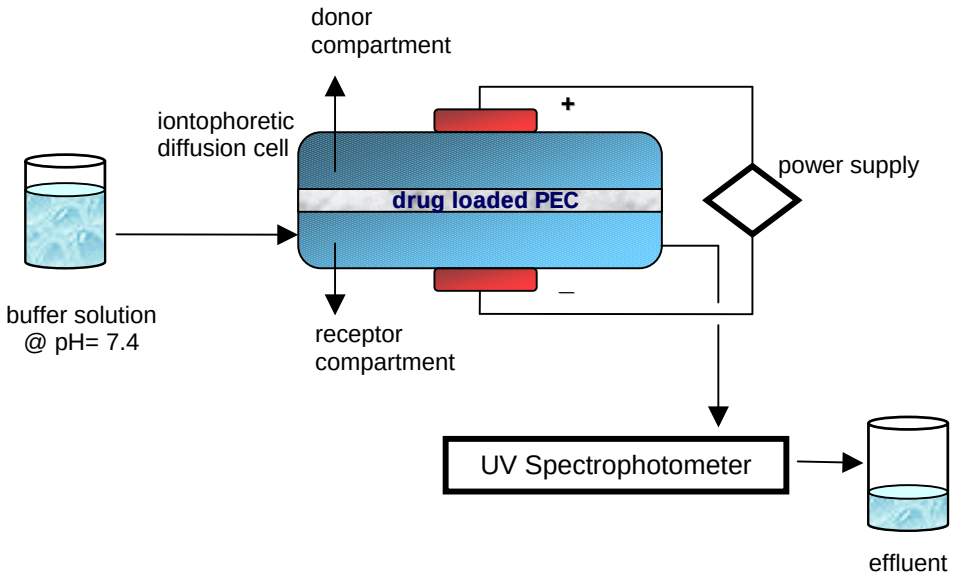

Figure 4.4. Iontophoretic drug release set-up.

A custom-made diffusion cell, schematically shown in Figure 4.5, was used within the system. This cell includes two polytetrafluoroethylene (PTFE) parts joined end to end and an o-ring in between. The membrane is sealed with two gaskets and fixed in the middle as the parts are joined and externally squeezed. Silver/silver chloride disc electrodes (Diameter = 1 cm) were used during the experiments to prevent electrolysis of water. The silver electrode was placed in the anodal compartment and the silver chloride electrode in the cathodal compartment.

The design of the cell enables the *in situ* analysis of amount of the drug delivered to the receptor solution. This was achieved by designing a small volume for the receptor chamber, which is 4.2 ml. The diameter of the opening between the compartments is 13 mm, which gives an active membrane are of 3.2 cm^2. The design of the cell ensures an undisturbed laminar flow in the receiver side and mixing was not required.

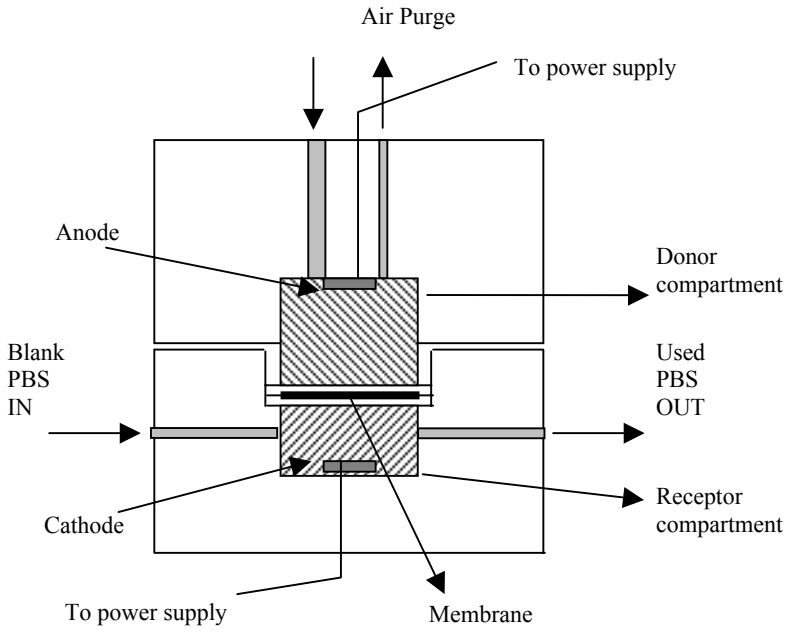

Figure 4.5. Custom-made diffusion cell for iontophoresis applications.

The upper chamber, having a volume of 5 ml, was filled with PBS or drug dissolved in PBS for release studies or permeability studies, respectively, via injection. As the experiment started, the PBS solution was pumped through the receptor chamber and then passed through the flow-cell installed in the UV visible spectrophotometer, which was connected to a computer. The data was recorded and monitored by the use of software. The effluent leaving the flow-cell was collected in a beaker.

Maximum current density applied was 0.5 mA/cm^2, which has been reported as the maximum acceptable density for the iontophoretic transdermal delivery producing minimal skin damage and irritation (Van der Geest et al. 1998).

CHAPTER 5

RESULTS AND DISCUSSION

5.1. Part I. Properties of the SF and HA Dispersions

Silk fibroin (SF) aqueous solution was obtained by the dissolution of degummed silk fibers in high strength aqueous salt solution of $CaCl_2$ at the amounts proposed by the Ajisawa's method. Eventually, aqueous fibroin solution was obtained by dialysis process following dissolution. It has been known that treatment with high salt concentration of salt solutions results in smaller polypeptide chains. For this reason, molecular weight of the fibroin solution prior to regeneration was investigated.

Silk fibroin presented a polydisperse molecular weight distribution. Size exclusion chromatography analysis of the various SF solutions showed that the average molecular weight of the prepared SF solution was 90 kDa, with a maximum of 240 kDa and minimum of 16 kDa. In literature, the results of SDS-PAGE analysis of native fibroin from silk glands was given and clear protein bands having molecular masses of 350 and 25 kDa were obtained by Yamada et al. (2001). The polydispersity in the results with the knowledge of the molecular mass of the native silk fibroin denoted that the native fibroin molecule degraded into a mixture of polypeptides of various sizes during the preparation of the fibroin solution.

The pH of the prepared aqueous fibroin solutions (10 wt%) were in the range of 6.2 - 6.7. In the study of Kim et al. (2004), it has been reported that fibroin solutions prepared with LiBr resulted in a pH range of 6.5-6.8, whereas the solutions prepared with Ajisawa's method by the use of $CaCl_2$, had the pH values within the range of 5.6-5.9 due to formation of fibroin cluster by the Ca^{2+} ions. Relatively higher pH range obtained showed that Ca^{2+} ions could be excluded from the solution medium before the formation of ion bridging induced by this divalent ion.

Prior to complexation experiments, electrophoretic mobilities (μ_e) of the two biopolymers were investigated in order to predict the most appropriate region for the formation of the electrostatic complexes (Figure 5.1). The μ_e of the hyaluronic acid (HA) was negative during all analysis and increased with increase of pH, i.e. -3 e.m.u.

at pH 3.08 vs -4.5 e.m.u. at pH 5.01. The pK_a value of hyaluronic acid was determined as 2.5, which was compatible with the pK_a value of the carboxyl groups that was 2.5, but lower than the reported pK_a value of HA, which was given as 2.9.

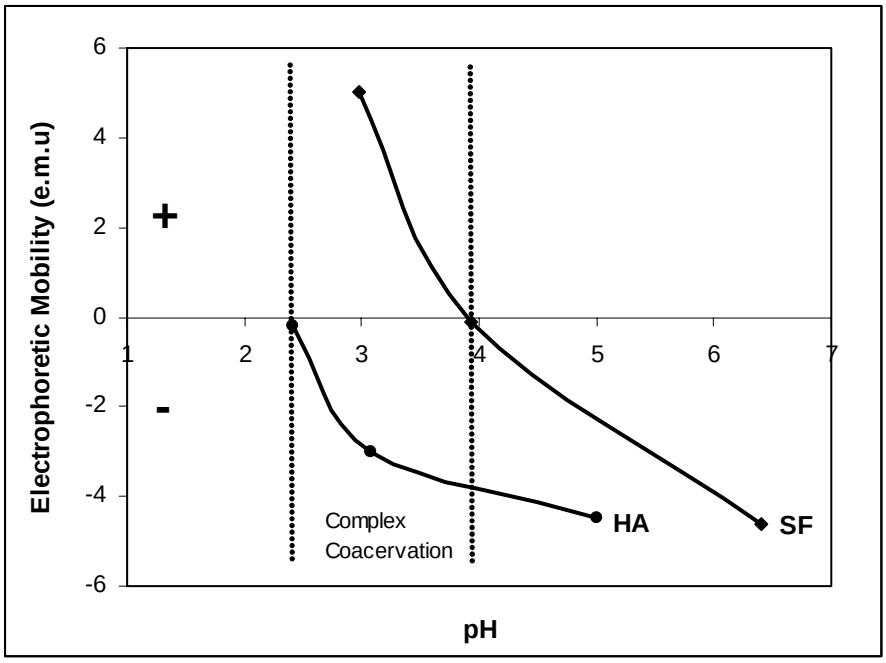

Figure 5.1. Electrophoretic mobility of 0.1 wt% biopolymer dispersions at 20°C.

μ_e of silk fibroin decreased by increasing the pH (5 e.m.u. at pH 2.97 to -0.1 e.m.u. at pH 3.93). The variation of μ_e was dependent on the charge balance between the amino and carboxyl groups carried by fibroin. A zero value was obtained around pH 3.9, which indicated the isoelectric point (IEP) of the prepared SF sample. In literature, it has been given within the range of 3.8 - 4.2. According to these measurements, strong electrostatic interactions between the two biopolymers should be effective in the 2.5 - 3.9 pH window, where the μ_e of biopolymers are of opposite charge.

5.2. Part II. SF-HA Complexation

Studies on complex formation between SF and HA were based on the effect of pH. As the pH of the medium strongly affects the charge density of the biopolymers, it determines the strength of complexation. In this part of the thesis, the pH-window of complexation has been established using turbidimetric, gravimetric, conductometric and

viscosimetric analysis as well as macroscopic observations. On the other hand, the influence of total biopolymer concentration (C_p) and the ratio of the two biopolymers (R = SF:HA weight ratio) on complexation have been shown.

Electrophoretic mobility studies represented in the previous section showed that silk fibroin is in the protonated form, positively charged, below pH 3.9, wheras above the pH 2.5 hyaluronic acid is in the deprotonated form, and hence negatively charged. For this reason, complex coacervation was expected between these pH values.

5.2.1. Turbidimetric Titration under Acidification

Turbidity is proportional to both the molecular weight and the concentration of the particles in a system. Therefore, turbidimetric analysis presents a powerful technique in monitoring the formation of coacervate complexes. Turbidimetric titrations were performed to obtain qualitative information about the interaction of SF and HA.

The mixtures of SF and HA showed good compatibility when mixed and a transparent solution was obtained with no precipitate formation above the pH of 5. Turbidimetric curves of the acid titrated SF-HA mixtures were shown in Figure 5.2 and Figure 5.3 in terms of NTU (Nephelometric Turbidity Unit) vs. pH. These figures revealed that complexation between SF and HA were in the favor of the proposed pH-window.

Figure 5.2 represented the titration curves of SF and HA mixtures for the C_p's of 0.5 wt% and 2.5 wt% at constant SF:HA weight ratio (R) of 32:1. At pH > IEP_{SF}, both SF and HA are negatively charged and hence repulsive Coulombic forces prevented the complexation. This showed that biopolymers were soluble in the mixture and the system exhibited a blend of two biopolymers miscible in each other. In this region the turbidity was constant and low comparable to those of the pure biopolymer solutions. Further decrease of the pH led to the increase in turbidity. All curves illustrated that turbidity represented a gradual increase until a certain pH value as the pH of the mixture approached to the isoelectric point of fibroin (IEP_{SF} = 3.9). The very first small variations in turbidimetric signals in a polyelectrolyte mixture were considered as the pH_c (pH critical) as the formation of primary soluble intrapolymeric complexes by numerous researchers. This variation was seen within the pH range of 4.5 - 6. However, these small variations can be more clearly seen by light scattering (Weinbreck et al.

2003a), as it occurs on the molecular level. The possibility of such variations above IEP of the protein, on the wrong side of the IEP, was attributed to the existence of a local protein domain forming a charge patch with an effective charge opposite in sign to net protein charge (Grymonpré et al. 2001). Around pH 3.5 a strong increase in system turbidity was observed and this point was generally symbolized as pH_{ϕ}, coacervate formation pH (Turgeon et al. 2003). This significant increase in turbidity indicated the aggregation of the intrapolymeric complexes giving rise to coacervation, but not the beginning of phase separation.

These observations were in the favor of the formation of electrostatic complexes between the two biopolymers and can be confirmed by the sharp increase of the turbidity values of the dispersions as the protonated amino groups of the protein associated with the deprotonated carboxyl group of the polysaccharide.

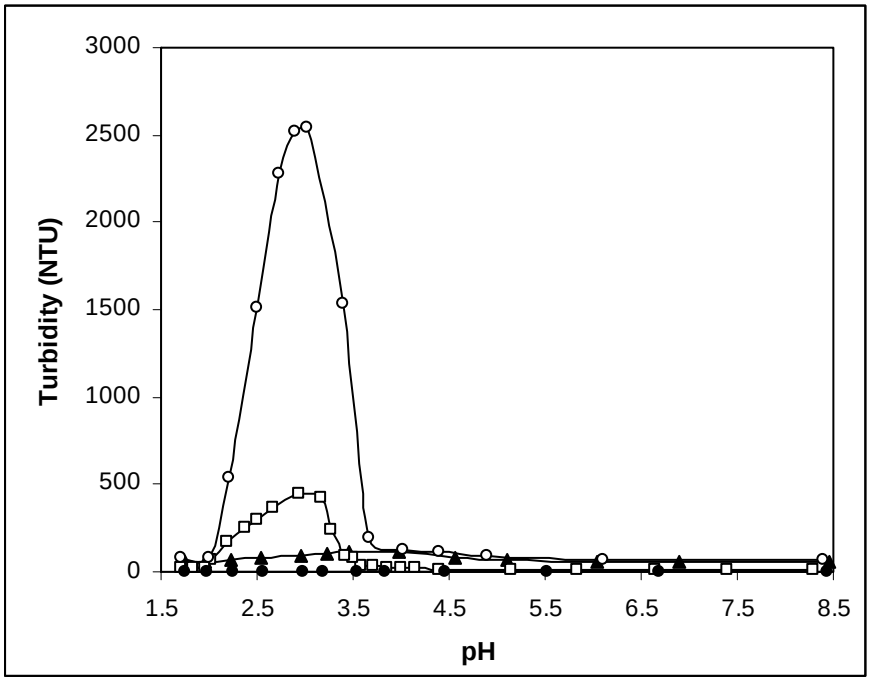

Figure 5.2. Turbidity of pure SF (▲) and HA (●) solutions; and SF-HA system as a function of pH for C_p=0.5% (○) and C_p=2.5% (□) with SF:HA ratio of 32:1.

The curves overlapped differing only by their intensities by the existence of small pH shifts and they showed a peak around pH 3.0. This revealed that complex coacervation was independent of total biopolymer concentration as reported by

Weinbreck et al. (2004). As demonstrated in earlier studies, total biopolymer concentration only influenced the amount and probably the size of the complexes formed. On the other hand, during turbidimetric titration analysis it was recognized that there was no coacervate formation below C_p of 0.1 wt% (results not shown here), which simulated the co-soluble highly diluted case for this system.

The curves were symmetrical and initial turbidity values reached through the pH of 2.5. It was also observed that the maximum turbidity levels reached with an abrupt elevation with small increases in the total biopolymer concentration.

Acidic titration was carried out after monitoring of pH dependent maximum complex formation to check whether the aggregated complexes were reversible. Turbidity decreased as the dissociation of the carboxyl groups was suppressed, and hence the interactions between the biopolymers were weakened. The elevated turbidity values was seen due to complex coacervation pH values even lower than 2.9 (reported pK_a of HA). This was attributed to lower pKa value (2.5) of the carboxylic groups (COO^-). Eventually, all coacervates dispersed spontaneously into soluble complexes. The final turbidity values were similar to that of the soluble complexes formed prior to coacervation. Therefore, one can conclude that the formation/dissociation of the aggregated complexes were reversible.

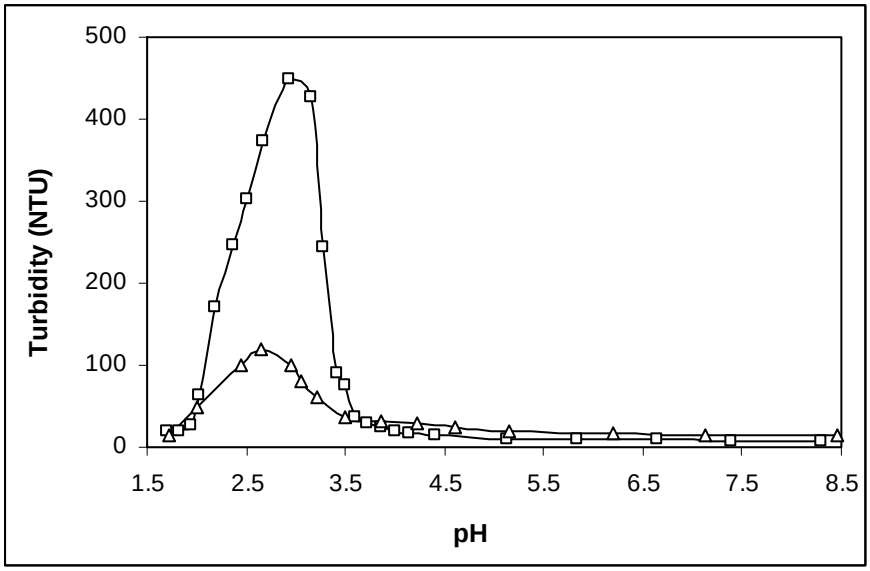

Figure 5.3. Turbidity of SF-HA system as a function of pH for SF:HA ratio of 32:1 (○) and 16:1 (△) for C_p=0.5% .

On the other hand, as represented in Figure 5.3, as the SF:HA ratio was decreased, the maximum turbidity signifying the concentration and the molecular weight of the coacervates also decreased, which showed that SF was the limiting biopolymer for the coacervation. Moreover, the pH value where the maximum turbidity was obtained shifted to lower pH values, since fewer SF molecules were available per HA chain and a more acidic pH was necessary to provide more positive charges on SF. Therefore, charge compensation and stabilization and hence aggregation of the coacervates could be established by further protonation and resultant increase in the electrophoretic mobility of protein at lower pH levels for lower SF:HA ratio. Consequently, the pH at which the maximum complexation was obtained increased when the SF/HA ratio was increased.

All the curves exhibited similar trends, with maximum turbidity around pH 3.0, which reported as the charge neutralization of the coacervates. Consequently, by turbidimetric titration, the complex coacervation between SF and HA was observed around the pH range of 2.5 - 3.5 as expected. The results showed that there occurred a pH-dependent two-step increase and symmetrical decrease of turbidity in the biopolymer mixture, pronounced as complex coacervation, and this was dominantly due to an electrostatic interaction between the SF and HA as given in Eqn. (5.1) below.

$$[HA\text{-}COO^{-}] + [SF\text{-}NH_3] \leftrightarrows [HA\text{-}COO^{-}]\,[NH_3^{+}\text{-}SF] \qquad (5.1)$$

During the whole pH range turbidimetric analysis was performed, HA solution did not exhibit any change in turbidity. However, there was a slight increase in the turbidity of the SF solution around the isoelectric point. This was accepted as a typical behaviour of proteins since they aggregate around their isoelectric point as a result of charge neutralization.

Complex coacervation could also be evidenced by naked-eye observations by the whitening of the biopolymer mixture as shown in Figure 5.4. At pH 7.12, the mixture was transparent, where there observed a change in the solution color as the pH was decreased and finally at pH 3.3 it was translucent with a white color. The centrifuged sample, which had a pH of 3.3, presented the complete phase-separation. Both phases were homogeneous.

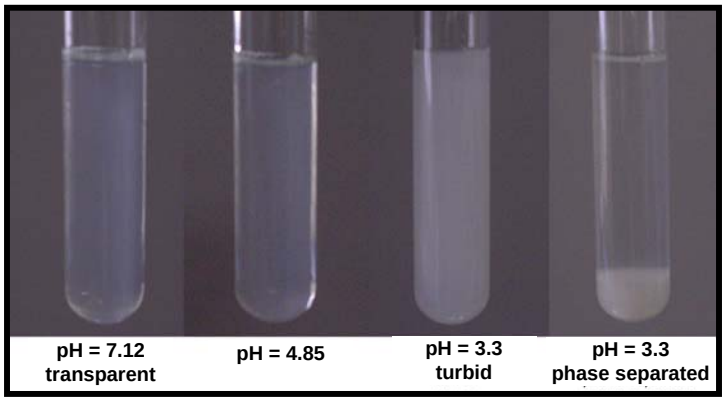

Figure 5.4. Formation of soluble and insoluble complexes with respect to pH.

Centrifugation was applied since settling of the coacervates was very slow. It was indicated by the study of Weinbreck et al. (2004) that coacervate droplets settle down faster if they are fully charge-balanced than if some residual charges are present. The prepared SF:HA mixture at pH 3.0 was in excess of HA, therefore SF was in insufficient quantity and it could not totally compensate the negative charges of the HA. For this reason, a surface layer of HA stabilized the coacervates as the case reported for *β*-lactoglobulin and acacia-gum by Sanchez et al. (2002). The stabilization of the coacervates inhibited the interactions between coacervate droplets, and rearrangement of the coacervates was needed that resulted in longer time to settle down.

5.2.2. Titration of HA by SF: Conductometric Monitoring

To get more insight into complex coacervation of SF and HA, HA was titrated with SF at pH 3.0, where maximum coacervation was established in turbidimetric analysis. The response of the system to SF titration was analyzed in terms of conductivity (mS/cm) of the system vs. added amount of SF (ml).

The conductometric curve, shown in Figure 5.5, showed a certain decrease and at a point change in the slope. Obviously the conductivity approached a constant value as the complexation proceeded. The decrease of the slope revealed that the complex formation began to form when the titration begins and the amount of formation increased during the titration procedure through the formation of intermolecular polyelectrolyte complexes through reversible transient ionic bridges. Instant turbidity formation after each addition of SF solution, but abrupt disappearance of the whitening

by stirring supported this approach. Thus, the initial sharper slope can be explained by the efficient pairing of active groups on SF and HA, which was partially and most probably regionally avoided and screened by existence of counter ions in the solution. On the other hand, coacervation may be also avoided because of the low energetic interest of the biopolymers in one phase due to high excess of HA. Consequently, the regular ionic crosslink between the monomeric units of the both polyion was interrupted because the monomer polyions cannot come to the mutual position as reported by Acar and Tulun (1996).

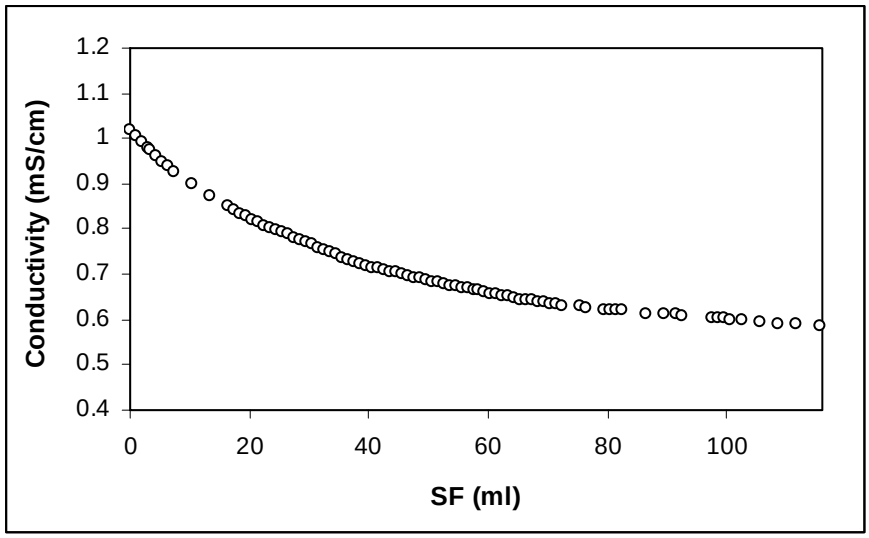

Figure 5.5. Conductometric titration at pH 3.0.

By the SF addition proceeded, the critical size/charge ratio was reached, where coacervation started as the polyions rearranged themselves with a different coiling mechanism for an efficient pairing active groups due to stronger ionic interaction and higher affinity of the biopolymers. Thus, the slope of the curve changed, at which point the mixture also became translucent, as the effect of counter ions was overcome and so–called microgel clusters formed trough cooperative coupling. This was also consistent with the knowledge of the screening effect of the ions on complex coacervation by addition of salt (de Kruif et al. 2004).

The formed coacervate clusters were negatively overcharged due to residual charges on HA chains. Therefore, as more SF was added after the critical value, HA was buried within the ionic crosslinks. Thus, the conductivity reached to a certain value by further charge stabilization of the formed regular crosslinks.

On theoretical basis, SF carries 0.12 mmol amino groups and HA carries 2.5 mmol carboxyl groups per gram. As shown in conductivity vs. added SF plot, around 45 ml the plot showed a change in slope. This corresponded to a charge ratio (COO^-/NH_3^+) of approximately 5, which can be assumed as the required critical charge ratio for the coacervation to start. It has been observed during several runs repeated that as the pH was decreased, the required amount of SF decreased up to five times and the coacervation occurred more abruptly. This was attributed to the increase in the fraction of the protonated amino groups, and the decrease in the fraction of the deprotonated carboxyl groups at lower pH values.

5.2.3. Gravimetric Analysis

The yield and stoichiometry of the SF-HA coacervation was investigated by gravimetric analysis. Figure 5.6 represented the yield of complex formation with respect to SF amount in the complex mixture. As the initial SF:HA ratio was decreased, the coacervation yield decreased. The gravimetric analysis showed that maximum amount of precipitate obtained was close to 30%. This revealed that there existed an optimum SF:HA ratio ratio as well as an optimum pH for maximum amount of coacervate formation, where a large volume of highly concentrated polymers would be obtained. On the other hand, the UV analysis of the supernatants showed that there was high excess of both polymers that not incorporated in coacervate formation. This can be attributed to excess amount of HA employed to the system, smaller peptide chains of SF and the soluble complexes formed by the small peptide chains of SF and HA. It was reported that efficiency of coacervation was affected by the molecular weight of the protein and the polymers of smaller molecular weight formed smaller intrapolymer complexes of higher solubility (Wang et al. 1996).

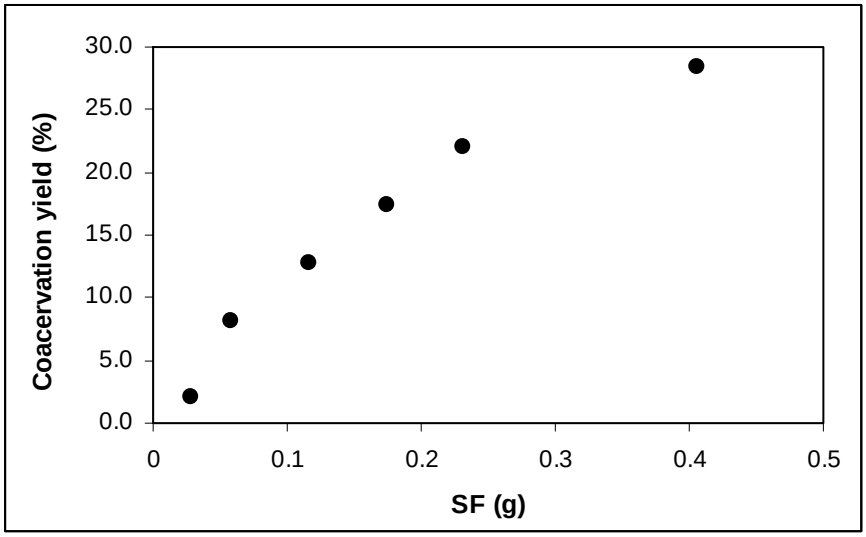

Figure 5.6. Coacervation yield (%) vs. SF (g) in the complex mixture.

The repeated gravimetric analysis showed that coacervate formation was also affected by the stirring time of the coacervate mixture. On the other hand, the trials for the contribution of higher amounts of SF in the biopolymer mixture did not permit the phase separation of the coacervates to achieve higher coacervation yields. It has been reported that when biopolymer concentration exceeds a critical value, biopolymer become limitedly co-soluble. The reason was shown as the large size and the rigidity of biopolymer molecules. Therefore, the entropy of mixing of biopolymers was several orders of magnitude smaller than that of the monomers. It was reported that biopolymer incompatibility may occur even the corresponding monomers were miscible in all proportions. Biopolymer incompatibility was observed between SF and HA biopolymer mixture when the concentration of SF exceeded 3 wt%. In literature, this value changed within the range of 2 – 12 wt% biopolymer concentration with respect to the charge density and the structure of the protein whether it is globular or fibrous (Tolstoguzov 2003).

Coacervate phase recovered from the complexation system was dried and weighed. The amount of coacervate formed with respect to ratio of available amino groups per carboxyl groups in the system was shown in Figure 5.7. By the addition of extra positive binding sites, the coacervate amount increased exponentially, since higher amounts of HA could be bound to protein chains. This exponential increase could be explained by the much higher molecular weight of HA. As the active binding sites were

increased, contribution of a larger molecule to the coacervate cluster was induced, resulting in a dramatic increase in the coacervate formation.

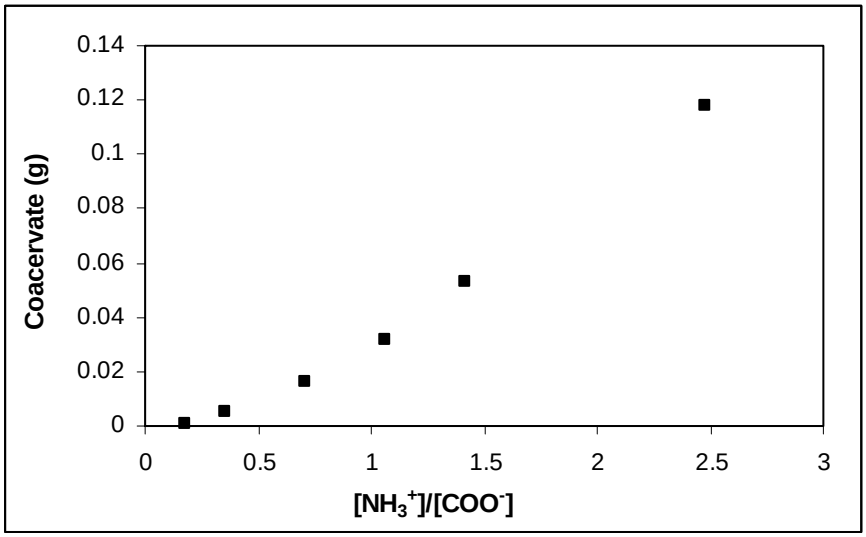

Figure 5.7. Coacervate (g) recovered from the complex mixture vs. ratio of the charges of the biopolymers at constant pH.

The observed increase in coacervate amount after 1:1 pairing of the charged groups and the abrupt increase in coacervate amount showed that coacervation is a very flexible system. The system is capable of adapting its chain conformation and charge distribution by shifting the dissociation pH values of the charged groups to maintain the overall charge balance of the system. Similar case was observed in the system of whey protein/gum arabic coacervates (Weinbreck et al. 2004). It was reported that higher the initial protein to polysaccharide ratio, higher the ratio of the protein to polysaccharide in the coacervate phase regardless of the pH. It was unexpected since the biopolymers were mutually charge balanced at each pH with respect to protein polysaccharide ratio. Therefore, one can conclude that the complex formation betweeen SF and HA exhibited a non-stoichiometric behaviour, which is also the case for similar protein-polysaccharide systems.

Furthermore, the supernatant pH was lower than the initial adjusted pH level of the complex system at the end of the settling of the coacervates. The decrease in pH can be explained by Eqn. (5.2) similar to the chitosan-hyaluronic acid system (Lee et al. 2003), if it was assumed that the pH of the supernatant was only induced by the presence of an excess acid extracted during the formation of the complexes.

$$[\text{HA-COOH}] + [\text{SF-NH}_3^+] \leftrightarrows [\text{HA-COO}^-]\,[\text{SF-NH}_3^+] + [\text{H}^+] \quad (5.2)$$

According to Eqn. (5.2), the protons separated from carboxyl groups moved to the supernatant solution during the formation of the coacervates as the HA deprotonated. Since at the pH level adjusted, the dissociation of the carboxyl groups is constant, this showed that HA was incorporated into the system excessively. This also indicated the non-stochiometric behaviour of the system. On the other hand, during acid titration of the system (especially at the beginning of coacervation), before reaching a value, the pH of the homogeneous (not phase-separated) coacervate mixture showed an increasing trend. This increase can be explained by the Eqn. (5.3) below

$$[\text{HA-COO}^-] + [\text{SF-NH}_2] + [\text{H}^+] \leftrightarrows [\text{HA-COO}^-]\,[\text{SF-NH}_3^+] \quad (5.3)$$

Most carboxyl groups were in the deprotonated state just below the isoelectric point of fibroin. However, the amino groups of fibroin is in $-NH_2$ form. Thus, as the pH of the system was adjusted to a pH level, this level showed positive deviations as the amino groups were protonated. This may also lead to a conclusion that the response of the hyaluronic acid to titration, thus deprotonation was faster that the protons released by the deprotonation of carboxyl groups did not compensate this deviation.

The induced conformational and structural change of the coacervate phase by the incorporation of the biopolymers in excess amounts also indicated that the biomaterials as various processed forms of the complex coacervates such as films, matrices can be prepared with differing diffusion and barrier properties.

5.2.4. Viscosimetric Analysis

The viscosity measurements aimed to investigate the compatibility of the polymers in the mixture and the association between forming the interpolymer complexes in solution. If the viscosity, concentration, and weight fractions of the polymers are known, the following equation constituting the additivity rule of the biopolymers can be established (Lee et al. 2003):

$$(\eta / c)_m = w_1(\eta_1 / c_1) + w_2(\eta_2 / c_2) \quad (5.4)$$

where subscripts (1) and (2) refer to SF and HA, respectively; c is the total biopolymer concentration; w_1 and w_2 are the weight ratios of the corresponding two biopolymers in the mixture; η_1/c_1 is the dynamic viscosity of SF at concentration of c_1; and η_2/c_2 is the dynamic viscosity of HA at concentration of c_2.

Table 5.1. Calculated vs. measured viscosity.

pH	R	Calculated Viscocity[a] (cP)	Measured Viscosity[b] (cP)
2.3	32	0.83	1.66
2.3	16	1.20	1.87
3.2	32	1.72	1.69
3.2	16	2.82	1.63
7.5	32	2.17	2.30
7.5	16	3.82	4.53

a: Viscosity calculated by Eqn. (5.4).
b: Viscosity measured at room temperature.

Measured and calculated viscosity values of SF-HA mixtures at varying weight ratio (r) and pH was given in Table 5.1. The results indicated that within the pH window for complex formation viscosity of the mixtures showed a negative deviation from the calculated viscosity values by Eqn. (5.4). This was attributed to formation of a compact interpolymer complex. On the other hand, the positive deviation occurred outside this window, which was attributed to good compatibility and gel-like association between biopolymers by Lee et al. (2003). It was reported that the viscosity decreased by a drastic reduction of the two polyelectrolytes through complexation, and formation of the compact complexes. In the gel-like complexes, expanded complexes, the viscosity may increase (Lee et al. 1997).

The viscosity of the SF/HA mixture, regardless of the total biopolymer concentration and the ratio of the biopolymers in the mixture, decreases at the pH of complex formation. It was demonstrated by Bungenberg de Jung (1929) that the decrease in viscosity before and during the actual complexation was induced by the reduction of the amount of liquid occluded inside the complexes. The decrease in viscosity of the polyelectrolyte systems and low viscosity close to the point of complexation was reported to be consistent with intrapolymer condensation.

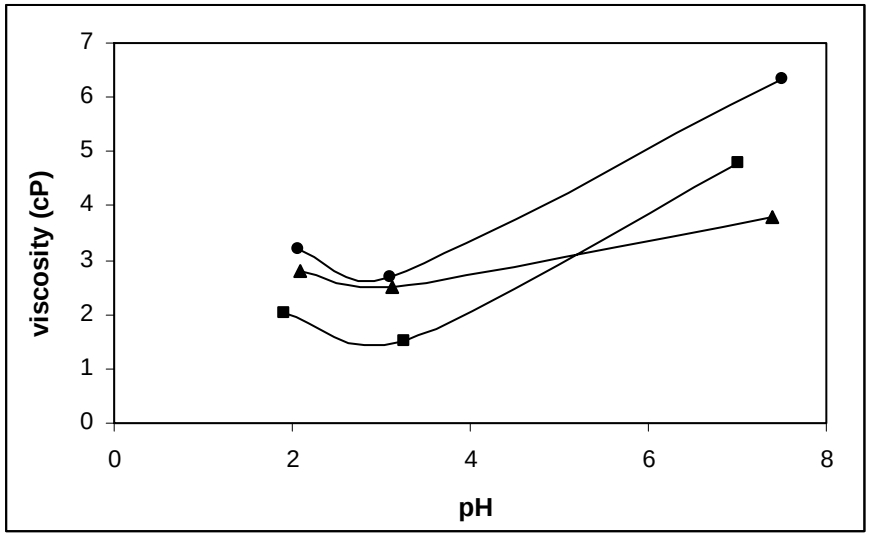

Figure 5.8. Viscosity vs. pH for C_p=1.5% and SF:HA=32 (■) ; C_p=0.5% and SF:HA=32 (▲); C_p=0.5% and SF:HA=16 (●).

The effect of pH on the viscosity of the complexation mixture was shown in Figure. The viscosity measured at three pH levels (above, within and below the proposed pH window, 2.5 - 3.9, for complexation) were calculated as the average of the viscosity values recorded between the shear stress range of 40 - 200 cm^{-1}. Larger variations below 40 cm^{-1}, as seen in Figure 5.8, were excluded during calculations.

The viscosity of the mixture decreased due to coacervate formation between the oppositely charged SF and HA around pH 3.0. Complex formation led to the shrinkage of the intrapolymer complex chains that decreased the viscosity of the system with more compact complex formation. The system turned into a colloidal dispersion from a blend of two biopolymers, which no more contributed their intrinsic viscosimetric properties into the system. Moreover, the viscosity of a dilute polymer mixture was expressed to be directly related to the size of the particles (Weinbreck et al. 2003b). Then one can conclude that the strongest and larger coacervates at higher amounts were formed at the minimum viscosity in relation with turbidimetric analysis.

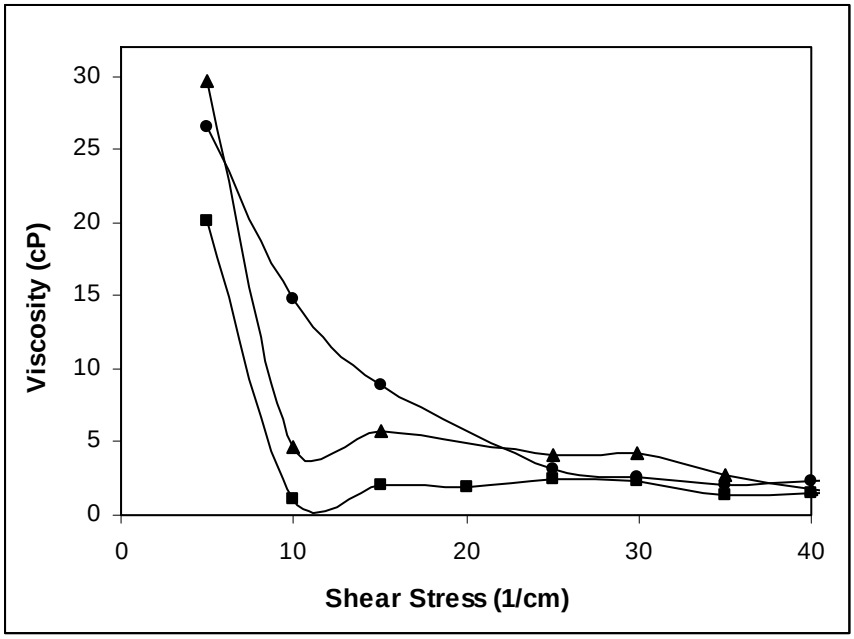

Figure 5.9. Viscosity vs. shear stress plots of SF-HA complex mixtures at pH=3.0. The curves represent C_p=1.5% and SF:HA=32 (■) ;C_p=0.5% and SF:HA=32 (▲); C_p=0.5% and SF:HA=16 (●).

Rather lower viscosity of the C_p=1.5% and SF:HA=32 case may be attributed to more compact and higher yielded complex formation and the viscosity increase due to increase in pH was less pronounced. In case of C_p=0.5% and SF:HA=16, the higher values for viscosity was obtained due to higher excess of HA. This was attributed to much higher viscosity of HA as compared to SF solutions and also by selective binding of HA to the poorly flexible chains of SF to form a precipitate of the complex with the increased amount of HA.

The complexation mixture systems showed a limited shear thinning behaviour below the shear stress of 10 cm^{-1} as shown in Figure 5.9. In combination with the previous findings, sharper curves indicated stronger electrostatic interaction between biopolymers. Moreover, the phase separated coacervate phase was highly viscous while leaving very dilute solution above. In literature, this was confirmed and the coacervate phase was expressed as *viscous particle dispersion* rather than a concentrated viscoelastic polymer solution (de Kruif et al. 2004).

5.3. Formation and Characterization of SF-HA Complex Films

The complex mixtures, prepared at the proposed pH window (pH 2.5 - 3.5), casted and dried under controlled temperature and relative humidity resulted in homogeneous transparent films. The preliminary evaluation of the films was their solubility in water. The films immersed in both water and various buffer solutions were insoluble, whereas pure SF and HA films prepared exhibited fast dissolution in aqueous media. At each mixing ratio or mixing order, within the proposed pH range, insoluble complex films with differing yields were obtained regardless of 1:1 pairing of the charged groups or the weight ratios. Tsuchida et al. (1972) and Kabanov et al. (1980), respectively suggested that when one of the biopolymers was in high excess, or when the host polymer was dropped upon the guest polymer, coacervation did not occur, and this suggestion was opposed by Dragan et al. (1996). Formation of insoluble complexes even at high excess of one of the biopolymers was shown as a proof for a greater stability of the polyelectrolyte complexes obtained in these conditions and an argument for a tight structure that could be achieved. A similar result was obtained for the complex formation between chitosan and carboxymethylcellulose (Argüelles-Monal et al. 1990). The complex was insoluble irrespective of the mixing way and of the excess of the complementary polymers. However, the situation could differ for other protein-polysaccharide systems with respect to charge density and molecular conformation of the biopolymers.

The complex films underwent a color change in aqueous media; they turned to milky white as shown in Figure 5.10. Such a color change was not observed for the pure SF and HA films prepared and dried under same conditions. The-color changing phenomenon in complex films was related to aggregative state of two biopolymers by Wang et al. 1997, that is analogous to the color change of the biopolymer mixture during the aggregation of the intrapolymer complexes with respect to induced pH changes. When the pH reached a critical value at a specific biopolymer ratio and total biopolymer concentration, deprotonated carboxylic acid groups of HA associated with the protonated amino groups of SF, which led to the complexation of the SF and HA chains. The orientation probably caused the refraction change of the light, so the casting solution turned milky-white (Wang et al. 1997). As the films were casted and left to drying, the milky-white gradually disappeared and dry transparent yellowish films were

obtained. Upon exposition to aqueous environment, they regained the milky-white appearance due to the associated complexes in the film.

Figure 5.10. Appearence of dry (a) and wet (b) insoluble SF-HA complex film.

Mechanical properties of the materials are of primary importance for determining the performance in case of varying stress conditions. The pure SF film displayed the typical behavior of brittle materials, as reported. On the other hand, SF-HA complexes was effective in inducing only a slight improvement on the mechanical properties of SF films. As HA content increased, more flexible films at dry state were obtained. The films were much more flexible before washed and excess of HA was removed. During the parallel studies carried out, SF was crosslinked with EDC (1-ethyl-(3-3-dimethylaminopropyl)carbodiimide hydrochloride), and SF-HA complex was enhanced by EDC. These studies also showed that as the amount of HA in the insoluble system was increased by the inducing effect of EDC, more flexible films were obtained. It was also reported that EDC also increased the flexibility of the crosslinked films (Bayraktar et al. 2005). Incorporation of EDC or plasticizer, such as glycerol can be applied to the system to enhance the flexibility on dry state, however, this thesis mainly focuses on pure SF-HA complexes. In wet state, SF-HA films were strong and flexible, applicable to further analysis.

5.3.1. Morphological Examination of the SF-HA Complex Films

Milky suspension of fine coacervates formed by the complexation of SF and HA casted and dried at 20°C and 65% RH. The resultant film was examined by scanning electron microscopy (SEM) and Atomic Force Microscopy (AFM). Insoluble SF-HA complex films (F4 and F5) had smooth surfaces with finely distributed roundish particles as shown in Figure 5.11. In other words, the films displayed so-called sea-island morphology, which was also met in the SEM photographs of chitosan-alginate polyelectrolyte complexes (Freddi et al. 1999).

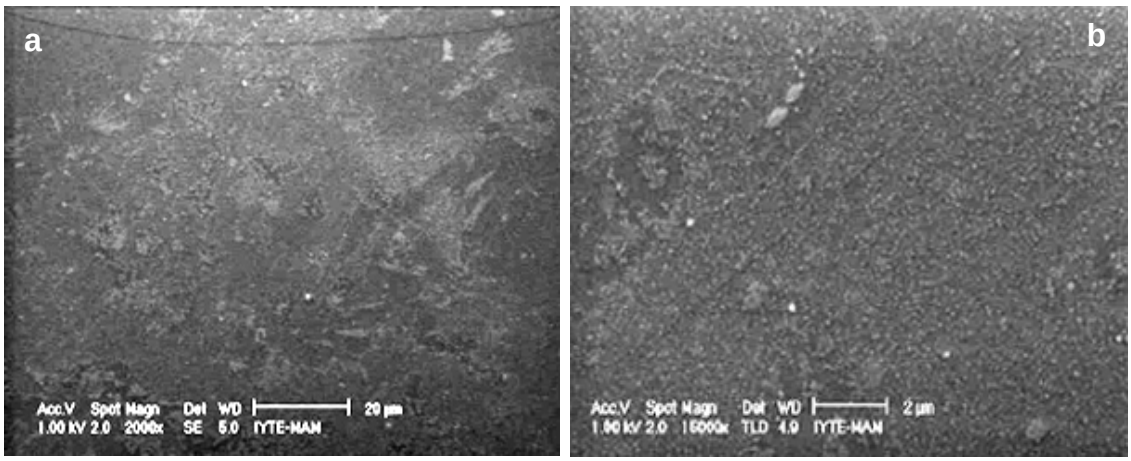

Figure 5.11. SEM photographs of the SF-HA complex film magnified at 2000x (a) and 15000x (b).

Figure 5.12 (a), (b) and (c) represented the cross-sectional view of the SF/HA complex film (F4). The upper side of the film shown in Figure 5.12 (b) was porous exhibiting a network-like morphology whereas the lower side of the film had a dense characteristic, resulting in an asymmetric cross-section structure. The porous and dense sections were magnified (2 μm) in Figure 5.12 (b) and (c), respectively. This may show up due to settling of the coacervate particles with higher molecular weight on the lower side of the film while leaving the upper side of the film poor in coacervates that led to a loose network structure. Asymmetric cross-sectional morphology was only met for the case when SF:HA weight ratio was 20, which corresponded to 1:1 pairing of the charges in the complex. When this ratio was exceeded, films resulted in denser membranes with a symmetric cross-sectional view. This was attributed to faster settling of the

coacervates at higher mixing ratios. Above this ratio, more compact and strongly associated complexes may form, resulting in a denser structure. Dense layer particle size was around 55 nm and this layer had a colloidal microstructure. The thickness of the film shown in Figure 5.12 was 87 μm.

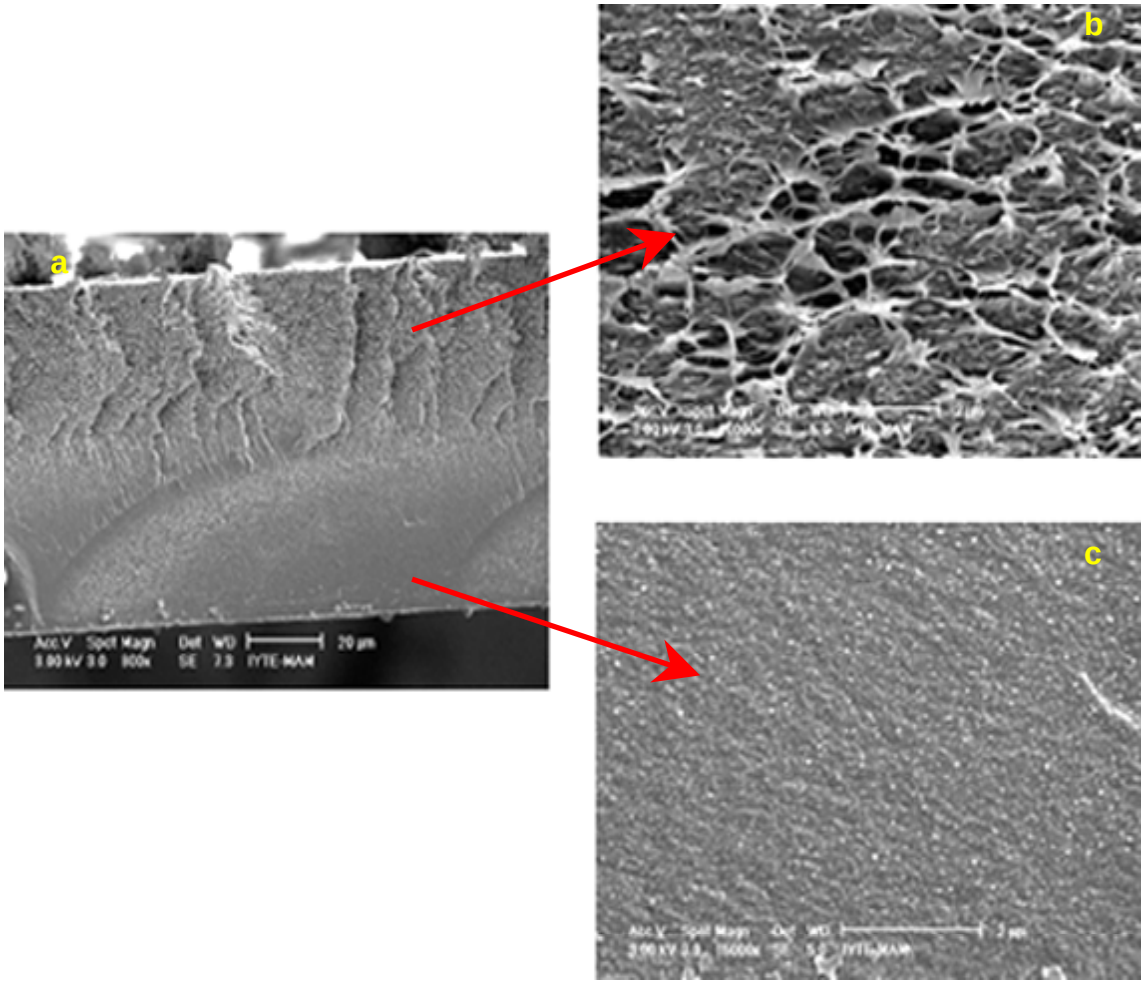

Figure 5.12. Cross section images of SF/HA complex film with magnification 100x (a), porous (b) and dense (c) regions of insoluble SF/HA film (15000x).

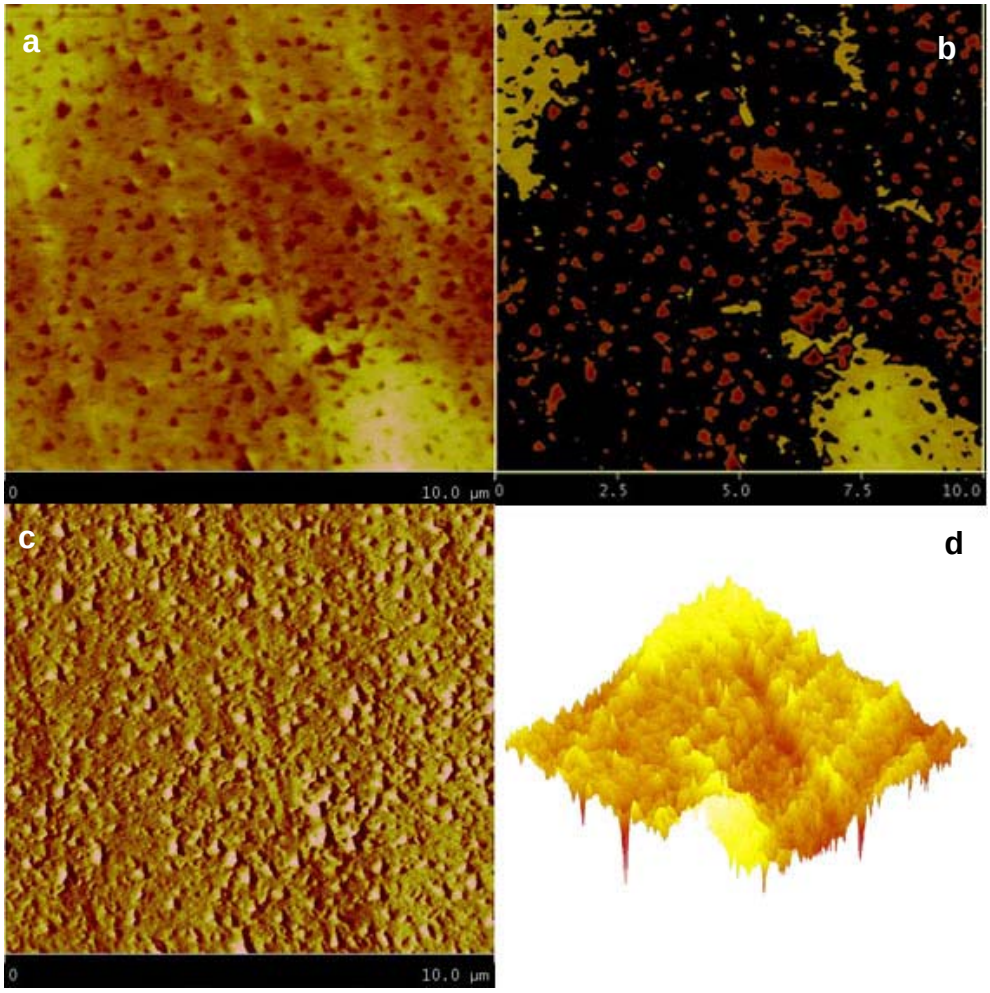

Figure 5.13. AFM images of SF-HA PEC film with height view (a), view of roughness analysis (b), deflection view (c) and 3D height view (d).

SF-HA complex film (F5) was immersed in water for 1 day and the water was refreshed periodically to remove the excess amounts of biopolymers and dried again under controlled conditions. This resulted in porous film with a low roughness. Figure 5.13 (a) showed the 2D height image and (d) 3D height image, whereas (b) exhibited the deflection image and (c) showed image transition for the roughness analysis of the air-surface of the film shown in Figure 5.13 (b). The formation of a porous structure and the resulting network seen was attributed to the removed HA from the complex. Unreacted excess HA had probably stabilized the complex coacervates at the upper side of the film as a filler. When the film was immersed in water, loosely resided HA dissolved in water creating channels (functioning as an excipient) in the biopolymer matrix. High amount of HA in the immersion solution also supported this suggestion. The average pore size of the films was 215 nm and the porosity was homogeneous

throughout the film with a narrow pore-size distribution. Mean roughness of the 50x50 μm^2 scanned area was 4.716 nm and for the 10x10 μm^2 scanned area it was 3.697 nm, which were comparable. Drying caused height elevations (lighter colored areas) as seen in AFM images of all films, however apart from these elevations, the films had a smooth texture.

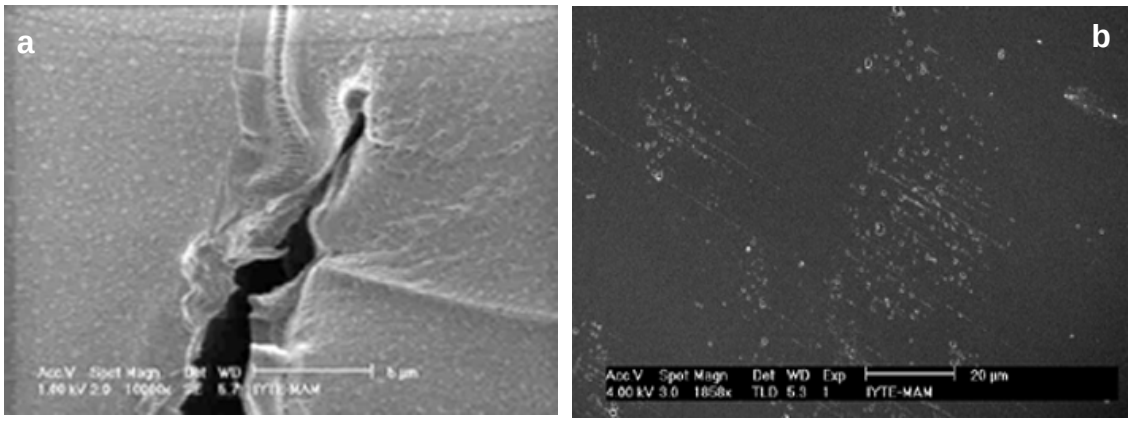

Figure 5.14. SEM photograph of SF-HA complex films dried under controlled conditions (a) and at room temperature (b).

Figure 5.14 represented the insoluble SF-HA complex film (F5) dried at 20°C and 65% RH (a) and the complex film (F7) dried at room temperature (b). F5 was insoluble and F7 was partially-soluble in water. Although same SF:HA weight ratio was employed to both films, F5 resulted in a dense homogeneous texture, whereas F7 exhibited a rather loose and heterogeneous structure. This effect was also clearly observed on AFM images of the complex films dried at room temperature as shown in Figure 5.15 below. The formation of and the size of the complex coacervates was uneven, whereas the variation of the environmental conditions and relatively faster drying kinetics resulted in both macroscopic and microscopic cracks on the surface of the films. In this figure, both height (a, c) and deflection (b, d) images of the contact mode AFM were obtained to show these cracks on the scanned areas of 50x50 μm^2 (a, b) and 10x10 μm^2 (c, d).

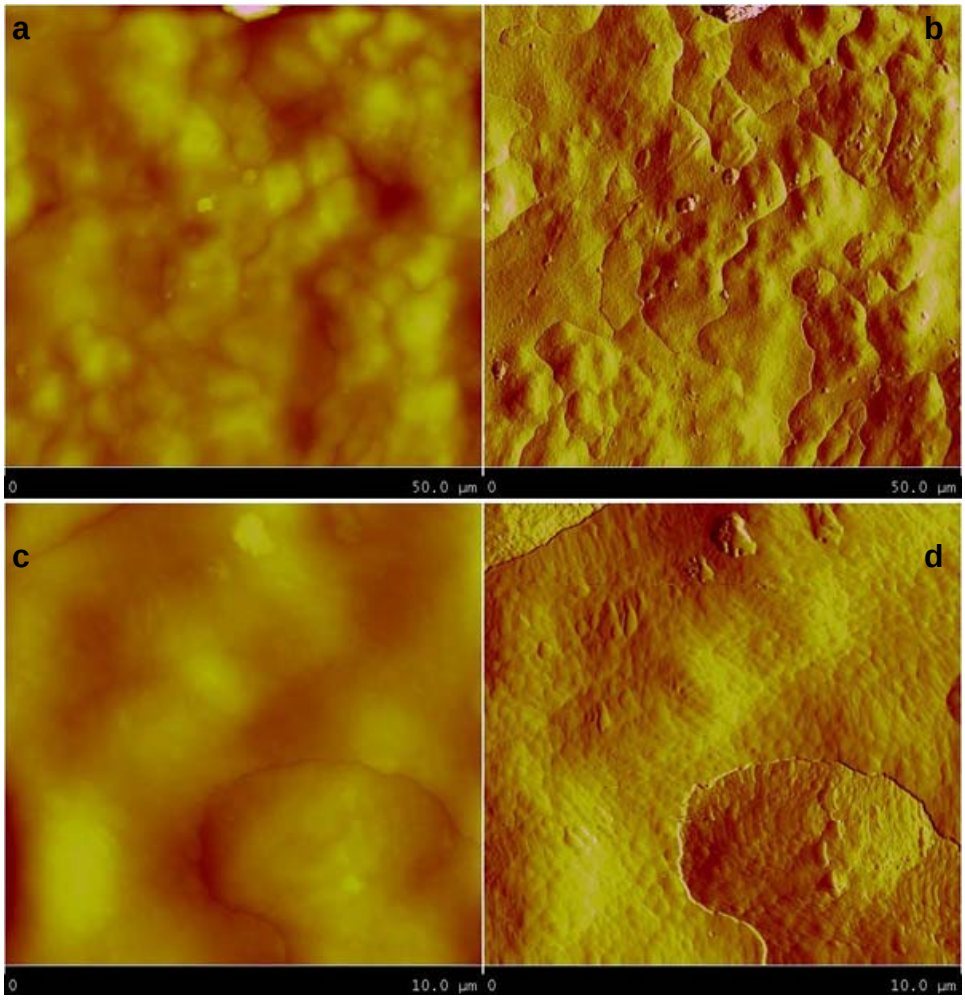

Figure 5.15. AFM images showing the formation of cracks on the complex film dried at room temperature given as height image for 50x50 μm^2 (a) and for 10x10 μm^2 (c); deflection image for 50x50 μm^2 (c) and for 10x10 μm^2 (d).

On the other hand, no crack formation was observed on the film dried at 20°C and 65% RH (F4) (Figure 5.15 (a)). This was attributed to the gradual evaporation of water, permitting films to dry at a proper rate, which led to the formation of homogeneously sized and distributed complex coacervates resulting in continuous films. It was observed that drying conditions had a strong effect on the film formation and the resultant film properties.

The SF control sample (F1) with silk-II conformation were compact and flat with a height of 0.582 nm, whereas the formation of complexes resulted in an average height of 39.55 nm on the surface of the SF-HA complex film (Figure 5.16 (a)). Pure SF sample exhibited densely packed small-sized grains (Figure 5.16 (b)). It was reported that β-sheet SF films may exhibit several types of morphologies such as small particles,

grains or nanofibrils (Putthanarat et al. 2002). The complex coacervates were seen as roundish grains which also confirmed that they were liquid droplets. The lighter areas showed high degree of aggregation of the coacervate droplets.

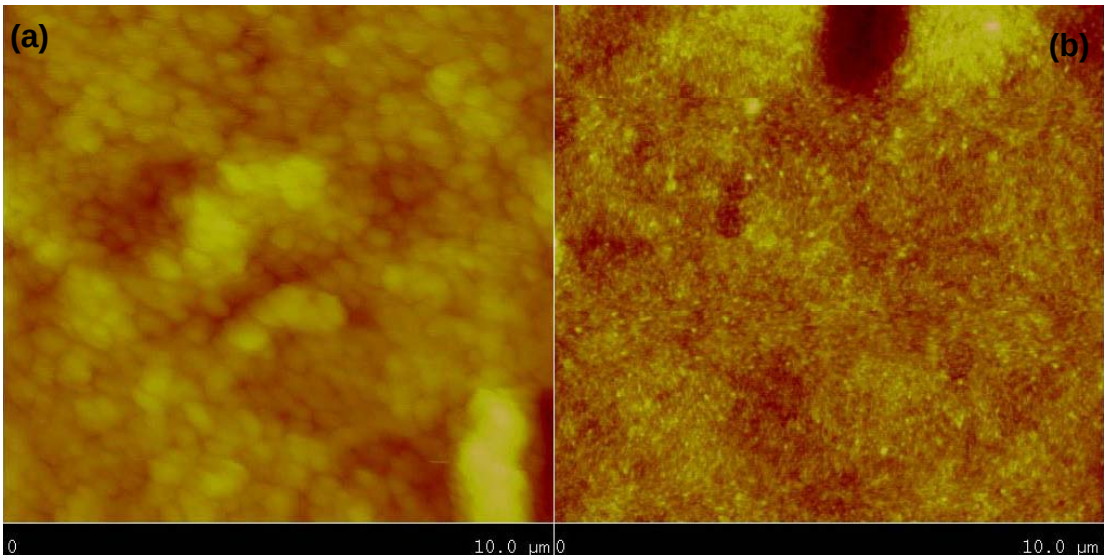

Figure 5.16. AFM images of SF-HA complex film (a) and SF control sample with silk II conformation (b) dried under controlled controlled conditions.

5.3.2. Thermal Analysis

Differential scanning calorimeter (DSC) is one of the techniques that has been applied to study the molecular conformation of silk-based materials and hence their physical and structural characteristics. Figure 5.17 below represented the DSC curves of the films prepared at different conditions.

The secondary structure of *B.mori* silk fibroin (SF) consists of the major conformation including random coils (silk I) and β-sheet (silk II). The following evaluation of the molecular conformation of SF did not differentiate between random coils and silk I structures. It was claimed that distinction between the silk I and random coil was impossible even from IR spectra (Asakura et al. 1985). For this reason, both conformations were shown as silk I.

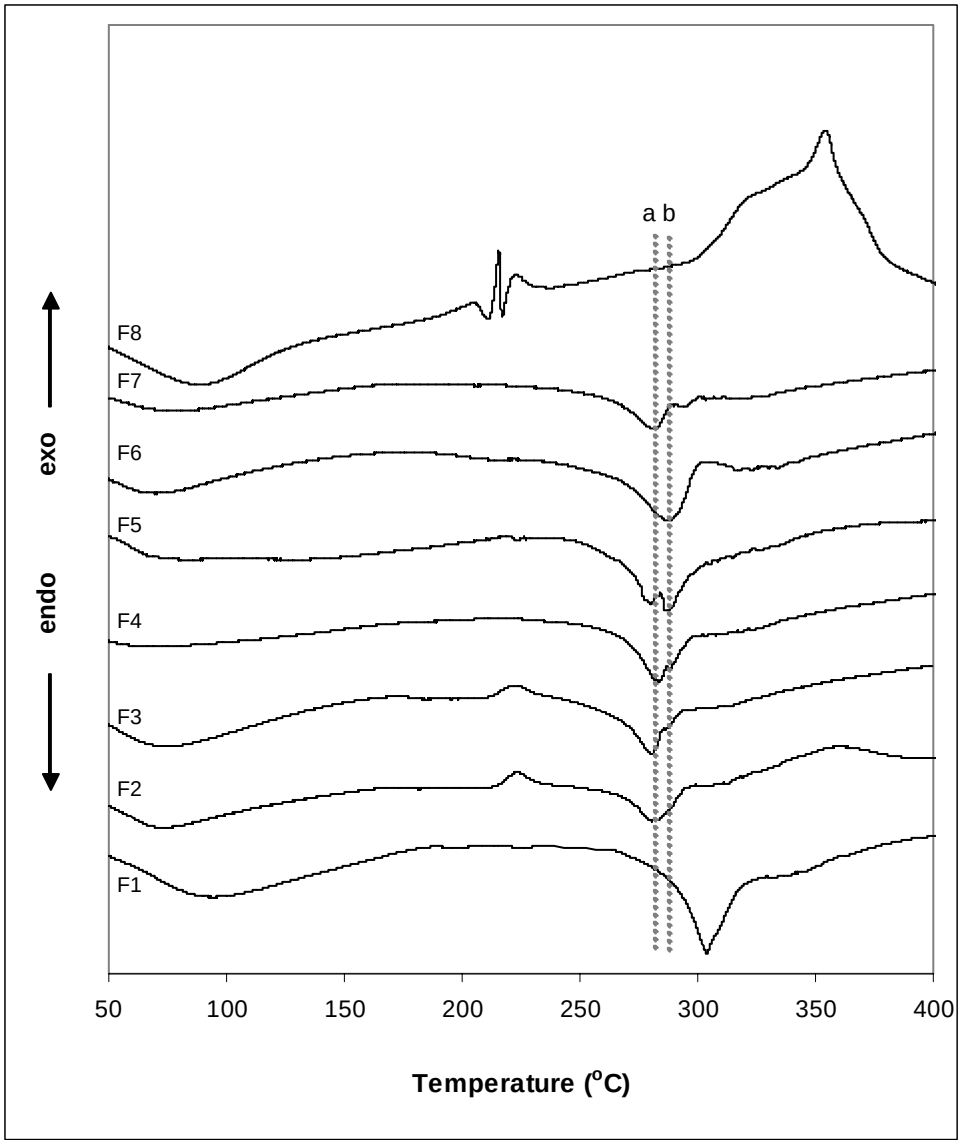

Figure 5.17. DSC curves of the films. Pure SF film-II (F1), pure SF film-I (F2), SF-HA blend (SF:HA=20) (F3), SF-HA complex film (SF:HA=20) (F4), SF-HA complex film SF:HA=30) (F5), phase-separated coacervate network (F6), coacervate film (F7), pure HA film (F8).

The pure SF films, F1 and F2, were both prepared at pH 5.5, but dried at 45°C and 20°C, respectively. Due to heat treatment, F1 was water insoluble and exhibited a strong endothermic peak at 305°C, which was attributed to thermal degradation of SF film with silk II conformation. On the contrary, F2 film, which was water soluble, showed an exothermic peak around 225°C due to crystallization of the amorphous fibroin from random coil (silk I) to β crystals (silk II). The peak of thermal decomposition of F2 shifted to a lower temperature (285°C as shown by the dashed line-

a) with less intensity, by the lower degree of molecular orientation when compared to DSC trace of the F1 with β-sheet (silk II) conformation. The peak positions were consistent with reported DSC traces of the silk-I and silk-II type fibroin (Xu et al. 2005, Um et al. 2001 and Gotoh et al. 1997).

F3 represented the DSC trace of the SF-HA physical mixture prepared at pH 5.5 with a SF:HA weight ratio of 20, which corresponded to 1:1 pairing of the charged groups on the biopolymers. During the preparation of this mixture, no turbidity was seen as naked-eye observation. F3 exhibited a very similar curve to that of F2 with silk I structure. An exotherm was seen at 225°C with a lower intensity and a narrower but higher intensity endotherm at 285°C. The appearance of the endotherm also showed that SF/HA blending did not introduce crystallization. No effect of HA was observed in this curve or either in other curves including HA, of which DSC trace was shown with F8. This was attributed to partition of HA in the mixtures in very small weight amounts. The only difference between the traces of the physical mixture of SF-HA and pure SF film with silk I structure was the appearance of a shoulder around 290°C (shown by dashed line-b). This was assigned to the formation of soluble interpolymer complexes above the isoelectric point of SF due to local positive charge patches. This was consistent with the obtained pH-window for the formation of soluble complexes in the turbidimetric analysis. On the other hand, preparation of SF-HA complex film at pH 3.2 at the same weight ratio introduced the formation of silk II structure to F4. As soon as two materials were mixed, turbidity (white-milky appearence) was observed during the preparation of the complex mixture at the specified pH. The resultant SF-HA complex film exhibited silk II conformation, and thermal degradation endotherm did not shift to a higher temperature as seen in case of F1 with a positive shift of 20°C. On the other hand, the shoulder seen on F3 around 290°C was sharper in case of F4 was attributed to transition of soluble intermolecular complexes to insoluble intrapolymeric complexes, which resulted in insoluble SF-HA complex films. This shoulder turned into an endotherm at the DSC curve F5, which was also prepared at pH 3.2 but at higher SF:HA ratio of 30. This increase beyond 1:1 stoichiometry was consistent with previous results showing the rearrangement of the charge distribution of the coacervate complexes leading to higher coacervation yields. Therefore, as the SF:HA ratio increases, complexes with higher thermal stability was obtained due to more compact complexation with stronger ionic interactions.

F6 exhibited the DSC trace of the coacervate phase centrifuged, filtered and dried under controlled conditions. Prior to centrifugation, complex mixture was prepared at pH 3.2 with a SF:HA ratio of 30. This procedure resulted in particles resembling a network like structure. DSC curve of the coacervate phase showed a broader endotherm at 290°C, which supported the appearence of a new peak at this temperature attributed to SF-HA complexation. The complex mixture prepared under same conditions waited for a gravity-induced phase separation, which was established in 2 hours without centrifugation and left drying at room conditions. DSC curve of the resultant coacervate film, which was partially-soluble, was shown with F7. The endotherm showing the thermal degradation of this film was very similar to that of soluble fibroin film with silk I structure (F2). However, the crystallization exotherm at 225°C was not seen, and the endotherm showing the coacervate formation just appeared as a plateau. Another point was that macroscopic and microscopic cracks were observed on this film as given by the AFM images of this film. Formation of partially-soluble films with crack formation under specified conditions signified the effect of drying conditions. Partial insolubility of the film (F7) was attributed to silk I to silk II transition.

The exothermic peak at 225°C given as a marker of silk I conformation disappeared in all films prepared at pH 3.2. Moreover, the thermal decomposition did not shift to a higher temperature, which shows higher thermal stability gained by silk II conformation, for these cases. This was attributed to pH-induced conformational transition of SF, which probably occured at a lower yield when compared with the intensity and decomposition temperature shifts between the DSC traces of F1 and F2. These observations revealed that SF/HA complex films did not induce a transition to β-sheet conformation, and complexation increased the thermal stability by 10°C which may be concluded as the result of the specific interactions between SF and HA, whereas SF in the complex films underwent a transition to β-sheet by some degree.

5.3.3. X-Ray Diffraction Analysis

The following X-ray diffraction (XRD) analyses were performed to get more insight into characterization of the SF-HA complex films. Figure 5.18 represented the XRD patterns of F1 (SF film with silk-II conformation), F2 (SF film with silk-I conformation), F4 (SF-HA complex film, r = 20), F5 (SF-HA complex film, r = 30) and F8 (HA film) as previously exhibited in DSC analysis. In the figure the DSC patterns of the films were placed in the order of increasing crystallinity.

SF film with silk-I conformation (F2) showed a weak and wide pattern around 2θ=20° with a spacing of 4.8 Å due to noncrystalline form as the typical characteristic diffraction pattern of amorphous silk fibroin (Saitoh et al. 2004). HA-film also showed up a very broad pattern around 2θ=35°. On the other hand, F1 showed a typical diffractogram of β-sheet crystalline structure, which had three diffraction peaks: a major peak at 17.4° and two minor peaks at 14.3 and 26.3°.

The diffractograms of F4 and F5 showed that crystalline and amorphous phases coexisted SF-HA complex films. F4 (r=20) showed lower crystalline peaks at 14.3, 16.9 and 25.5° and weak and broad peak around 20° representing noncrystalline structure, whereas F5 (r=30) exhibited a new broad peak at 7.5°, three crystalline peaks at 14.4, 17 and 25.4° and a stronger and narrower peak at 20°. The peaks representing the crystalline phases had lower intensity with small shifts when compared to that of F1 and the intensity diminishes as SF:HA weight ratio increased. Small shifts and untypical peaks may be caused by the shear forces being effective on casting and drying, giving rise to β-sheet characteristics. On the other hand, it was reported that the appearance of unknown peaks or spacings may be due to other types of conformations such as helical and β-turns or distorsions by the presence of conformers and/segments in which torsion angles deviate from those of silk-I or silk-II (Ayutsede et al. 2005).

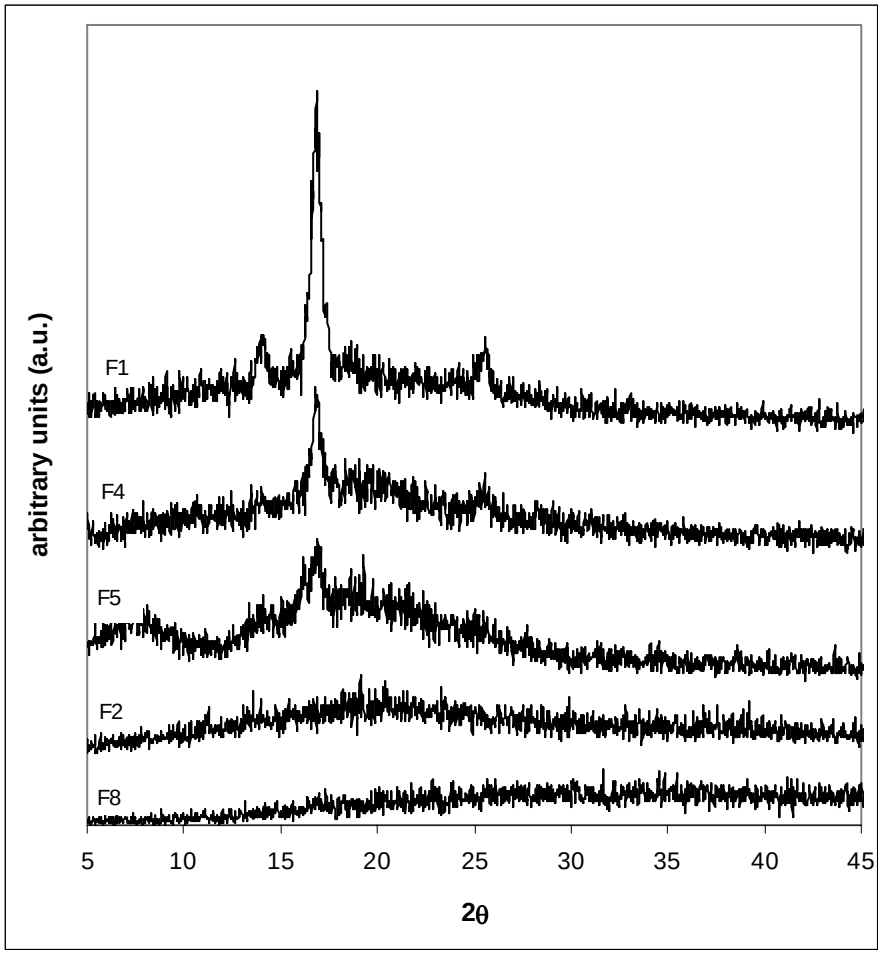

Figure 5.18. X-ray diffraction patterns of SF film-II (F1), SF film-I (F2), SF-HA complex film (SF:HA=20) (F4), SF-HA complex film (SF:HA=30) (F5), HA film (F8).

These findings denoted that complexation between SF and HA through ionic interactions reduced the crystallinity, which was induced by the lower pH values that favored the β-sheet conformation for SF. Similar behavior was seen for the chitosan-gelatin polyelectrolyte complex (Yin et al. 1999). It was reported that the crystalline peaks appeared on the XRD profiles of the complex became weaker with increasing the gelatin content. The weakening of the crystalline peaks induced by increasing the protein content of the complex was attributed to strong interactions between gelatin and chitosan that led their good compatibility.

5.3.4. FT-IR Analysis

Another instrumental technique, infrared spectroscopy (IR), was employed to determine the molecular conformation and orientation of SF-HA complex films. IR spectrum in the 1800-800 cm^{-1} range of control can be a fingerprint of prepared films since it contains various absorption bands related to different chemical and structural features of the prepared films. ATR-IR spectra of the SF-HA complex films, Figure 5.19, showed small but still significant changes with respect to the SF control film, which was prepared at pH 3.2 to check the conformation transition observed in DSC analysis. SF-HA complex film was also prepared at 3.2, with a SF:HA ratio of 20, simulating the film shown as F4 in the previous analysis. The resultant pure SF film showed slow and partial dissolution in water compared to that SF film prepared at pH 5.5.

Amide I-IV bands are conformationally sensitive bands for polypeptides and proteins. Their intensity and position of these bands give information about the molecular conformation of the materials examined in IR spectrum. In amide I and amide II regions of the IR spectra of the films, instead of a single characteristic peak, bands were observed. In literature, amide I (-CO- and –CN- stretching) appeared to be in the region of 1655-1660 cm^{-1}, amide II (-NH- bending) in the region of 1531-1542 cm^{-1} and amide III (-CN- stretching) at 1230 cm^{-1} were attributed to silk I conformation. On the other hand, the appearance of amide I in the region of 1620-1630 cm^{-1}, amide II in the region of 1515-1530 cm^{-1} and amide III at 1240 cm^{-1} characterized the β-sheet conformation (Ayutsede et al. 2005, Freddi et al. 1999, Wang et al. 1997). The appearance of strong and broad peak of SF-HA complex film (c) at 1240 cm^{-1} represented that the dominant conformation was silk I, when compared to the β-sheet dominant conformation of SF control film (b) which showed 1231 cm^{-1} absorption band of the silk II conformation. On the contrary, SF-HA complex film, as well as the SF control film, represented absorption bands of 1637 cm^{-1} and 1508 cm^{-1} with accompanying peaks of 1654 cm^{-1} and 1540 cm^{-1}. In addition, the appearance of 950 cm^{-1} (-NH- stretching) absorption band on IR spectra of the complex film favored the existence β-sheet crystals. Consequently, IR spectra of the films showed that SF-HA complex film, as well as the SF control film, comprised mixtures of silk I (α) and silk II (β) type conformations and complexation did not introduce a positive effect on

crystallization; on the contrary, decreased the crystallinity which may enhance during drying. The pH-induced crystalline structure of SF was disturbed by formation associative compact structures and/or the crystalline phases may be buried into the complexes with respect to higher degree of hydrophobicity due to charge stabilization of the complexes and the β-sheet conformation.

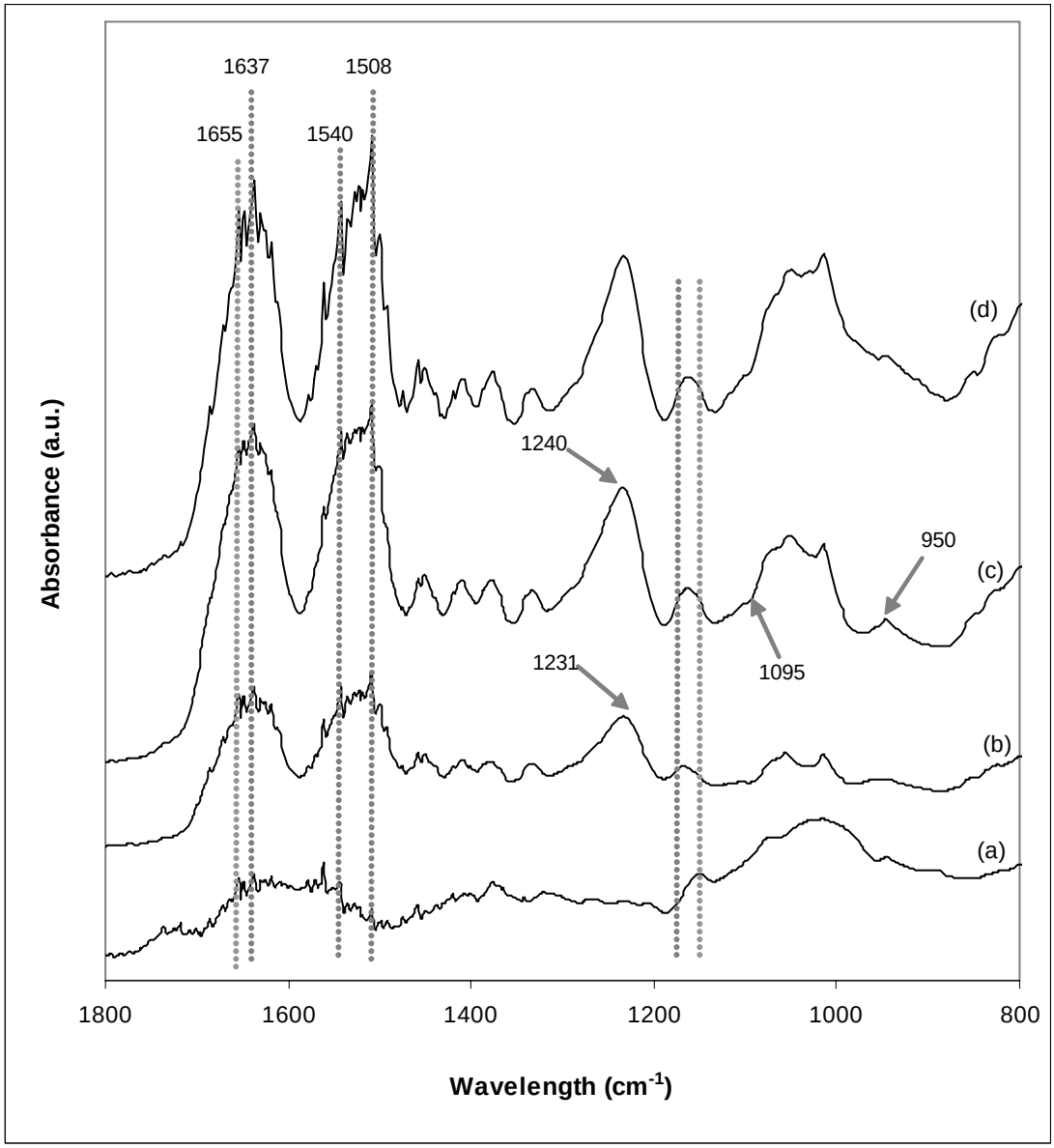

Figure 5.19. ATR-IR spectra of the casted films; HA (a), SF (b); SF-HA complex film (c) and drug loaded SF-HA complex film (d).

In addition to all, even though new conspicuous peak did not appear, considerable increase in amide I, amide II, amide III bands and at 1410 cm^{-1} corresponding to valency vibration of carboxylate ion and formation of a shoulder at 1095 cm^{-1} corresponding to –C=O- stretching for the SF-HA film evidenced the complex formation between the amino groups of SF and carboxyl groups of HA.

SF-HA complex film (F9), shown in Figure 5.19 (d), was loaded with the model drug, timolol maleate, and the characteristic IR spectra of the drug loaded film (d) exhibited the highest increase in intensity, which showed that drug molecules that were positively charged at the mixing pH probably formed linkages with the excess of the deprotonated carboxylic acid groups of HA.

5.3.5. Swelling Tests

The investigations on swelling ability of SF-HA films were carried out in the media of pH 2.5 - 7.4. The weight of the films increased rapidly and equilibrated within 3 hours. The swollen membranes had the milky-white appearance during all swelling experiments. Figure 5.20 and Figure 5.21 showed the pH-dependent swelling kinetics for the SF-HA complex film (F4) at 37° and 50°, respectively. The films swelled more in alkaline condition and shrank in acidic condition regardless of the temperature of the salt-free phosphate buffer solutions. The relatively higher swelling in alkaline condition occured since the carboxyl groups on SF and the unreacted pendent groups on HA probably dissociated into carboxyl anion in alkali condition, which caused the ionic repulsion between anionic groups in the network resulted in the conformational stretching and the films swelled. On the other hand, the films shrank in acidic condition with respect to the coiled conformation owing to the ionic affinity.

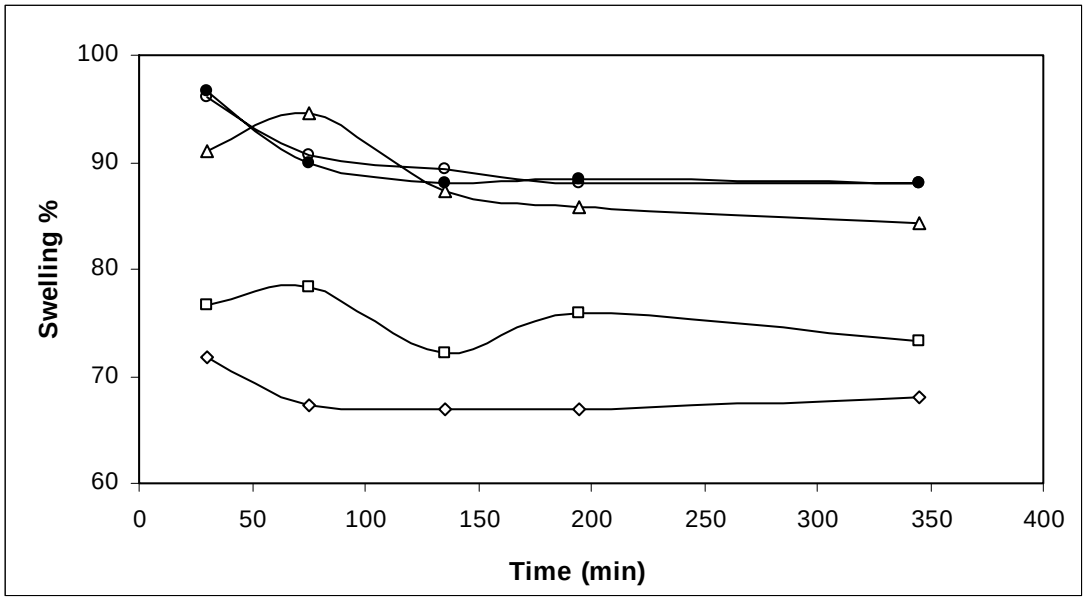

Figure 5.20. pH-dependent swelling kinetics of the SF-HA complex film at 37°C. pH 2.5 (◊); 3.2 (□); 6.5 (○); 5.5(Δ); 7.4 (•).

The plots showed that the reason of swelling was mostly due to ionic repulsion of the pendent groups on SF since the swelling ratios above and below the IEP of the protein was similar and dissociation of carboxyl groups on HA would be completed up to these pH levels since it had a very low pK_a value. In the region of 2.5 - 4, the carboxyl groups on SF are in the form of –COOH with the excess H^+ ions present in the solution. As the pH increased, H^+ ion from carboxyl group combined with OH^- in alkali and the carboxyl groups dissociated into carboxyl anion.

The pH value and the degree of dissociation calculated according to Eqn. (5.5) are shown in Table 5.2. pK_a of HA was taken as 2.5 with respect to electrophoretic mobility measurements (Sutani et al. 2002).

$$\alpha = \frac{1}{10^{(pK_a - pH)} + 1} \tag{5.5}$$

Degree of dissociation of the carboxyl groups on HA does not show any changes above the pH of 4 - 4.5, which confirmed that dissociation of carboxyl groups on HA mostly occurred within the pH window of 2.5 - 4.5. Thus, the alterations in swelling at alkaline pH were due to dissociation of the carboxyl groups of SF creating higher ionic repulsion with the existed negatively charged groups.

Table 5.2. Degree of dissociation for HA with respect to pH.

pH	α
2.5	0.50
3.2	0.83
4.5	0.99
5.5	1.00
6.5	1.00
7.4	1.00

In general, for the polyampholyte gels, there occurs a u-shaped swelling profile having a minimum around the IEP of the polyampholyte showing the interaction of the anionic and cationic units. Shrinking at neutral pH was described by the presence of excess amino groups. In our case, there observed only an increase in swelling with the increase of pH approving that the cationic units were already consumed through complexation with the dissociated units of the HA. Therefore, in all pH levels the complex membrane was negatively charged. On the other hand, higher charge density of HA caused swelling of the membranes even at highly acidic conditions. Minimum equilibrium swelling percentage was recorded as 68% at pH 2.5 and 37°C.

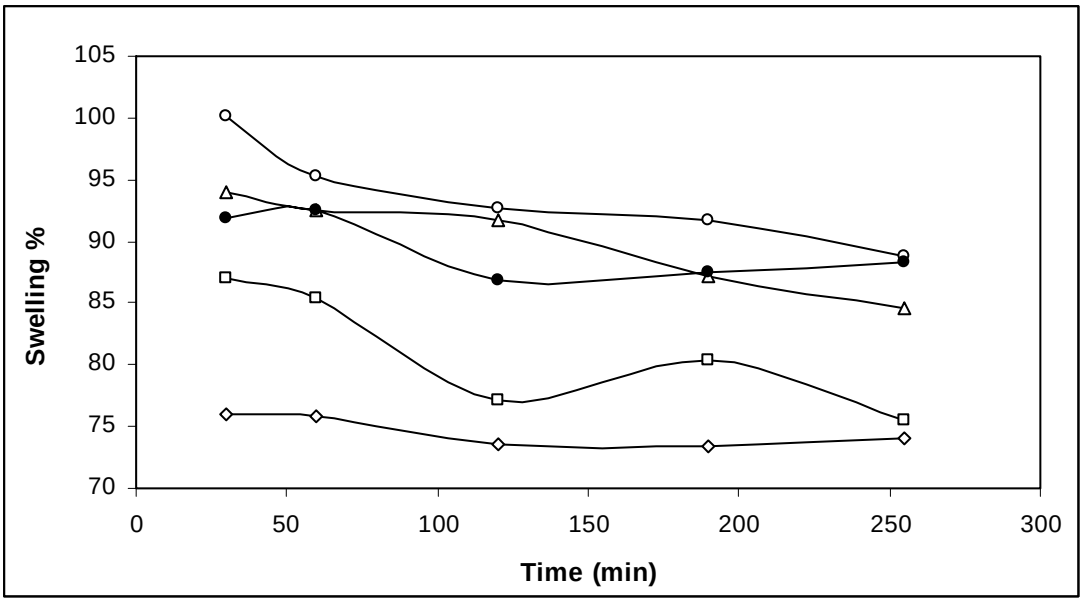

Figure 5.21. pH-dependent swelling kinetics of the SF-HA complex film at 50°C. pH 2.5 (◊); 3.2 (□); 6.5 (○); 5.5(Δ); 7.4 (●).

Equilibrium swelling of the complex films was found to be independent of temperature as shown in Figure 5.22 below for all pH levels studied. This indicated that complex coacervates were surrounded and stabilized by the excess of HA through high yield of complexation. As a result, the water molecules was highly ordered around these groups at the temperatures examined. Temperature dependent swelling was reported for membranes mostly having hydrophobic moieties (Yoshizawa et al. 2004).

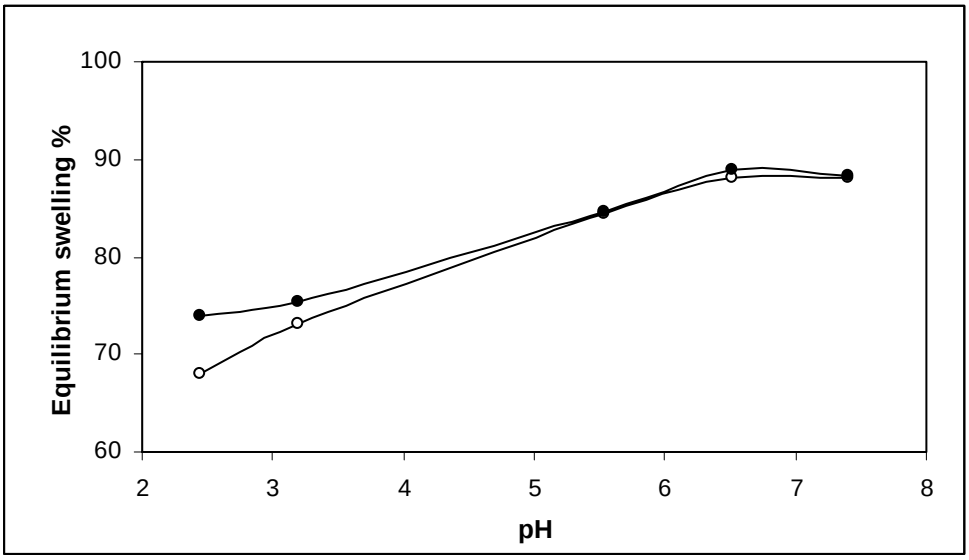

Figure 5.22. Equilibrium swelling percentages of the SF-HA complex films with respect to pH at 50°C (•) and 37°C (○).

Table 5.3 represented equilibrium swelling (%) of the various types of SF-based films at 37°C based on the pH and ionic strength of the swelling environment. Minimum swelling was obtained for the pure SF films with silk-II conformation due to its highly rigid structure and no change in swelling was observed with respect to changes in ionic strength. Maxiumum swelling was obtained at 0.1 M NaCl concentration and pH 7.4 which was attributed to increase in ionic osmotic pressure generated from mobile counterions in the network. Further increase of the ionic strength of the medium up to 1.0 M NaCl decreased the swelling levels, which denoted the effect of high concentration of counterions may hinder the ionic interactions between the carboxyl groups lowering the elastic-retractive force exerted on the network due to ionic repulsion.

Furthermore, loaded SF-HA complex film exhibited lower degree of swelling, which was attributed to formation of stronger complexes during preparation of the films and this was consistent with IR analysis of F9 film.

Table 5.3. Equilibrium swelling of various SF films with respect to pH and ionic strength.

Film Label	**pH**	**NaCl Conc. [M]**	**Equilibrium Swelling Ratio (%)**
SF-HA Film (F4)	10.0	-	86
SF-HA Film	7.4	-	85
SF-HA Film	6.5	-	84
SF-HA Film	5.5	-	81
SF-HA Film	3.2	-	70
SF-HA Film	2.4	-	67
SF-HA Film	7.4	0.1	95
SF-HA Film	7.4	1.0	75
Insoluble SF Film (F1)	7.4	0.1	53
Insoluble SF Film	7.4	-	53
Drug Loaded SF-HA Film (F9)	7.4	0.1	66

In addition to all, complex films prepared with SF and HA were found to be highly resistant to both acidic and alkaline conditions even at elevated temperatures up to 50°C as no disintegration or disassociation was observed during the experiments.

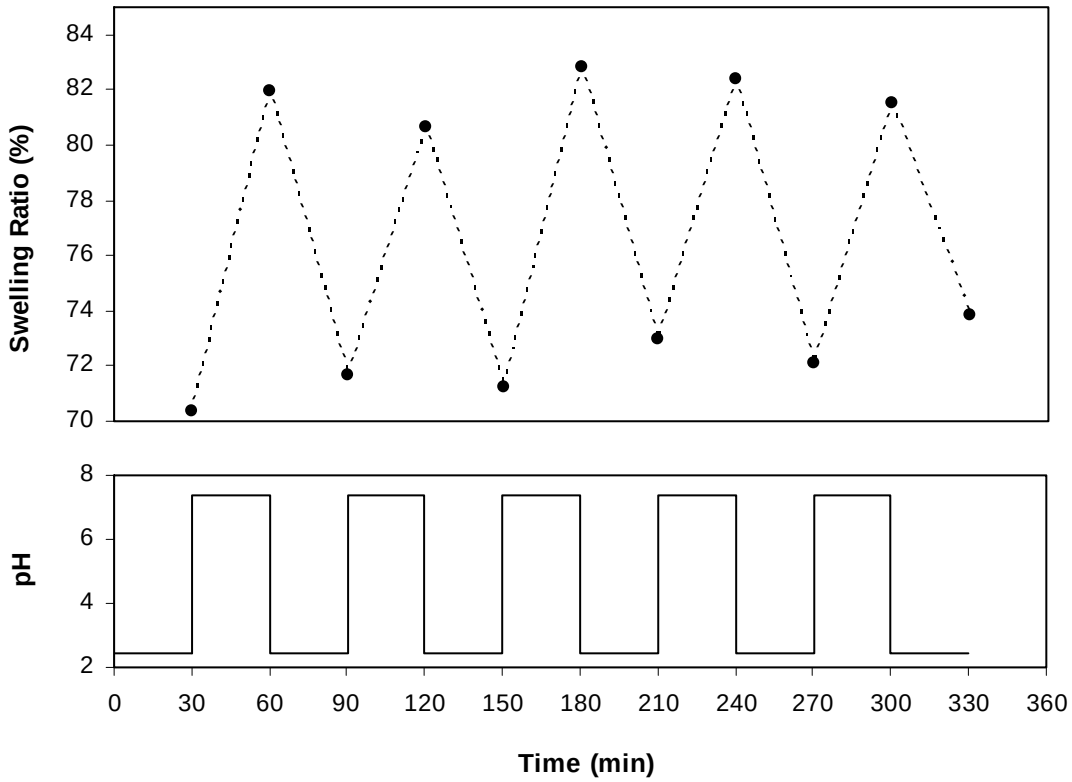

Figure 5.23. pH responsive changes of water content in SF-HA complex films.

Figure 5.23 shows pH responsive changes of the swelling ratio (%) in the SF-HA film. The biopolymeric film swelled at alkaline condition (pH 7.4) and shrank at acidic condition (pH 2.5). Expansion and shrinkage was repeatedly reversible in response to change in pH.

In literature, numerous drug delivery systems based on swelling-controlled mechanism in response to variations in environmental conditions, e.g. pH, have been reported (Gupta et al. 2002). The polymeric network mesh-size of these systems showed changes with swelling, which permitted or prevented the release of the drugs. Swelling experiments employed to SF-HA complex films showed the films responded to the variations in pH regardless of the changes in temperature, which represented that SF-HA complex films may be utilized in pH-responsive systems for intelligent drug delivery.

5.4. Drug Permeability and Release Studies

5.4.1. Permeability of TM Through SF-HA Complexes

The permeation of the model drug, timolol maleate (TM), through SF-HA complex film was studied in buffer solution at pH 2.5 and 7.4, at the minimum and maximum swelling conditions determined at the previous section, respectively. Figure 5.24 showed the permeation behaviour of TM through SF-HA complex film (F4) at different pH media at 37°C.

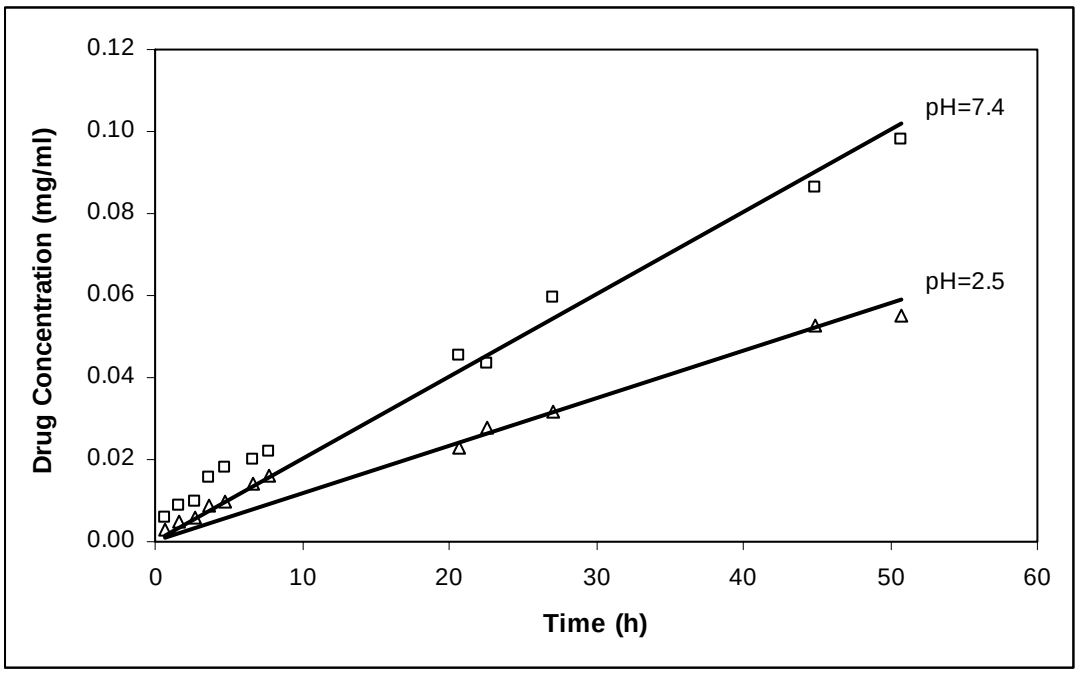

Figure 5.24. Timolol maleate concentration in permeate through SF-HA complex film at pH 7.4 and 2.5.

Overall equation for permeation of the permeation is given by Eqn. (5.6):

$$J = P(C_D - C_R) \tag{5.6}$$

where J is the overall flux; P is the overall permeation coefficient; C_R is the solute concentration in the receptor vial at time t and C_D is the initial solute concentration of the donor vial.

Permeation of drugs was assumed to obey Fickian's law. As such, permeability coefficients are determined based on the following Eqn. (5.7) (Li et al. 2002):

$$\ln\left(\frac{C_D - C_R}{C_D}\right) = -A\left(\frac{1}{V_D} + \frac{1}{V_R}\right)Pt \qquad (5.7)$$

where V_D and V_R is the volume of the donor and receptor vial respectively (V_R = 180 ml, V_D = 20 ml), A is the effective area of permeation (A=1.5 cm^2). Thickness of the film was 200 μm.

The evaluated permeabilities of the SF-HA complex films were $12.3x10^{-3}$ cm/s and $7.1x10^{-3}$ cm/s at pH 7.4 and 2.5, respectively. The results revealed that the direct correlation between the decreasing of the permeability (P), as shown in Figure 5.24, with the decreasing pH. The dependence of P on pH was explained by free volume in the film (Yoshizawa et al. 2004). In the systems having the swelling capability, the effective free volume is derived from the free volume of water, and the transport of solutes is presumed to permeate through the free-water region in the swollen film (Fang et al. 1998). As shown in Figure 5.24, SF-HA complex film swelled at higher rates at high pH. Due to the fact that the total volume of pores and channels in a unit volume increases, the amount of solute transport increase with respect to swelling. On the contrary, as the volume of the pores decreased at low pH, P decreased.

5.4.2. Passive vs. Iontophoretic Delivery of TM

The profiles for the passive (current density: I/A = 0) delivery and iontophoretic (current density: I/A = 0.5 mA/cm^2) transport of TM through SF-HA film (F4) were represented in Figure 5.25 (a) and Figure 5.25 (b), respectively. Drug loading (5 mg/ml) was employed to the donor compartment at the 15^{th} min. The iontophoretic delivery dose was 60 mA.min (1.5 mAx20 min) for each pulses, which were followed by 20 min of passive initial section as shown in Figure 5.25 (d). The higher release observed for the first pulse of the iontophoretic application could be due to a burst effect in which the drug present on the surface layer of the membrane was released instantly upon contact with the receptor solution, maintained under sink conditions. It was also observed that lag time of the membranes decreased after each pulse, which showed that applied electric field also caused reversible changes in the membrane morphology. This was

assigned as reversible since passive drug delivery rate was reached to initial values after each pulse.

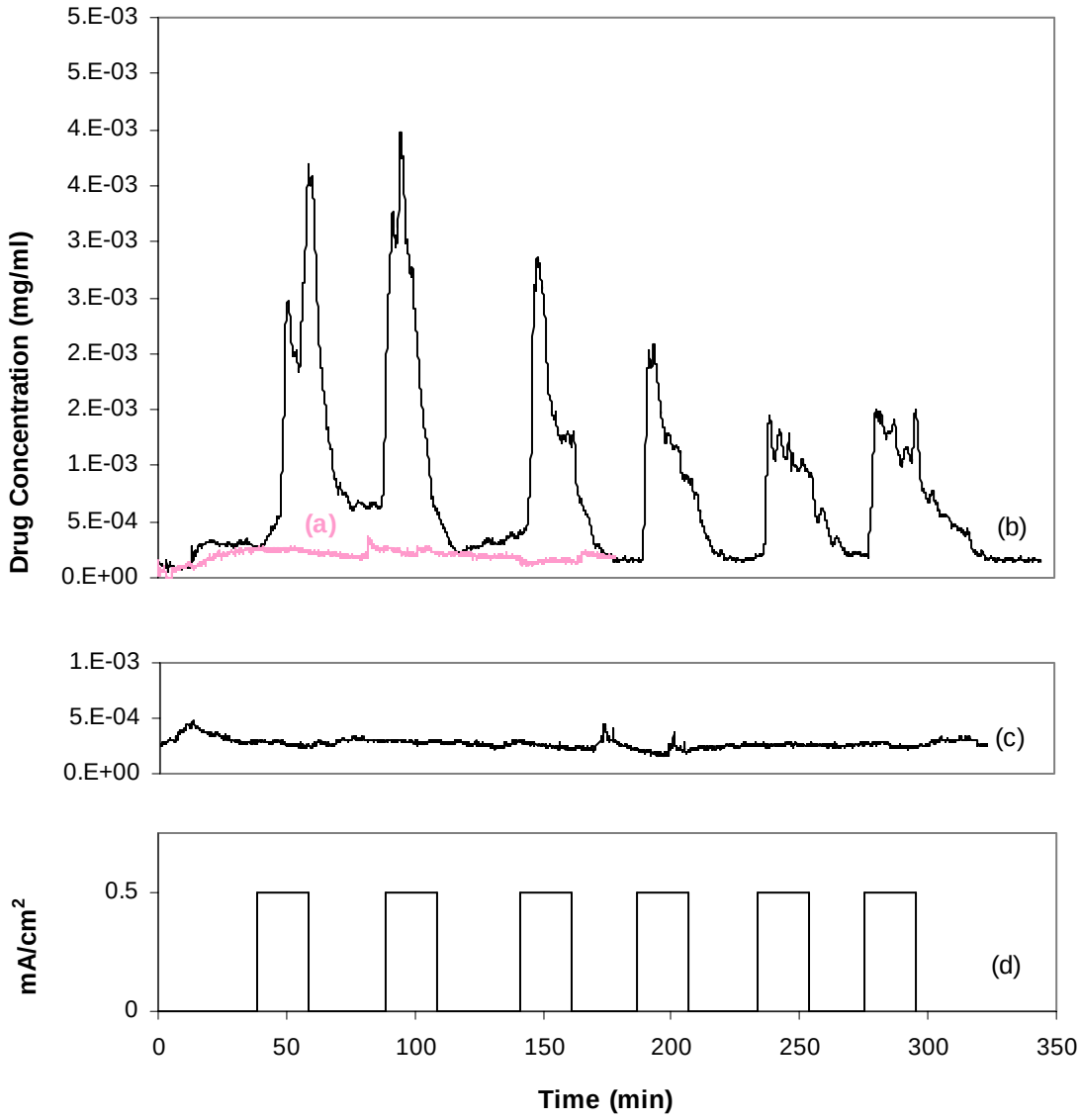

Figure 5.25. TM delivery profiles through SF-HA complex film. TM permeation through the film in passive mode (a), iontophoretically assisted TM permeation form the film (b), release (c) from the drug loaded film, (d) applied electric field profile.

Consequently, the instantaneous flux raised as the current was applied and then declined when the current application was terminated, and this process was repeated on subsequent applications. This showed that the release of TM by permeation through

SF/HA complex membranes was enhanced by iontophoresis applied in pulsate fashion. This represented that these membranes can be modulated for iontophoresis applications.

Total mass balance calculations showed that the decline on the peaks caused by two reasons: decrease in the drug concentration in the donor compartment and fouling caused by adsorption of the drug on the membrane surface. In literature, it was reported that high adsorption of the drug to the membrane, besides the loss of valuable drug molecule, probably caused fouling of the material, which influences the membrane's permeability (Stamatialis et al. 2002). Since the film was shown to be negatively charged in all pH levels, and the drug molecule was positively charged, ionic interactions may have accelerated the possible adsorption mechanism.

Drug release from the drug loaded SF-HA complex films (F9), Figure 5.25 (c), with or without current application was practically same. Formation of strong interactions between the drug and the coacervate complexes led to indistinguishable release. Denser membrane structure formed due to strong interactions did not permit the drug release from the film even up to 65% swelling was observed. This also showed that swelling degree as well as the porosity and pore size distribution had an important effect on drug release.

These results showed that SF-HA complex system can be used in iontophoretic drug delivery systems as a membrane controlling the release of the drug rather than a drug loaded matrix. The response of the system to electric field may have achieved by two mechanisms: electro-repulsion (migration) of the drug through the complex film under the applied electric field and/or the response of the complex film to the applied electric field, which would have increased the permeability of the film.

CHAPTER 6

CONCLUSION

This study focused on formation of silk fibroin (SF) – hyaluronic acid (HA) complexes and the potential use of SF-HA complex films in drug release systems.

SF-HA complex coacervation was investigated and it was shown that the complexation was dominantly induced by pH that determined charge states of the biopolymers. Thus, the pH range for the formation of insoluble and soluble complexes were determined with respect to pH of the complex mixture. Insoluble complex coacervate formation was observed within the pH range of 2.5-3.5. It was shown that the complexes were formed due to electrostatic interactions between SF and HA in this pH window, where these two biopolymers were oppositely charged. It was revealed by turbidimetric analysis that the formation of insoluble complexes were reversible and independent of total biopolymer concentration. Gravimetric analysis performed at constant pH showed that total biopolymer concentration and ratio of the biopolymers in the complex mixture influenced the amount and probably the size of the complexes formed. Formation of the insoluble complex was confirmed and detailed by conductometric and viscosimetric analysis. The complexation was evidenced by the decrease of the complex mixture viscosity by the formation of dispersion composed of aggregated coacervates. Formation of stronger and larger coacervates were confirmed by the minimum viscosity and the maximum turbidity observed in the system. These analyses determined the appropriate conditions for complexation of these two biopolymers conditions for the preparation of the complex films.

The complex solutions were formed at pH 3.2 with a SF:HA weight ratio of 20-30 where higher complexation yields may be obtained. The mixtures casted and dried at 20°C and 65% RH resulted in insoluble complex films irrespective of the mixing order or mixing ratio. The films had a homogeneous texture with slightly improved mechanical properties. It was also shown that drying had a crucial effect on the formation of the insoluble continuous films. The instrumental analysis performed revealed the consequences of complex formation between HA and SF. It was also

shown that the complex films comprised mixtures of crystalline and non-crystalline regions.

Swelling tests performed on the complex films exhibited that the films swelled more in alkaline condition and had a pH-responsive swelling behavior. No effect of temperature was observed on swelling characteristics of the films at various pH conditions. The films loaded with the model drug, timolol maleate (TM) showed less swelling which was attributed to formation of stronger interaction between the positively charged drug molecules and negatively charged excess of HA during the formation of drug loaded films. This result was confirmed with the FT-IR analysis.

SF-HA complex films exhibited higher permeability for TM at alkaline condition which was consistent with the swelling tests. Swelling test also revealed that SF-HA complexes can be good candidates for intelligent drug delivery systems, in which drug release is based on the response of the system to the environmental conditions.

Drug release studies showed that the drug permeation through SF-HA complex films was enhanced by iontophoresis. The permeation of TM was controlled by the applied electric field in pulsatile fashion. On the other hand, drug loaded complex film did not give any response to the electric field which was reasonable with the formation of stronger complexes leading to formation of denser films.

Consequently, SF-HA complex films were found to be promising for iontophoretic drug delivery applications for membrane-permeation-controlled systems, rather than a matrix system in which drug was imprinted.

REFERENCES

Acar, N. and Tulun, T. 1996. "Studies on the Interaction of Poly (4-vinylpyridiniumchloride) with Poly(sodiumphosphate) in an Aqueous Solution by Conductometry", *Journal of Polymer Science: Part A: Polymer Chemistry*, Vol. 34, pp. 1251-1260.

Alexandar, S.A. and Donoff, R.B. 1980. "The Glycosaminoglycans of Open Wounds", *Journal of Surgical Research*, Vol. 29, pp. 422-429.

Altman, G.H., Diaz, F., Jacuba, C., Calabro, T., Horan, R.L., Chen, J., Lu, H., Richmound, J., Kaplan D.L. 2003. "Silk-Based Biomaterials", *Biomaterials*, 24, pp.401-416.

Arai, T., Wilson, D.L., Kasai, N., Freddi, G., Hayasaka, S., Tsukada, M. 2002. "Preparation of Silk Fibroin and Polyallylamine Composites", *Journal of Applied Polymer Science*, Vol. 84, pp. 1963-1970.

Argüelles-Monal, W., Garciga, M., Peniche-Covas, C. 1990. "Study of Stoichiometric Polyelectrolyte Complex Between Chitosan and Carboxymethyl Cellulose", *Polymer Bulletin*, Vol. 23, pp. 307-313.

Asakura,T., Kuzuhara, A., Tabeta, R., Saito, H. 1985. "Conformation Characterization of Bombyx mori Silk Fibroin in the Solid State by High Frequency 13C Cross Polarization-Magic Angle Spinning NMR, X-Ray Diffraction and Infrared Spectroscopy", *Macromolecules*, Vol.18, p. 1841.

Ayutsede, J., Gandhi, M., Sukigara, S., Micklus, M., Chen, H.-E., Ko, F. 2005. "Regeneration of *Bombyx mori* Silk by Electrospinning. Part3: Characterization of Electrospun Non woven Mat", *Polymer*, Vol. 46, pp. 1625-1634.

Baker, R. and Kochinke, F. 1989. "Controlled Release of Drugs: Polymers and Aggregate Systems", *Transdermal Drug Delivery Systems*, Edited by M. Rosoff, VCH, New York, p. 283.

Balazs, E.A. and Leshchiner, A. 1986. "Crosslinked Gels of Hyaluronic Acid and Products Containing Such Gels", *US Patent 4,582,865*.

Banga, A.K. and Chien, Y.W. 1993. "Hydro-gel Based Iontotherapeutic Delivery Devices for Transdermal Delivery of Peptide/Protein Drugs", *Pharmaceutical Research*, Vol. 10, 697-702.

Banga, A.K., Bose, S., Ghosh, T.K. 1999. "Iontophoresis and Electroporation: Comparisons and Contrasts", *International Journal of Pharmaceutics,* Vol. 179, pp.1-19.

Banga, A.K., Katakam, M., Mitra, R. 1995. "Transdermal Iontophoretic Delivery and Degradation of Vasopressin Across Human Cadaver Skin, *International Journal of Pharmaceutics and Pharmaceuticals*, Vol. 116, pp. 211-216.

Barbani, N., Lazzeri, L., Cristallini, C., Cascone, M.G., Polacco, G., Pizzirani, G. 1999. "Bioartificial Materials Based on Blends of Collagen and Poly(Acrylic Acid)", *Journal of Applied Polymer Science*, Vol.72, pp. 971-976.

Barker, R. 1987. *Controlled Release of Biologically Active Agents*, (Plenum Press, New York-London).

Bayraktar, O., Malay, Ö., Özgarip, Y., Batıgün, A. 2005. "Silk Fibroin as a Novel Coating Material for Controlled Release of Theophylline", *European Journal of Pharmaceutics and Biopharmaceutics*, Vol. 60, pp. 373-381.

Brannon-Peppas, L. 1997. "Polymers in Controlled Drug Delivery", *Medical Plastics and Biomaterials*, http://www.devicelink.com/mpb/archive/97/11/003.html.

Bungenberg de Jong, H.G. 1949. "Crystallization -Coacervation-Flocculation", In H.R.Kruyt (Ed.), pp. 232-258, *Colloid Science*, Amsterdam, Elsevier.

Bungenberg de Jong, H.G. and Kruyt, H.R. 1929. "Coacervation (Partial Miscibility in Colloid Systems)", *Proc. K. Ned. Akad. Wet.*, Vol. 32, pp. 849-856.

Burgess, D.J. 1990. "Practical Analysis of Complex Coacervate Systems", *Journal of Colloid and Interface Science*, Vol. 140, pp. 227-238.

Burgess, D.J. 1994. "Complex Coacervation: Microcapsule Formation", in P.L. Dubin et al. (Eds.), *Macromolecular Complexes in Chemistry and Biology*, Springer Verlag, Berlin, pp. 285-300.

Burgess, D.J. and Carless, J.E. 1984. "Microelectrophoretic Studies of Gelatin and Acacia for the Prediction of Complex Coacervation", *Journal of Colloid Interface and Science*, Vol. 98, pp. 1-8.

Burgess, D.J. and Carless, J.E. 1985. "Manufacture of Gelatin/Gelatin Coacervate Microcapsules", *International Journal of Pharmaceutics*, Vol. 27, pp. 61-70.

Burgess, D.J. and Carless, J.E. 1986. "Complex Coacervate Formation Between Acid- and Alkaline- Processed Gelatins", in *Coulombic Interactions in Macromolecular Systems*, Eisenberg A., Bailey F.R., Eds., ACS Symposium Series 302, American Chemical Society, Washington DC, pp. 251-260.

Burgess, D.J., Kwok, K.K. and Megremis, P.T 1991. "Characterization of Albumin-Acacia Complex Coacervation", *Journal of Pharmacy and Pharmacology*, Vol. 43, pp. 232-236.

Chang, S.L., Hofmann, G.A., Zhang, L., Deftos, L.J., Banga, A.K. 2003. "Stability of a Transdermal Salmon Calcitonin Formulation", *Drug Delivery*, Vol. 10, pp. 41-45.

Chen, J., Minoura, N., Osaki, T., Tanioka, A. 2000. "Effects of pH on the Transport of 5-Fluorouracil Across a Fibroin Membrane", *Transaction*, Vol. 56, pp. 302-308.

Chen, J., Minoura, N., Tanioka, A. 1994. "Transport of Pharmaceuticals Through Silk Fibroin Membrane", *Polymer*, Vol. 35, pp. 2853-2856.

Chen, W.-S., Henry, G.A., Gaud, S.M., Miller, M.S., Kaiser, J.M., Balmadeca, E. A., Morgan, R.G., Baer, C.C., Borwankar, R.P., Hellgeth, L.C., Strandholm, J.J., Hasenheuttl, G.L., Kerwin, P.J., Chen, C.C., Kratochvil, J.F., Lloyd, W.L. 1989 Microfragmented Ionic Polysaccharide/Protein Complexes Solution. *U.S. Patent 4,559,223*.

Chen, X., Li, W., Yu, T. 1997. "Conformation Transition of Silk Fibroin Induced by Blending Chitosan", *Journal of Polymer Science: Part B: Polymer Physics*, Vol. 35, pp. 2293-2296.

Choi, Y.S., Hong, S.R., Lee, Y.M., Sog, K.W. and Park, M.H. 1999. "Studies on Gelatin-Containing Artificial Skin: I. Preparation and Characterization of Crosslinked Gelatin-Hyaluronate Sponges", *Journal of Biomedical materials Reserach*, Vol. 48, pp. 631-639.

Cleland, R.L. 1968. "Ionic Polysaccharides. II. Comparison of Polyelectrolyte Behavior of Hyaluronate and Carboxymethyl Cellulose", *Biopolymers*, Vol. 6, pp. 1519-1529.

Conaghey, O.M., Corish, J., Corrigan, O.I. 1998. "The Release of Nicotin from a Hydrogel Containing Ion Exchange Resins", *International Journal of Pharmaceutics*, Vol. 170, pp. 215-224.

Coston, A.F. and Li, J.K.-J. 2001. "Iontophoresis: Modeling, Methadology, and Evolution", *Cardiovascular Engineering*, Vol. 3, pp. 127-136.

Dautzenberg, H. 2000. "Light Scattering Studies on Polyelectrolyte Complexes", *Macromolecular Symposium*, Vol. 162, pp. 1-21.

de Kruif, C.G. and Tuinier, R. 2001. "Polysaccharide Protein Interactions", *Food Hydrocolloids*, Vol. 15, pp. 555-563.

de Kruif, C.G., Weinbreck, F., de Vries, R. 2004. "Complex Coacervation of Proteins and Anionic Polysaccharides", *Current Opinion in Colloid and Interface Science*, Vol. 9, pp. 340-349.

Dickinson, E. 1998. "Stability and Rheological Implications of Electrostatic Milk Protein-Polysaccharide Interactions, *Trends in Food Science and Technology*, Vol. 9, pp. 347-354.

Dragan, S., Cristea, M., Luca, C., Simionescu, B.C. 1996. "Polyelectrolyte Complexes. I. Synthesis and Characterization of Some Insoluble Polyanion-Polycation Complexes", *Journal of Polymer Science: Part A: Polymer Chemistry*, Vol.34, pp. 3485-3494.

Dumitriu, S. and Chornet, E. 1998. "Inclusion and Release of Proteins from Polysaccharide-Based Polyion Complexes", *Advanced Drug Delivery Reviews,* Vol. 31, pp. 223-246.

Fang, E., Cheng, Q., Lu, X.B. 1998. "Kinetics of *In Vitro* Drug Release from Chitosan/Gelatin Hybrid Membranes", *Journal of Applied Polymer Science*, Vol. 68, pp. 1751-1758.

Fini, M., Motta, A., Torricelli, P., Giavaresi, G., Aldini, A.N., Tschon, M., Giardino, R., Migliaresi, C. 2005. "The Healing of Confined Critical Size Cancellous Defects in the Presence of Silk Fibroin Hydrogel", *Biomaterials*, Vol. 26, pp. 3527-3536.

Fletcher, K. 1998. "Drug Delivery: Strategies and Technologies", *PSST*, Vol.1, pp. 49-51.

Flynn, G.L., Yalkowsky, S.H., Roseman, T.J. 1974. "Mass Transport Phenomena and Models: Theoretical Concepts", *Journal of Pharmaceutical Sciences*, Vol. 63, p. 479.

Freddi, G., Romano, M., Massafra, M.R., Tsukada M. 1995. "Silk Fibroin/Cellulose Blend Films: Preparation, Structure, and Physical Properties", *Journal of Applied Polymer Science*, Vol. 56, pp. 1537-1545.

Freddi, G., Tsukada, M., Beretta, S. 1999. "Structure and Physical Properties of Silk Fibroin/Polyacrylamide Blend Films", *Journal of Applied Polymer Science*, Vol. 71, pp. 1563-1571.

Ghosh, S., Kobal, I., Zanette, D., Reeds, W.F. 1993. "Conformational Contraction and Hydrolysis of Hyaluronate in Sodium-Hydroxide Solutions", *Macromolecules*, Vol. 26, pp. 4685-4693.

Gibbs, D.A., Merrille, E.W., Smith, K.A., Balazs, E.A. 1968. "Rheology of Hyaluronic Acid", *Biopolymers*, Vol. 6, pp. 777-791.

Girard, M., Turgeon, S.L., Gauthier, S.F. 2002. "Interbiopolymer Complexing Between β-Lactoglobulin and Low- and High-Methylated Pectin Measured by Potentiometric Titration and Centrifugation", *Food Hydrocolloids*, Vol. 16, pp. 585-591.

Girard, M., Turgeon, S.L., Gauthier, S.F. 2003. "Thermodynamic Parameters of β-Lactoglobulin-Pectin Complexes Assessed By Isothermal Titration Calorimetry, *Journal of Agricultural Food Chemistry*, Vol. 51, pp. 4450-4455.

Gotoh, Y., Niimi, S., Hayakawa, T., Miyashita, T. 2004. "Preparation of Lactose-Silk Fibroin Conjugates and Their Application as a Scaffold for Hepatocyte Attachment", *Biomaterials*, Vol. 25, pp. 1131-1140.

Gotoh, Y., Tsukada, M., Baba, T., Minoura, N. 1997. "Physical Properties and Structure of Poly(ethylene glycol)-Silk Fibroin Conjugate Films", *Polymer*, Vol. 38, pp. 487-490.

Green, P., Shroot, B., Bernerd, F., Pilgrim, W.R., Guy, R.H. 1992. "*In Vitro* and *In Vivo* Iontophoresis of a Tripeptide Across Nude Rat Skin", *Journal of Controlled Release*, Vol.20, pp. 209-217.

Grimshaw, P., Nussbaum, J., Grodzinsky, A. 1990. "Kinetics of Electricity and Chemically Induced Swelling in Polyelectrolyte Gels", *Journal of Chemical Physics*, Vol. 93 pp.4462-4472.

Grimshaw, P.E., Grodzinsky, A.J., Yarmush, M.L., Yarmush, D.M. 1989. "Dynamic Membranes for Protein Transport", *Chemical Engineering Science*, Vol.44, pp. 827-840.

Grymonpré, K.R., Staggemeier, B.A., Dubin, P.L., Mattison, K.W. 2001. "Identification by Integrated Computer Modeling and Light Scattering Studies of an Electrostatic Serum Albumin-Hyaluronic Acid Binding Site", *Biomacromolecules*, Vol. 2, pp. 422-429.

Gupta, P., Vermani, K., Garg, S. 2002. "Hydrogels: from Controlled Release to pH-Sensitive Drug Delivery", *Drug Discovery Today*, Vol. 7, pp. 569-579.

Guy, R.H., Kalia, Y.N., Delgado-Charro, M.B., Merino, V., Lopez, A., Marro, D. 2000. "Iontophoresis: Electrorepulsion and Electroosmosis", *Journal of Controlled Release*, Vol. 64, pp. 129-132.

Hanawa, T., Watanabe, A., Tsuchiya, T., Ikoma, R., Hidaka, M., Sugihara, M. 1995. "New Oral Dosage Form for Elderly Patients: Preparation and Characterization of Silk Fibroin Gel", *Chemical and Pharmaceutical Bulletin*, Vol. 43, pp. 284-288.

Hossain, K.S., Ohyama, E., Ochi, A., Magoshi, J. and Nemoto, N. 2003. "Dilute-Solution Properties of Regenerated Silk Fibroin", *Journal of Physical Chemistry B*, Vol. 107, pp. 8066-8073.

Huang, Y.Y., Wu, S.M., Wang, C.Y. 1996. " Response Surface Method: A Novel Strategy to Optimize Iontophoretic Transdermal Delivery of Thyrotropin-Releasing Hormone", *Pharmaceutical Research*, Vol. 13, pp. 547-52.

Jain, S.K., Chourasia, M.K., Sabitha, M., Jain, A.K., Ashawat, M., Jha, A.K. 2003. "Development and Characteriation of Transdermal Drug Delivery Systems for Diltiazem Hydrochloride", *Drug Delivery*, Vol.10, pp. 167-177.

Jaskari, T., Vuorio, M., Kontturi, K., Urtti, A., Manzanares, J.A. and Hirvonen, J. 2000. "Controlled Transdermal Iontophoresis by Ion-Exchange Fiber", *Journal of Controlled Release*, Vol. 67, pp. 179-190.

Jensen, M., Hansen, P.B., Murdan, S., Frokjaer, S. and Florence, A.T. 2002. "Loading Into and Electro-Stimulated Release of Peptides and Proteins From Chondroitin 4-Sulphate Hydrogels", *European Journal of Pharmaceutical Sciences*, Vol. 15, pp. 139-148.

Jin, H.-J., Park, J., Valuzzi, R., Cebe, P., Kaplan, D.L. 2004. "Biomaterial Films of *Bombyx mori* Silk Fibroin with Poly(ethylene oxide)", *Biomacromolecules*, Vol. 5, pp. 711-717.

Kabanov, V.A., Zezin, A.B., Mustafaev, M.I., Kasaikin, V.A. 1980. *Polymeric Amines and Ammonium Salts*, edited by E.J. Goethals (Pergamon Press, Oxford), p. 173. 80

Kaibara, K., Okazaki, T., Bohidar, H.B., Dubin, P.L. 2000. "pH-Induced Coacervation in Complexes of Bovine Serum Albumin And Cationic Polyelectrolytes", *Biomacromolecules*, Vol.1, pp. 100-107.

Kang, G.-D., Nahm, J.-H., Pak, J.-S., Moon, J.-Y., Cho, C.-S., Yeo, J.H. 2000. "Effects of Poloxamer on the Gelation of Silk Fibroin", *Macromolecular Rapid Communications*, Vol. 21, pp. 788-791.

Kanikkannan, N., Singh, J., Romarao, P. 2001. "In Vitro Transdermal Iontophoretic Transport of Timolol Maleate: Effect of Age and Species", *Journal of Controlled Release*, Vol. 71, pp. 99-105.

Kim, S.J., Yoon, S.G., Lee, K.B., Park, Y.D. and Kim, S.I. 2003. "Electrical Sensitive Bahvior of a Polyelectrolyte Complex Composed of Chitosan/Hyaluronic Acid", *Solid State Ionics*, Vol., pp.

Kim, U.-J., Park, J., Kim, H.J., Wada, M., Kaplan, D.L. 2005."Three-Dimensional Aqueous-Derived Biomaterial Scaffolds from Silk Fibroin", *Biomaterials*, Vol. 26, pp. 2775-2785.

Kim, U.-J., Park, J., Li, C., Jin, H.-J., Valluzzi, R., Kaplan, D.L. 2004. "Structure and Properties of Silk Hydrogels", *Biomacromolecules*, Vol. 5, pp. 786-792.

Kokufuta, E. 1979. "Colloid Titration Behavior of Poly(ethyleneimine)", *Macromolecules*, Vol. 12, pp. 350-353.

Kost, J. and Langer, R. 2001. "Responsive Polymeric Delivery Systems", *Advanced Drug Delivery Reviews*, Vol. 46, pp. 125-148.

Kumar, M.N.V.R. and Kumar, N. 2001. "Polymeric Controlled Drug-Delivery Systems: Perpective Issues and Opportunities", *Drug Development and Industrial Pharmacy*, Vol. 27(1), pp. 1-30.

Kupperblatt, G.B. and Dickinson, B. 1999. "Iontophoretic Patch with Hydrogel Reservoir", *EP0904779*.

Lee, K.Y., Park, W.H., Ha, W.S. 1997. "Polyelectrolyte Complexes of Sodium ALginate with Chitosan or Its Derivatives for Microcapsules", *Journal of Applied Polymer Science*, Vol. 63, pp. 425-432.

Lee, S.B., Lee, Y.M., Song, K.W., Park, M.H. 2003. "Preparation and Properties of Polyelectrolyte Complex Sponges of Hyaluronic Acid and Chitosan and Their Biological Behaviors", *Journal of Applied Polymer Science*, Vol. 90, pp. 925-932.

Leisner, D. and Imae, T. 2003. "Interpolyelectrolyte Complex and Coacervate Formation of Poly(glutamic acid) with a Dendrimer Studied by Light Scattering and SAXS, *Journal of Physical Chemistry Bulletin*, Vol. 107, pp. 8078-8087.

Li, F., Li., W.G. and Yao, D. 2002. "Preparation of Oxidized Glucose-Crosslinked *N*-alkylated Chitosan Membrane and In Vitro Studies of pH-Sensitive Drug Delivery Behaviour", *Biomaterials*, Vol. 23, p. 343.

Li, M., Minoua, N. Dai, N., Zhang, L. 2001. "Preparation of Porous Poly(vinyl alcohol)-Silk Fibroin (PVA/SF) Membranes", *Macromolecular Materials and Engineering*, Vol. 286, pp. 529-534.

Liang, C.X. and Hirabayashi, K. 1992. "Improvements of the Physical Properties of Fibroin Membranes with Sodium Alginate", *Journal of Applied Polymer Science*, Vol. 45, pp. 1937-1943.

Luo, Y., Kirker, K.R., Prestwich, G.D. 2000. "Cross-linked Hyaluronic Acid Hydrogel Films: New Biomaterials for Drug Delivery", *Journal of Controlled Release*, Vol. 69, pp. 169-184.

Magoshi, J., Magoshi, Y., Becker, M.A., Kato, M., Han, Z., Tanak, T., Inoue, S.-i., Nakamura, S. 2000. "Crystallization of Silk Fibroin from Solution", *Thermochimica Acta*, Vol. 352-353, pp. 165-169.

Magoshi, J., Magoshi, Y., Becker, Nakamura, S. 1996. *Polymeric Materials Encyclopedia,* edited by J.C. Salamone, CRC Press, New York, p. 667.

Medi, B.M., Singh, J. 2003. "Electronically Facilitated Transdermal Delivery of Human Parathyroid Hormone", *International Journal of Pharmaceutics*, Vol. 263, pp. 25-33.

Meinel, L., Hofmann, S., Karageorgiou, V., Kirker-Head, C., McCool, J., Gronowicz, G., Zichner, L., Langer, R., Vunjak-Novakovic, G., Kaplan, D.L 2005. "The Inflammatory Responses to Silk Films In Vitro and In Vivo", *Biomaterials*, Vol. 26, pp. 147-155.

Meyer, K. and Palmer, J. 1934. "The Polysaccharide of the Vitrous Humor", *Journal of Biological Chemistry*, Vol. 107, pp. 629-634.

Minoura, N., 1996. *Polymeric Materials Encyclopedia*, edited by J.C. Salamone (CRC Press-USA), pp. 7744-7751.

Minoura, N., Tsukada, M., Nagura, M. 1990a. “Physico-chemical Properties of Silk Fibroin Membrane as a Biomaterial”, *Biomaterials*, Vol. 11, pp. 430-434.

Mitragotri, S., Blankschtein, D. and Langer R. 1995. "Ultrasound-Mediated Transdermal Protein Delivery", *Science*, Vol. 269, pp. 850-853.

Nam, J. and Park, Y.H. 2001. “Morphology of Regenerated Silk Fibroin: Effects of Freezing Temperature, Alcohol Addition and Molecular Weight”, *Journal of Applied Polymer Science*, Vol. 81, pp. 3008-3021.

Nemoto, N., Hossain, K.S., Magoshi, J. 1999. "Dynamic and Static Light Scattering of Dilute Aqueous Solutions of Silk Fibroin Collected from *Bombyx Mori* Silkworms", *Langmuir*, Vol. 15, pp. 4114-4119.

Nishida, S., Tanaka, Y and Uragami, T. 1993 "Water Insoluble Biocompatible Hyaluronic and Polyion Complex and the Method Same", *European Patent EP0544259*.

Nugroho, A.K., Li, L., Dijkstra, D., Wikström, H., Danhof, M., Bouwstra, J.A. 2005. "Transdermal Iontophoresis of the Dopamine Agonist 5-OH-DPAT in Human Skin *In Vitro*", *Journal of Controlled Release*, Vol. 103, pp. 393-403.

Okano, T. and Yoshida, R. 1993. *Biomedical Applications of Polymeric Materials*, Chief Editor T. Tsuruta, CRC Press, Florida, USA, pp. 408-410.

Panchagnula, R., Pillai, O., Nair, V.B. and Romarao, P. 2000. "Transdermal Iontophoresis Revisited", *Current Opinion on Chemical Biology*, Vol. 4, pp. 468-473.

Panchagnula, R. 1997. "Transdermal Delivery of Drugs", *Indian Journal of Pharmacology*, Vol. 29, pp. 140-156.

Park, S.J., Lee, K.Y., Ha, W.S., Park, S.Y. 1999. "Structural Changes and Their Effect on Mechanical Properties of Silk Fibroin/Chitosan Blends", *Journal of Applied Polymer Science*, Vol. 74, pp. 2571-2575.

Park, S.-N., Park, J.-C., Kim, H.O., Song, M.J., Suh, H. 2002. "Characterization of Porous Collagen/Hyaluronic Acid Scaffold Modified by 1-Ethyl-3-Dimethylaminopropyl)carbodiimide Cross-linking", *Biomaterials*, Vol. 23, pp. 1205-1212.

Peniche, C., Argüelles-Monal, W., Peniche, H. and Acosta, N. 2003. "Chitosan: An Attractive Biopolymer for Microencapsulation", *Macromolecular Bioscience*, Vol. 3, pp. 511-520.

Perez-Rigueiro, J., Viney, C., Llorca, J., Elices, M. 1998. "Silkworm Silk as an Engineering Material", *Journal of Applied Polymer Science*, Vol. 70, pp. 2439-2447.

Plashchina, I.G., Mrachkovskaya, T.A., Danilenkom, A.N., Kozhevnikov, G.O., Starodubrovskaya, N.Y., Braudo, E.E., Schwenke, K.D. 2001. "Complex Formation of Faba Bean Legumin with Chitosan: Surface Activity and Emulsion Properties of Complexes", in: E. Dickinson, R. Miller, *Food Colloids*, *Fundamentals of Formulation*, Royal Society of Chemistry, Cambridge, pp. 332-341.

Putthanarat, S., Zarkoob, S., Magoshi, J., Chen, J.A., Eby, R.K., Stone, M., Adams, W.W. 2002. "Effect of Processing Temperature on the Morphology of Silk Membranes", *Polymer*, Vol. 43, pp. 3405-3413.

Qian, J., Liu, Y., Liu, H., Yu, T., Deng, J. 1996. "An Amphoteric Biosensor Based on Immobilized Glucose Oxide Employing p-Benzoquinone as Electron Shuttle", *Journal of Chemical Technology and Biotechnology*, Vol. 67, pp. 281-285.

Raiman, J., Koljonen, M., Huikko, K., Kostiainen, R., Hirvonen, J. 2004. "Delivery and Stability of LHRH and Nafarelin Human Skin: The Effect of Constant/Pulsed Iontophoresis", *European Journal of Pharmaceutical Sciences*, Vol. 21, pp. 371-377.

Rujiravanit, R., Kruaykitanon, S., Jamieson, A.M., Tokura, S. 2003. "Preparation of Crosslinked Chitosan/Silk Fibroin Blend Films for Drug Delivery System", *Macromolecular Bioscience*, Vol. 3, pp. 604-611.

Saitoh, H., Ohshima, K., Tsubouchi, K., Takasu, Y., Yamada, H. 2004. "X-Ray Structural Study of Noncrystalline Regenerated *Bombyx mori* Silk Fibroin", *International Journal of Biological Macromolecules*, Vol. 34, pp. 317-323.

Sanchez, C., Meckloufi, G., Schmitt, C., Renard, D., Robert, P., Lehr, C.M., Lamprecht, A., Hardy, J. 2002. "Self-Assembly of β–Lactoglobulin and Acacia Gum in Aqueous Solvent: Structure and Phase-Ordering Kinetics", *Langmuir*, Vol. 18, pp. 10323-10333.

Schmitt, C., Sanchez, C., Desobry-Banon, S., Hardy, J. 1998. "Structure and Technofunctional Properties of Protein-Polysaccharide Complexes: A Review", *Critical Reviews in Food Science and Nutrition*, Vol. 38, pp. 689-753.

Schmitt, C., Sanchez, C., Despond, S., Renard, D., Thomas, F., Hardy, J. 2000. "Effect of Protein Aggregates on the Complex Coacervation between β–lactoglobulin and Acacia Gum at pH 4.2", *Food Hydrocolloids*, Vol. 14, pp. 403-413.

Schmitt, C., Sanchez, C., Thomas, F. and Hardy, J. 1999. "Complex Coacervation between β-lactoglobulin and Acacia Gum in Aqueous Medium", *Food Hydrocolloids*, Vol. 13, pp. 483-496.

Sebastiani, P., Nicoli, S., Santi, P. 2005. "Effect of Lactic Acid and Iontophoresis on Drug Permeation Across Rabbit Ear Skin", *International Journal of Pharmaceutics,* Vol. 292, pp. 119-126.

Sershen, S. and West, J. 2002. "Implantable, Polymeric Systems for Modulated Drug Delivery", *Advanced Drug Delivery Reviews*, Vol.54, pp. 1225-1235.

Simon, L.D., Charman, W.N., Charman, S.A., Stella, V.J. 1997. "Protein Transport Across Hydrated Hyaluronic Acid Ester Membranes: Evaluation of Ribonuclease A as a Potentially Useful Model Protein", *Journal of Controlled Release*, Vol. 45, pp. 273-285.

Simsek-Ege, F.A., Bond, G.M., Stringer, J. 2002. "Polyelectrolyte Complex Formation Between Alginate and Chitosan as a Function of pH, *Journal of Applied Polymer Science*,Vol. 88, pp. 346-351.

Singh, P. and Maibach, H.I. 1994. "Iontophoresis in Drug Delivery: Basic Principles and Applications", *Critical Reviews on Drug Carrier Systems*, Vol. 11, pp. 161-213.

Sofia, S., McCarthy, M.B., Gronowicz, G., Kaplan, D.L. 2001. "Functionalized Silk-Based Biomaterials for Bone Formation", *Journal of Biomedical Materials Research*, Vol. 2001, pp. 139-148.

Šoltés, L. and Mendischi, R. 2003. "Molecular Characterization of Two Host-Guest Associating Hyaluronan Derivatives", *Biomedical Chromatography*, Vol. 17, pp. 376-384.

Stamatialis, D.F., Rolevink, H.H.M., Koops, G.H. 2002. "Controlled Transport of Timolol Maleate Through Artificial Membranes Under Passive and Iontophoretic Conditions, *Journal of Controlled Release*, Vol. 81, pp. 335-345.

Surini, S., Akiyama, H., Morishita, M. Nagai, T., Takayama, K. 2003. "Release Phenomena of Insulin from an Implantable Device Composed of a Polyion Complex of Chitosan and Sodium Hyaluronate", *Journal of Controlled Release*, Vol. 90, pp. 291-301.

Sutani, K., Kaetsu, I., Uchida, K., Matsubara, Y. 2002. "Stimulus Responsive Drug Release from Polymer Gel. Controlled Release of Ionic Drug from Polyampholyte Gel", *Radiation Physics and Chemistry*, Vol. 64, pp. 331-336.

Sutinen, R., Paronen, P., Urtti, A. 1999. "Water-Activated, pH-Controlled Patch in Transdermal Administration of Timolol – I. Preclinical Tests", *Europan Journal of Pharmaceutical Sciences,* Vol. 11, pp. 19-24.

Tabata, Y. and Ikada, Y. 1998. "Protein Release from Gelatin Matrices", *Advanced Drug Delivery Reviews*, Vol. 31, pp. 287-301.

Terry, A.E., Knight, D.P., Porter, D., Vollrath, F. 2004. "pH Induced Changes in the Rheology of Silk Fibroin Solution from the Middle Division of *Bombyx mori* Silkworm", *Biomacromolecules*, Vol. 5, pp. 768-772.

Thacharodi, D. and Rao, K. 1995. "Development and In Vitro Evaluation of Chitosan-Base Transdermal Drug Delivery Systems for Controlled Delivery of Propranolol Hydrochloride", *Biomaterials*, Vol.16., pp. 145-148.

Tiebackx, F.W.Z. 1911. "Gleichzeitige Ausflockung zweier Kolloide", *Chem Ind. Kolloide*, Vol. 8, pp. 198-201. 26

Tolstoguzov, V. 2003. "Some Thermodynamic Considerations in Food Formulation", *Food Hydrocolloids*, Vol. 17, pp. 1-23.

Tomer, R., D,imitrijevic, D., Florence, A.T. 1995. "Electrically COntrolled Release of Macromolecules from Crosslinked Hyaluronic Acid Hydrogels", *Journal of Controlled Release*, Vol. 33, pp. 405-413.

Tomihata, K. and Ikada, Y. 1997. "Crosslinking of Hyaluronic Acid with Water-Soluble Carbodiimide", *Journal of Biomedical Materials Research*, Vol. 37, pp. 243-251.

Tsuchida, E., Osada, Y., Sanada, K. 1972. " Interaction of Poly (Styrene Sulfonate) with Polycations Carrying Charges in the Chain Backbone", *Journal of Polymer Science: Polymer Chemistry*, Vol. 10, pp. 3397.

Tsukada, M., Freddi, G., Minoura, N., Allara, G. 1994. "Preparation and Application of Porous Silk Fibroin Materials", *Journal of Applied Polymer Science*, Vol. 54, pp. 507-514.

Tuinier, R., Rolin, C., de Kruif, C.G. 2002. "Electrosorption of Pectin onto Casein Micelles", *Biomacromolecules*, Vol. 3, pp. 632-638.

Turgeon, S.L., Beaulieu, M., Schmitt, C., Sanchez, C. 2003. "Protein-Polysaccharide Interactions: Phase-Ordering Kinetics, Thermodynamic and Structural Aspects", *Current Opinion in Colloid and Interface Science,* Vol. 8, pp. 401-414.

Um, I.C., Kweon, H.Y., Park, Y.H., Hudson, S. 2001. "Structural Characteristics and Properties of the Regenerated Silk Fibroin Prepared from Formic Acid", *International Journal of Biological Macromolecules*, Vol. 29, pp. 91-97.

Valluzzi, R., Gido, S.P., Muller, W., Kaplan, D. 1999. "Orientation of Silk III at the Air-Water Interface", *International Journal of Biological Macromolecules*, Vol. 24, pp. 237-242.

Van der Geest, R., Danhof, M., Bodde, H.E. 1998. "Validation and Testing of a New Iontophoretic Continuous Flow Through Transport Cell", *Journal of Controlled Release*, Vol. 51, p. 85.

Vasil'ev, A.E., Krasnyuk, I., Ravikumar, S. and Tokhmakhchi, V.N. 2001. "Drug Synthesis Methods and Manufacturing Technology: Transdermal Therapeutic Systems for Controlled Drug Release (A Review)", *Pharmaceutical Chemistry Journal*, Vol. 35, pp. 613-626.

Wang, H., Li, W., Lu, Y., Wang, Z. 1997. "Studies on Chitosan and Poly(acrylic acid) Interpolymer Complex. I. Preparation, Structure, pH-Sensitivity, and Salt Sensitivity of Complex Forming Poly(acrylic acid): Chitosan Semi-Interpenetrating Polymer Network", *Journal of Applied Polymer Science*, Vol. 65, pp. 1445-1450.

Wang, Y., Thakur, R., Fan., Q., Minchniak, B. 2005. " Transdermal Iontophoresis: Combination Strategies to Improve Iontophoretic Drug Delivery", *European Journal of Pharmaceutics and Biopharmaceutics*, Vol. 60, pp. 179-191.

Wang, Y.-F., Gao, J.Y., Dubin, P.L. 1996. "Protein Separation via Polyelectrolyte Coacervation: Selectivity and Efficiency", *Biotechnology Progress*, Vol. 12, pp. 356-362.

WEB_1, 2003. Iontophoresis - Theory, by B. Gazelius (Periflux Systems), 10/03/2003. http://www.perimed.se/p_Applications/IontophoresisTheory.pdf

WEB_2, 2005. General Introduction/Coacervate Systems, by F. Weinbreck, 15/06/2005. http://www.library.uu.nl/digiarchief/dip/diss/2004-0422-110036/c1.pdf

WEB_3, 2005. Introduction to Protein Structure, Lecture 3 by T.M. Mareci, 29/06/2005. http://faraday.ufbi.ufl.edu/~thmareci/bch4024/lecture3.pdf

WEB_4, 2005. Hyaluronan: Structure and Physical Properties, 18705/2005. http://www.glycoforum.gr.jp/science/hyaluronan/HA01/HA01E.html

WEB_5, 2005. Biomaterials from Chemically-Modified Hyaluronan, 18/05/2005. http://www.glycoforum.gr.jp/science/hyaluronan/HA18/HA18E.html

WEB_6, 2005. Timoptic Ocudose Prescription Information, 10/06/2005. http://www.agingeye.net/glaucoma/timopticocudose.pdf

Weinbreck, F., de Vries, R., Schrooyen, P., de Kruif, C.G. 2003a. "Complex Coacervation of Whey Proteins and Gum Arabic", *Biomacromolecules*, Vol. 4, pp. 293-303.

Weinbreck, F., Nieuwenhuijse, H., Robijn, G.W., de Kruif, C.G. 2003b. "Complex Formation of Whey Proteins-Exocelluler Polysaccharide EPS B40", *Langmuir*, Vol.19, pp. 9404-9410.

Weinbreck, F., Tromp, R.H., de Kruif, C.G. 2004. "Composition and Structure of Whey Protein/Gum Arabic Coacervates", *Biomacromolecules*, Vol. 5, pp. 1437-1445.

Xu, Y., Zhang, Y., Shao, H., Hu, X. 2005. "Solubility and Rheological Behavior of Silk Fibroin (*Bombyx mori*) in *N*-Methyl Morpholine *N*-Oxide", *International Journal of Biological Macromolecules*, Vol. 35, pp.155-161.

Yamada, H., Nakao, H., Takasu, Y., Tsubouchi, K. 2001. "Preparation of Undegraded Native Molecular Fibroin Solution from Silkworm Cocoons", *Materials Science and Engineering C*, Vol. 14, pp. 41-46.

Yamada, H., Tsuboi, Y., Itaya, A. 2003. "AFM Observations of Silk Fibroin on Mica Substrates: Morphologies Reflecting the Secondary Structures", *Thin Solid Films*, Vol. 440, pp. 208-216.

Yamaura, K., Kuranuki, S., Suzuki, M., Tanigami, T., Matsuzawa, S. 1990. "Properties of Mixtures of Silk Fibroin/Syndiotactic-Rich Poly(vinyl alcohol)", *Journal of Applied Polymer Science*, Vol. 41, pp. 2453-2461.

Yin, Y.J., Yao, K.D., Cheng, G.X., Ma, J.B. 1999. "Properties of Polyelectrolyte Complex Films of Chitosan and Gelatin, *Polymer International*, Vol. 48, pp. 429-433.

Yoshizawa, T., Shin-ya, Y., Hong, K.J., Kajuiuchi, T. 2004 "pH- and Temperature-Sensitive Permeation Through Polyelectrolyte Complex Films Composed of Chitosan and Polyalkyleneoxide-Maleic Acid Copolymer", *Journal of Membrane Science*, Vol. 241, pp. 347-354.

Zhang, Y.-Q. 1998. "Natural Silk Fibroin as a Support for Enzyme Immobilization", *Biotechnology Advances*, Vol. 16, pp. 961-971.

Zhou, C.-Z., Confalonieri, F., Jacquet, M., Perasso, R.L., Li, Z.-G., Janin, J. 2001. "Silk Fibroin: Structural Implications of a Remarkable Amino Acid Sequence", *Proteins: Structure, Function, and Genetics*, Vol. 44, pp. 119-122.

APPENDIX A

PREPARATION OF DIALYSIS TUBING

The dialysis tubing was prepared by cutting 30 cm-long tubing from the roll. Initially the glycerin is removed by washing the tubes in running water for 3-4 hours. After the washing step, the sulfur components are removed by treating the tubes with a 0.3 % (w/v) sodium sulfide solution at 80°C for one minute. Then it is washed with hot water at 60°C for 2 minutes. It is followed by acidification with 0.2% (v/v) sulfuric acid and rinsing with hot water to remove the acid. As a result of this process, tubing is proposed to retain most proteins of molecular weight 12,000 and greater.

APPENDIX B

CALIBRATION CURVES

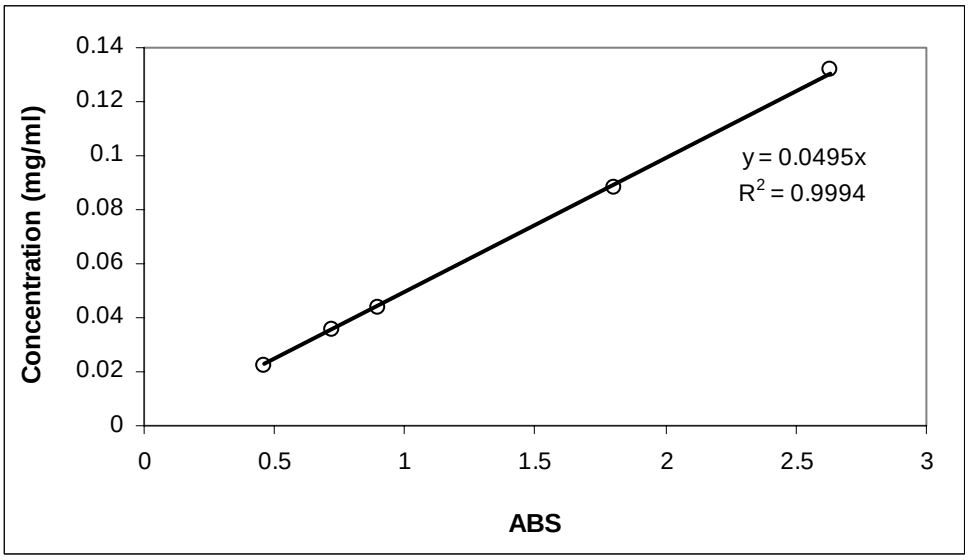

Figure B1. Calibration curve of TM dissolved in PBS at pH = 7.4 evaluated at λ = 294 nm in UV-visible spectrophotometer.

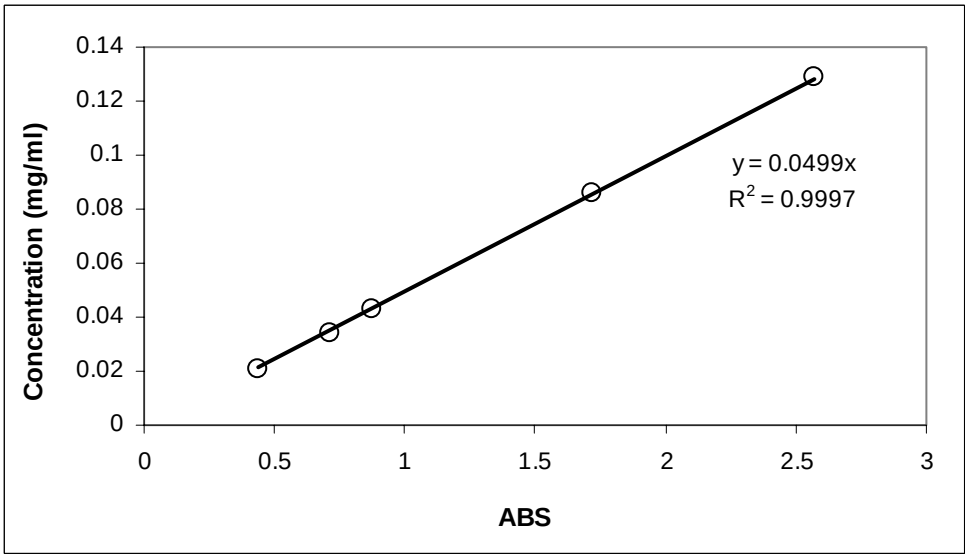

Figure B2. Calibration curve of TM dissolved in PBS at pH = 2.5 evaluated at λ = 294 nm in UV-visible spectrophotometer.

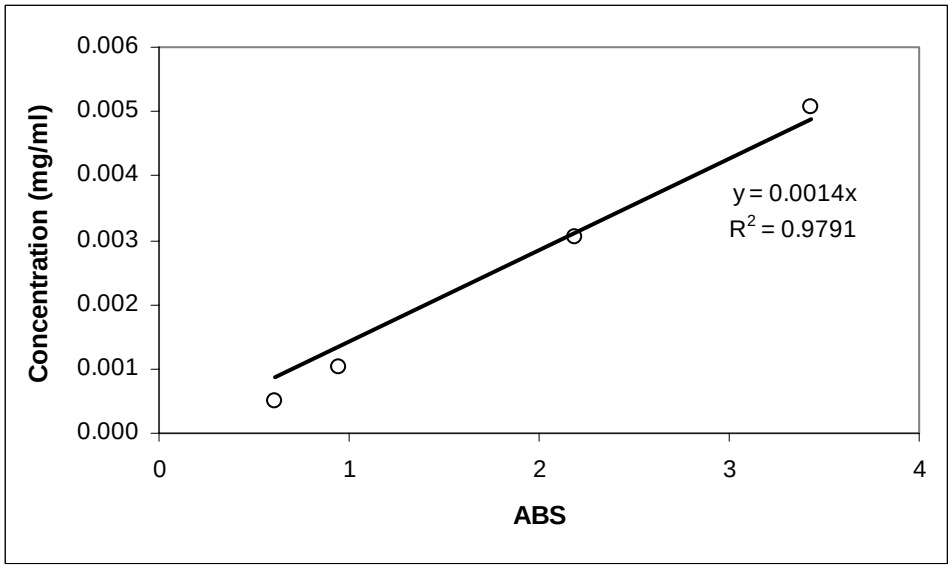

Figure B3. Calibration curve of aqueous SF solution evaluated at λ = 272 nm in UV-visible spectrophotometer.

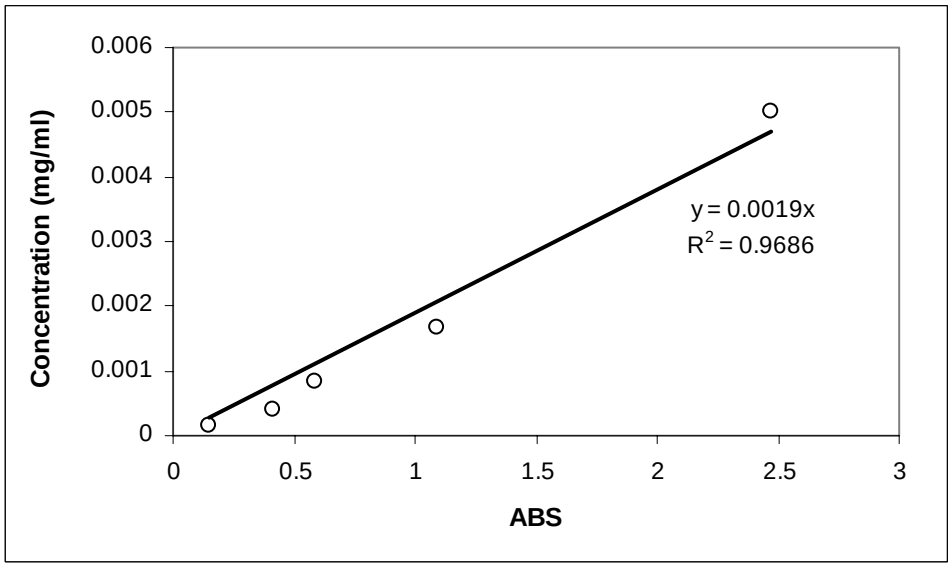

Figure B4. Calibration curve of aqueous HA solution evaluated at λ = 217 nm in UV-visible spectrophotometer.